IPAM workshop: Multiscale Geometric Methods in Astronomical Data Analysis

UCLA, November 9, 2004

Cosmological fields and the distribution of galaxies: Multiresolution morphology

Vicent J. Martínez

Observatori Astronòmic
Universitat de València

With thanks to John Peacock for some slices

In collaboration with:

J.-L. Starck, D. Donoho, E. Saar, S. Paredes, and S. Reynolds

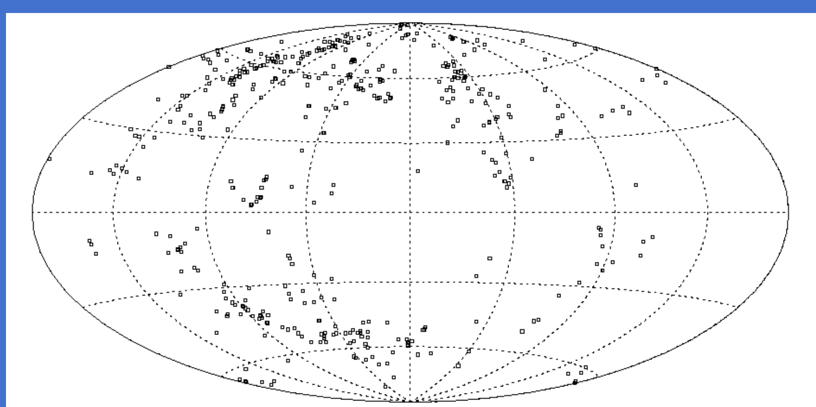

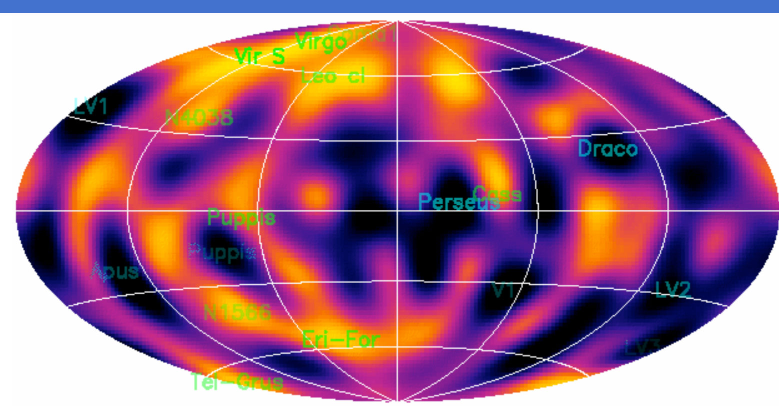

Outline of the talk:

- Galaxies everywhere

(on the sky and in the computer)

- Second-order statistics

(correlation function and power spectrum)

- Multiresolution morphology

(consistent estimation of the density field)

Outline of the talk:

- Galaxies everywhere

(on the sky and in the computer)

- Second-order statistics

(correlation function and power spectrum)

- Multiresolution morphology

(consistent estimation of the density field)

The first Hubble Deep Field

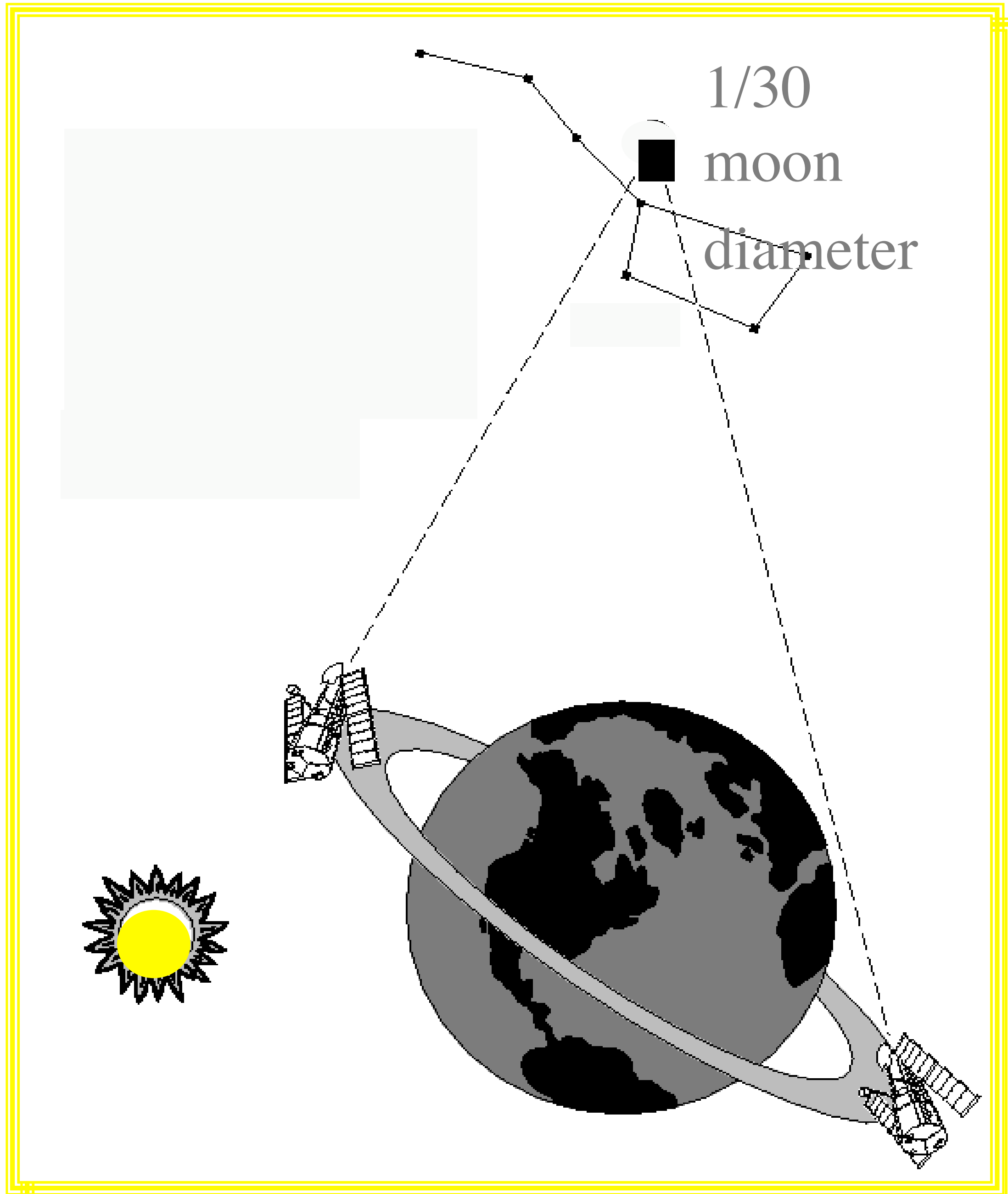

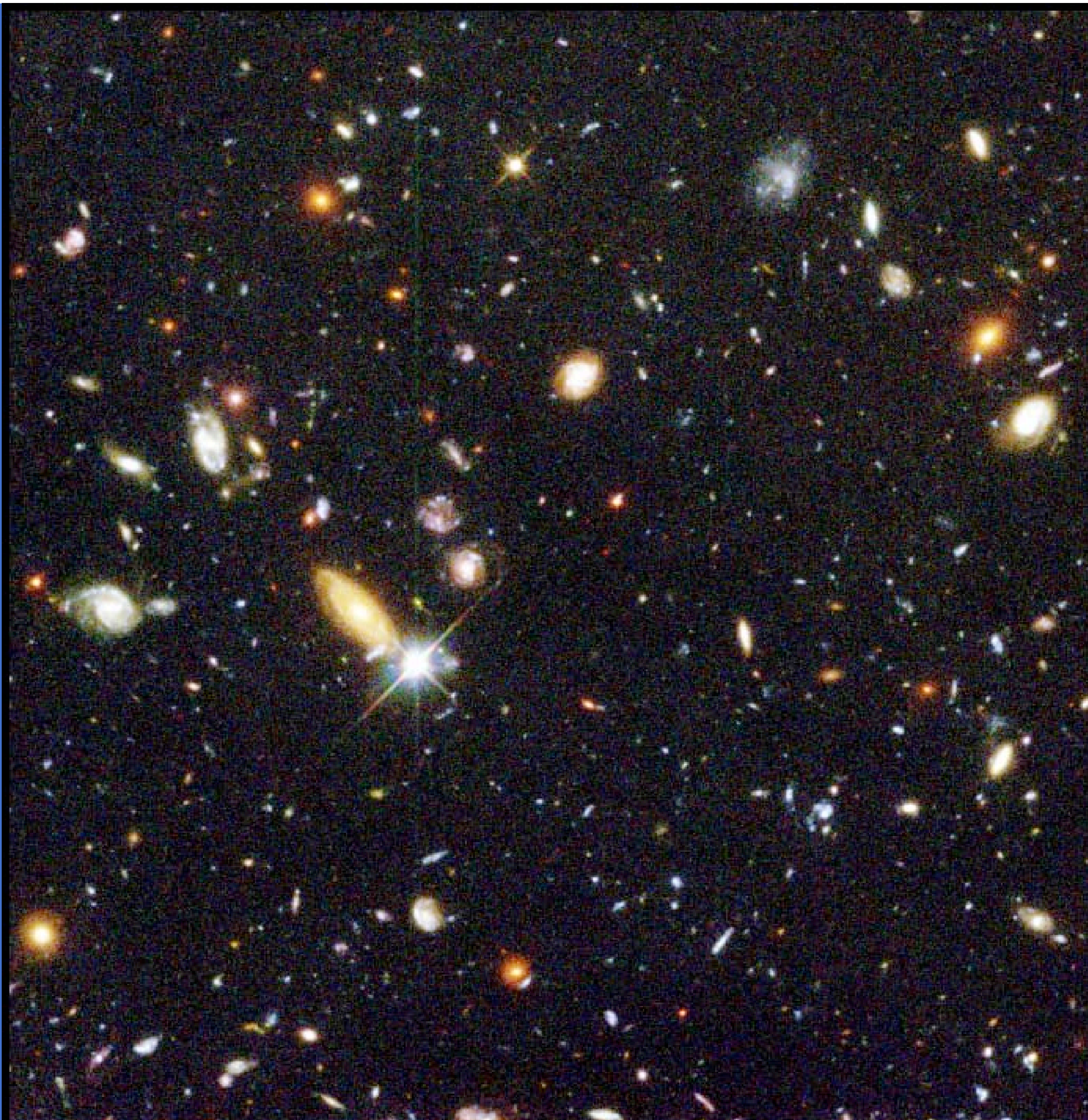

Hubble Deep Field HST • WFPC2

PRC96-01a • ST ScI OPO • January 15, 1996 • R. Williams (ST ScI), NASA

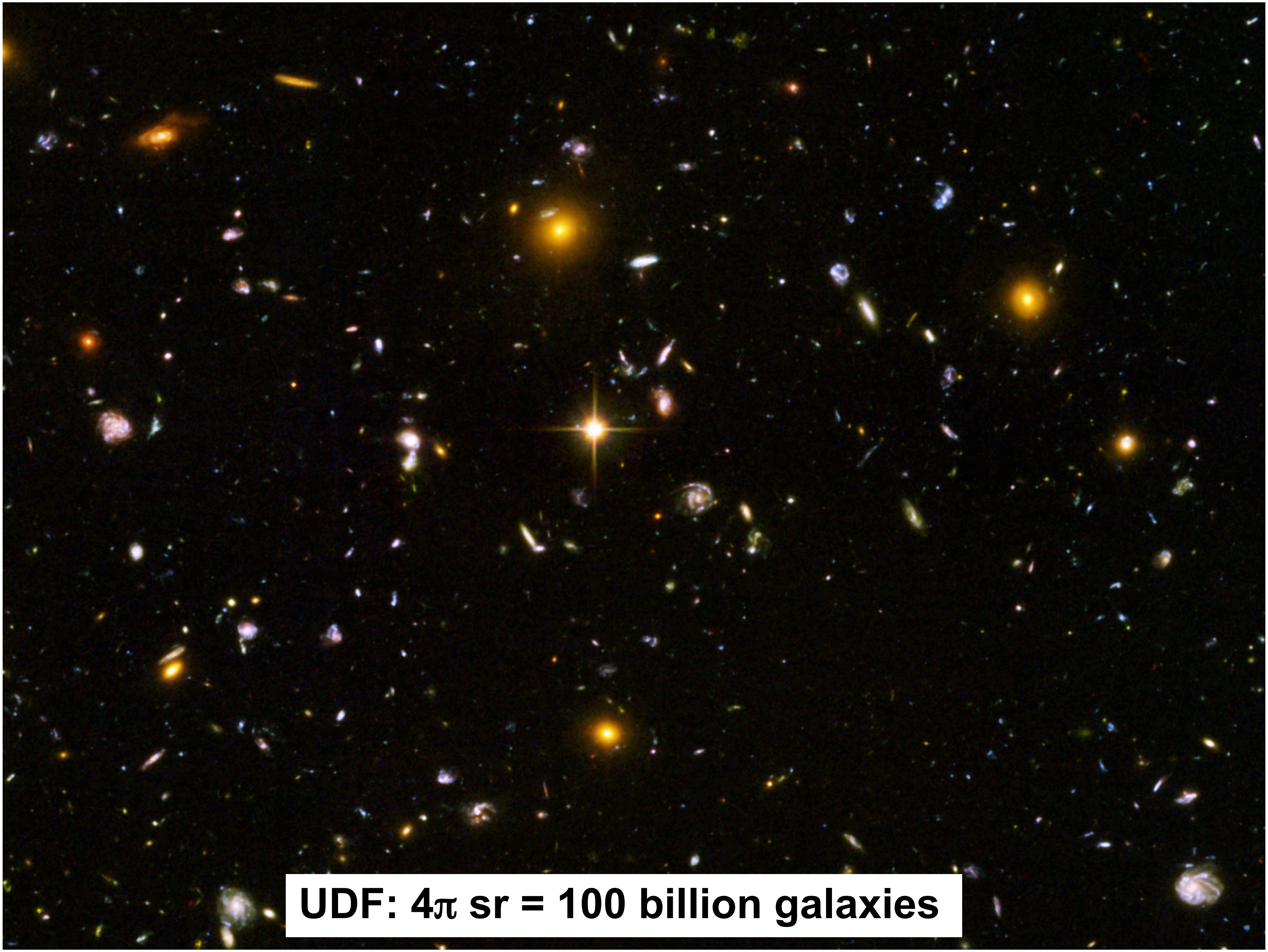
UDF: 4π sr = 100 billion galaxies

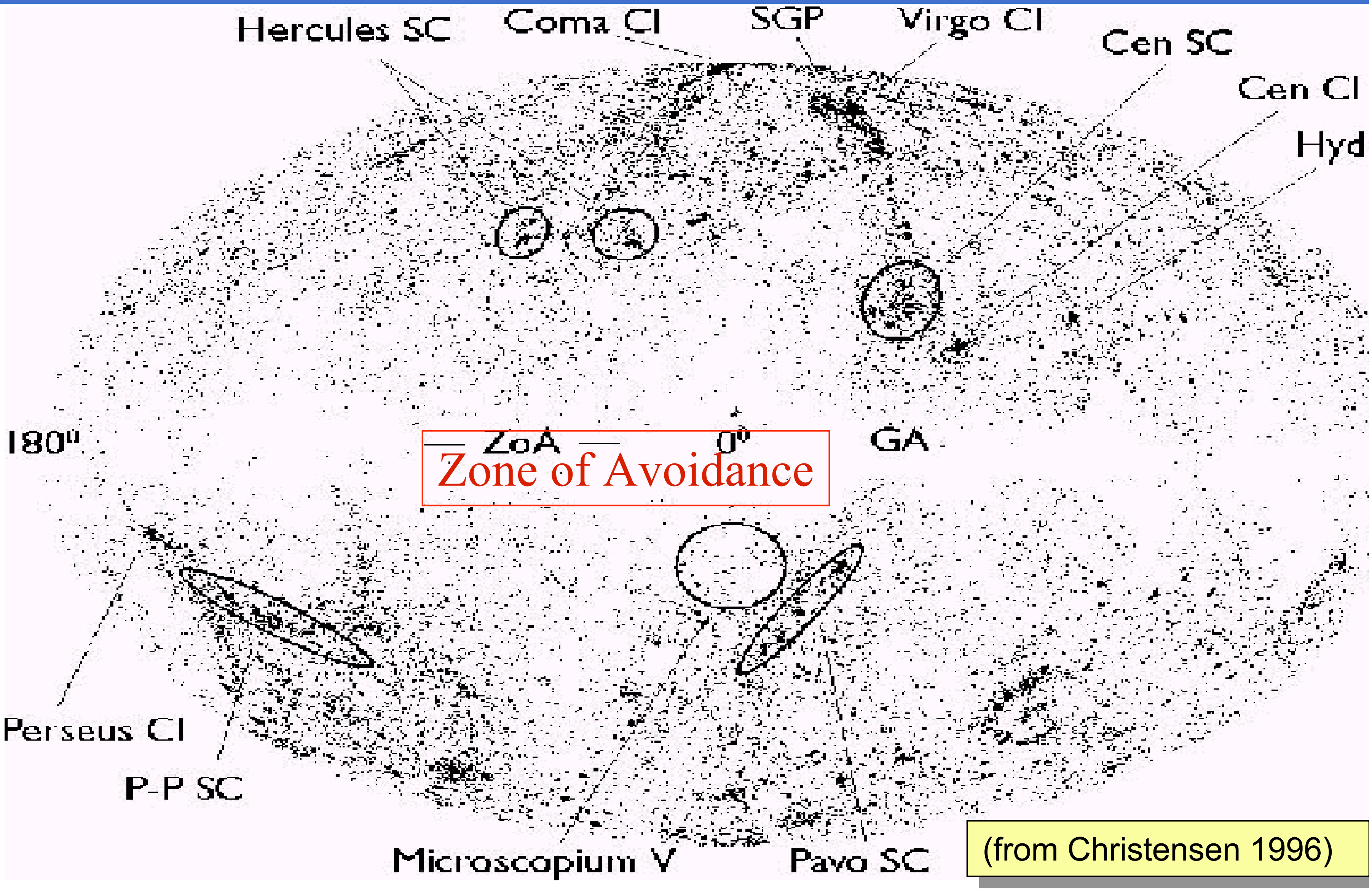

(from Christensen 1996)

Maps of the Galactic extinction

White is misty (opaque), black is transparent

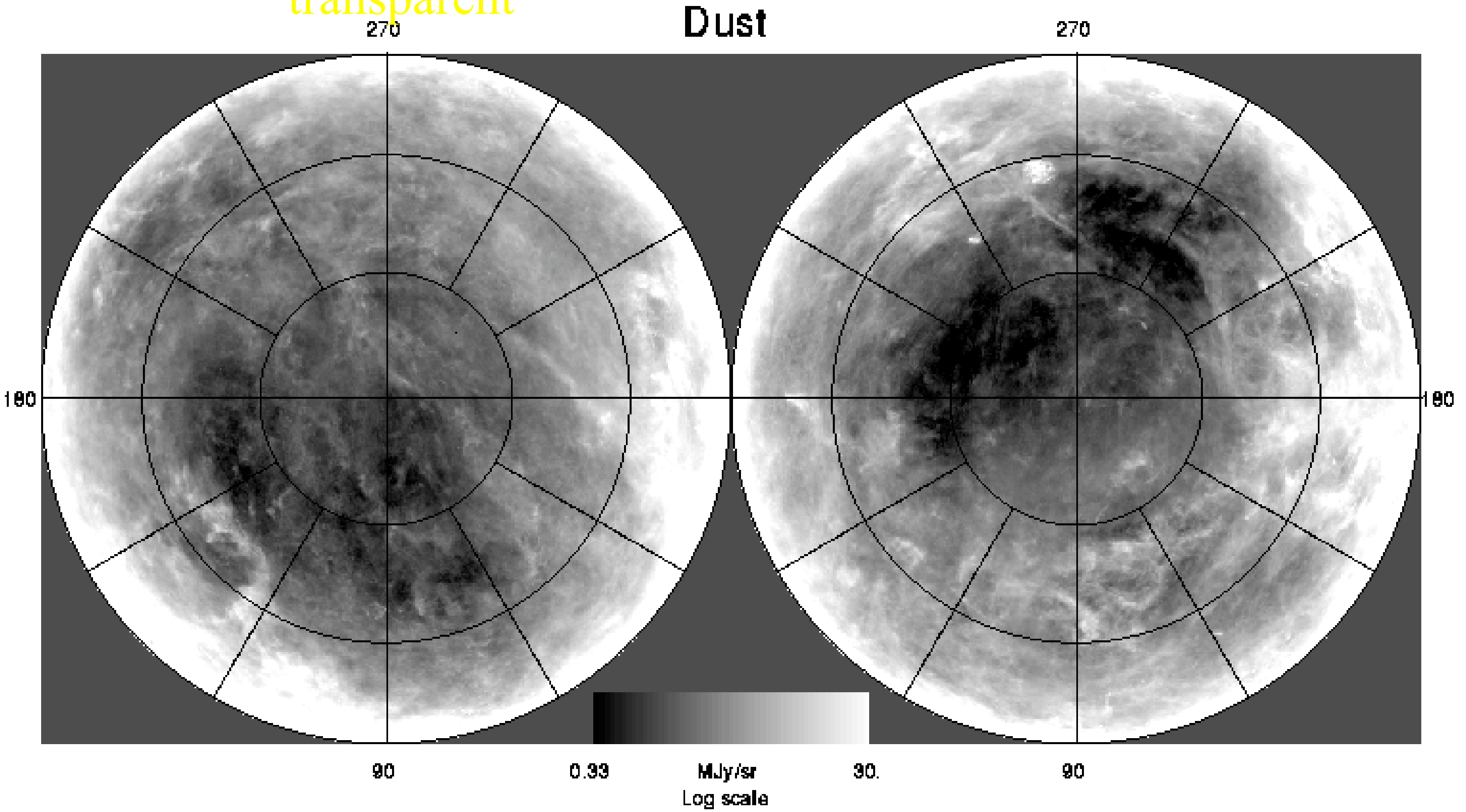

Coutersy of D. Schlegel, D. Finkbeiner, A. Kriegel, and M. Davis

J. Peacock,
JENAM '04

The distribution of the galaxies

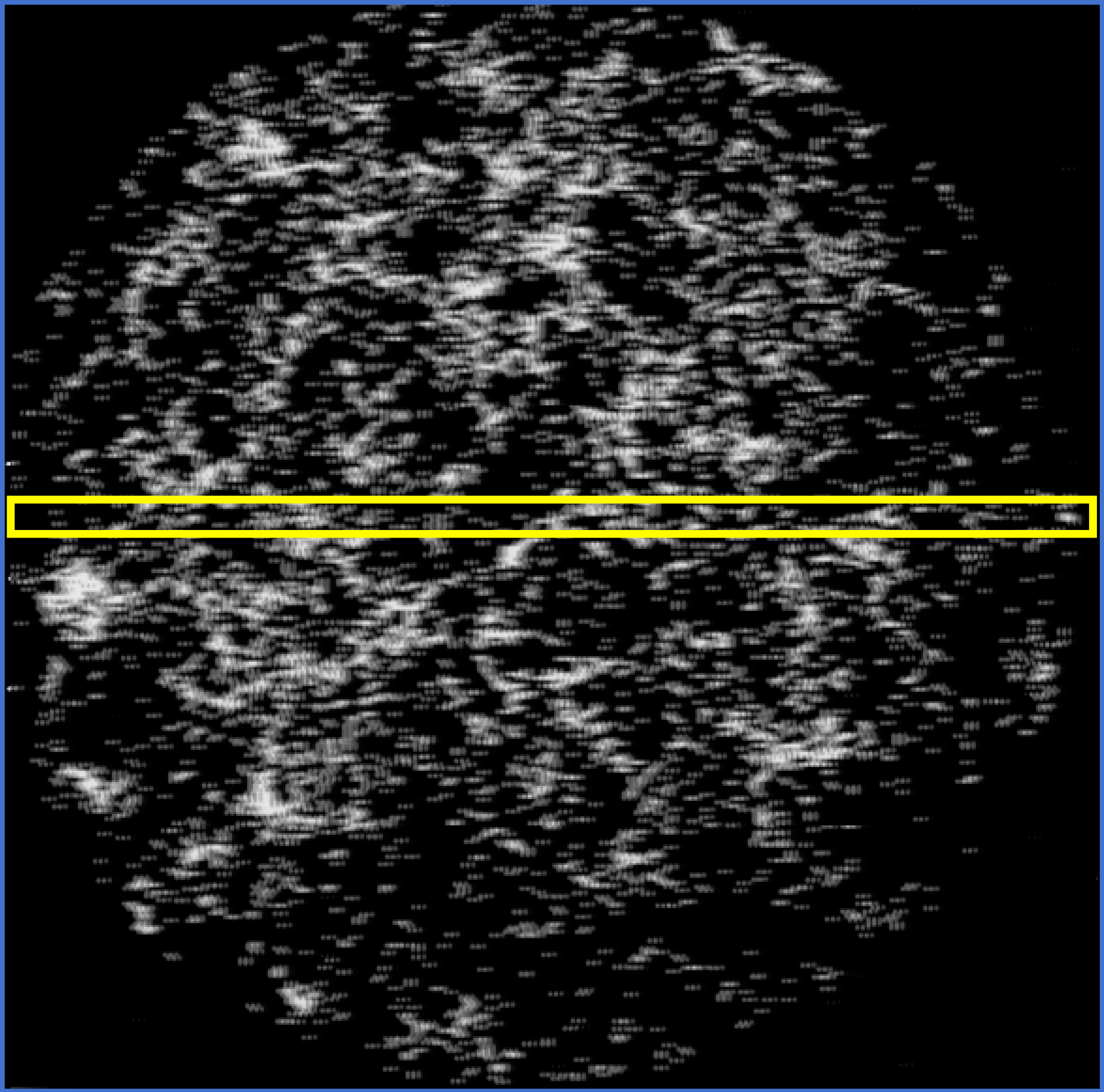

1930s:

Non-Poisson (Hubble)

1950s:

Shane & Wirtanen spend 10 years counting 1,000,000 galaxies by eye

- filamentary patterns?

1980s:

Take a strip and get redshifts

Mapping the Universe

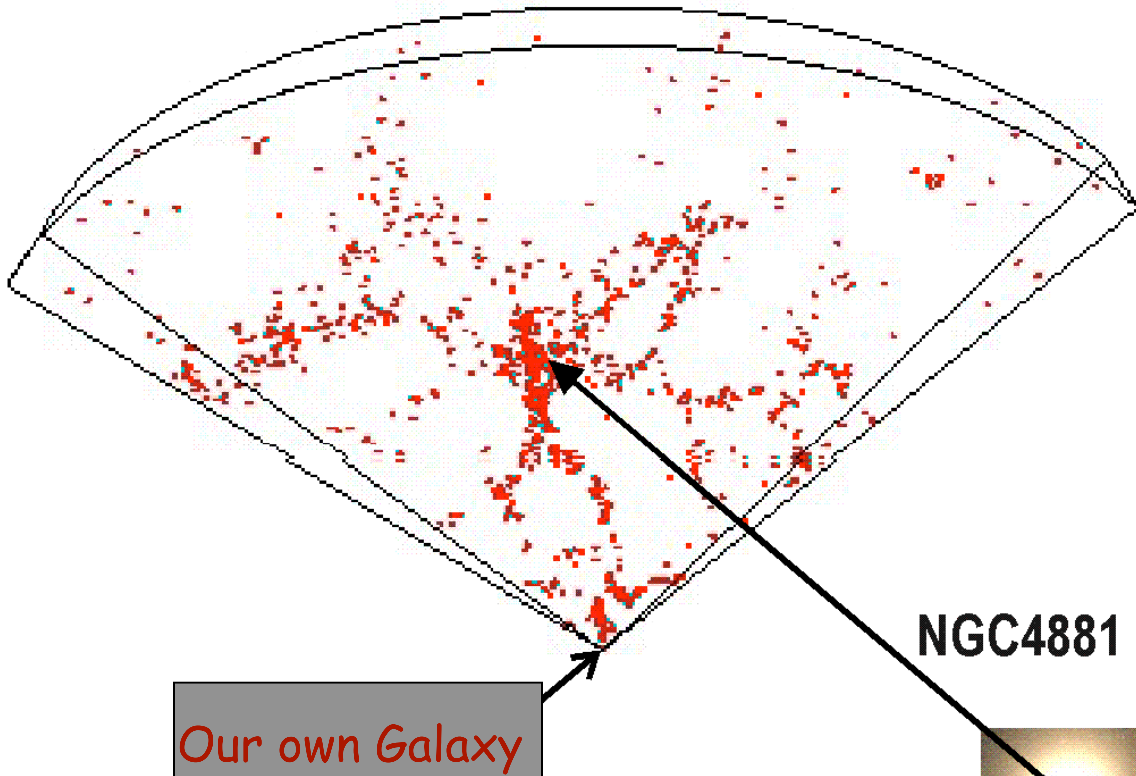

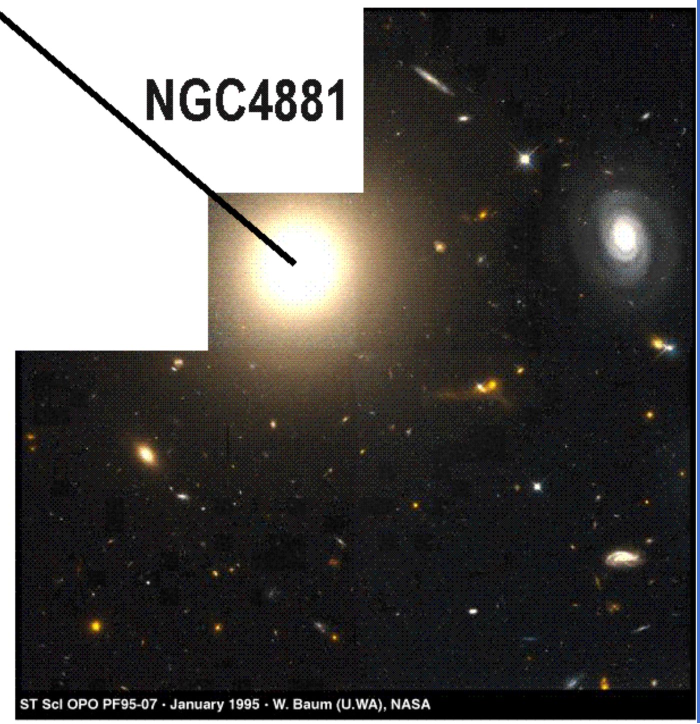

de Lapparent, Geller, and Huchra
(1986), ApJ, 302, L1

Cosmological Distances

D_l : luminosity distance

D_m : Mattig distance

D_a : angular diameter distance

r : comoving distance

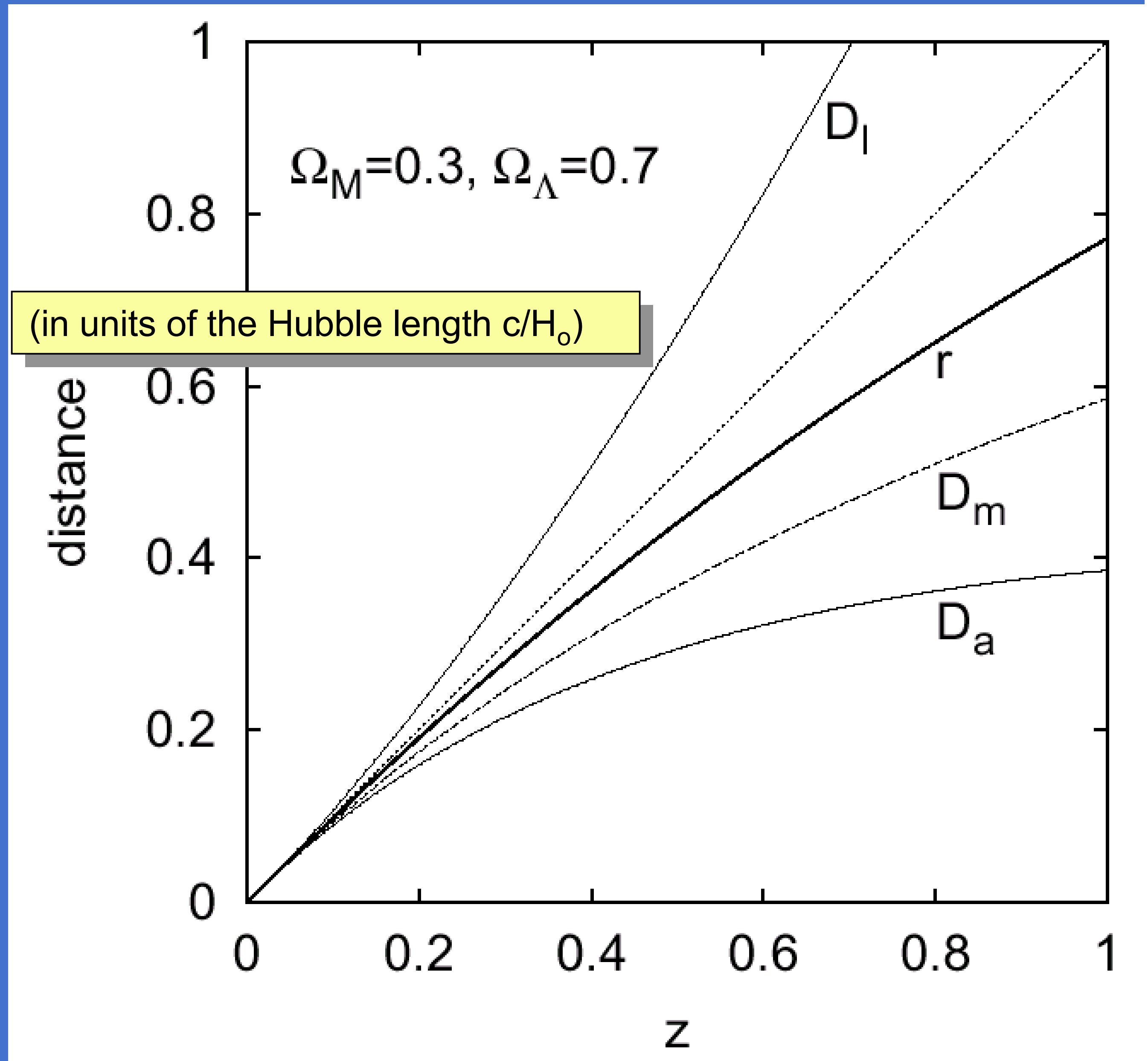

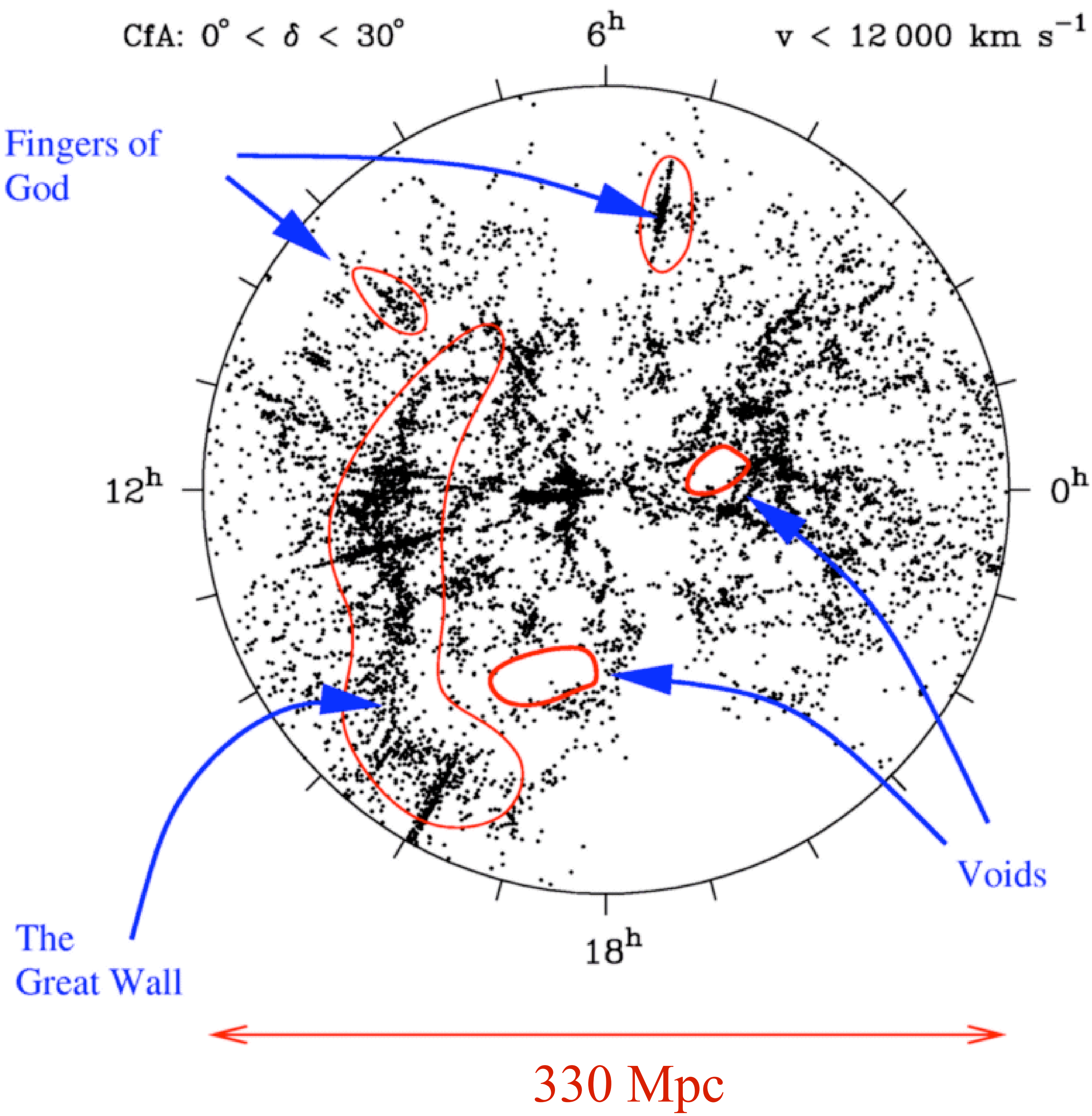

J. Peacock, JENAM '04

Redshift surveys (mid-1980s)

Inverting $v = cz = Hd$ gives an approximate distance.

Applied to galaxies on a strip on the sky, gives a 'slice of the universe'

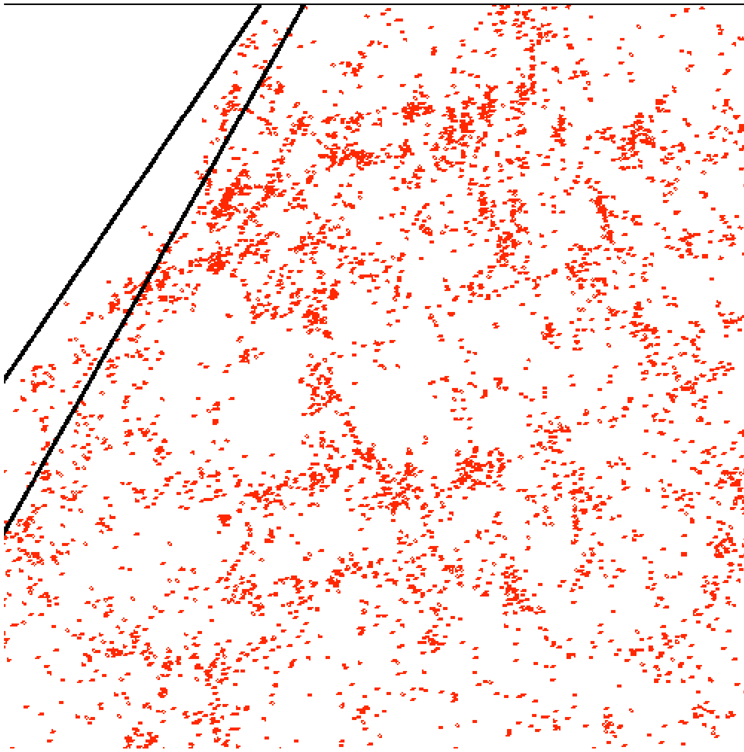

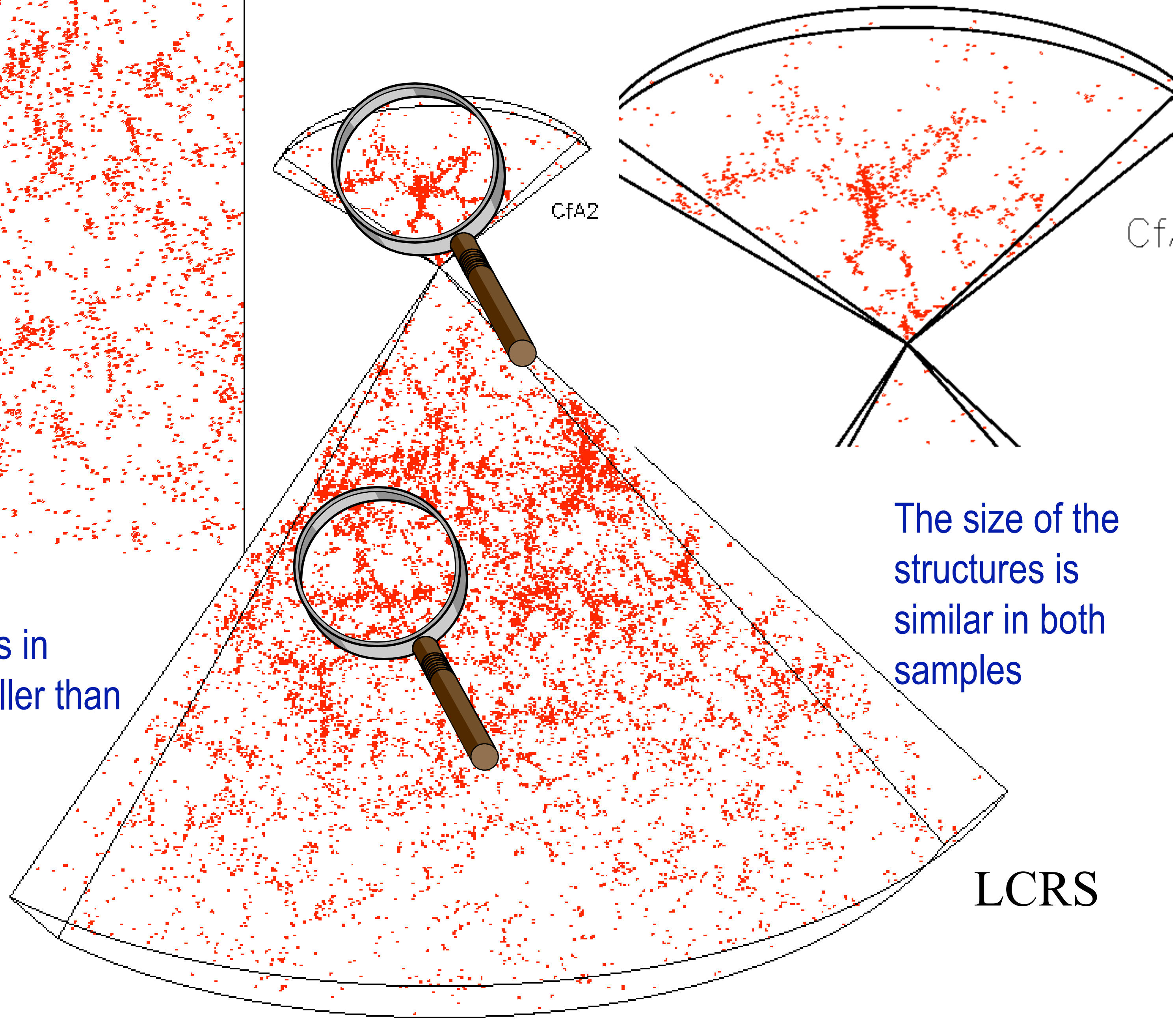

The largest structures in LCRS are much smaller than the survey size

The size of the structures is similar in both samples

“ The beginning of the end” or “the end of greatness” ...R. Kirshner

2dFGRS input catalogue from UKST/APM

- Galaxies: $b_J \leq 19.45$ from revised APM

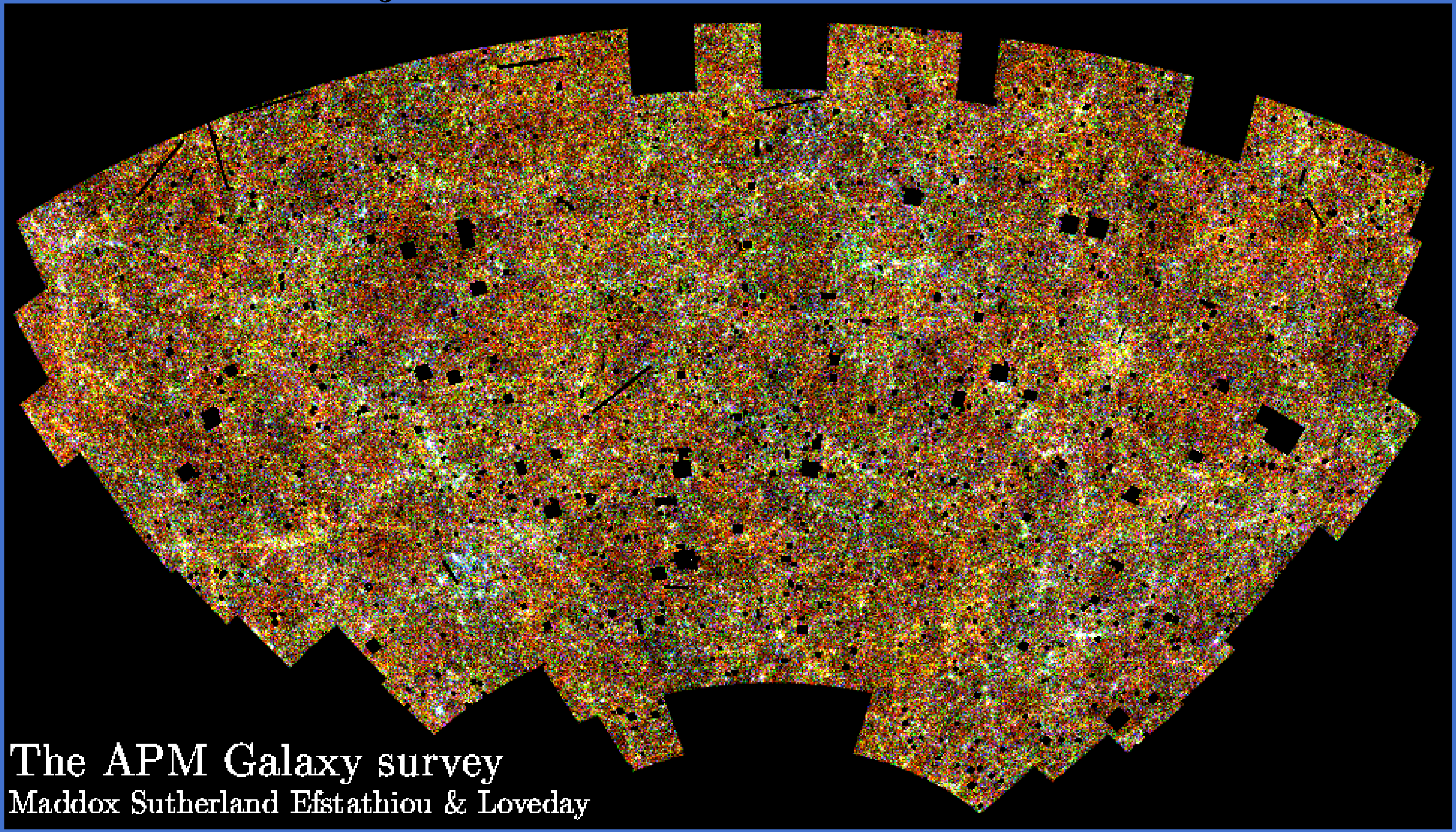

- Total area on sky ~ 2000 deg^2
- 250,000 galaxies in total, 93% sampling rate
- Mean redshift <z> ~ 0.1, almost all with z < 0.3

J. Peacock, JENAM '04

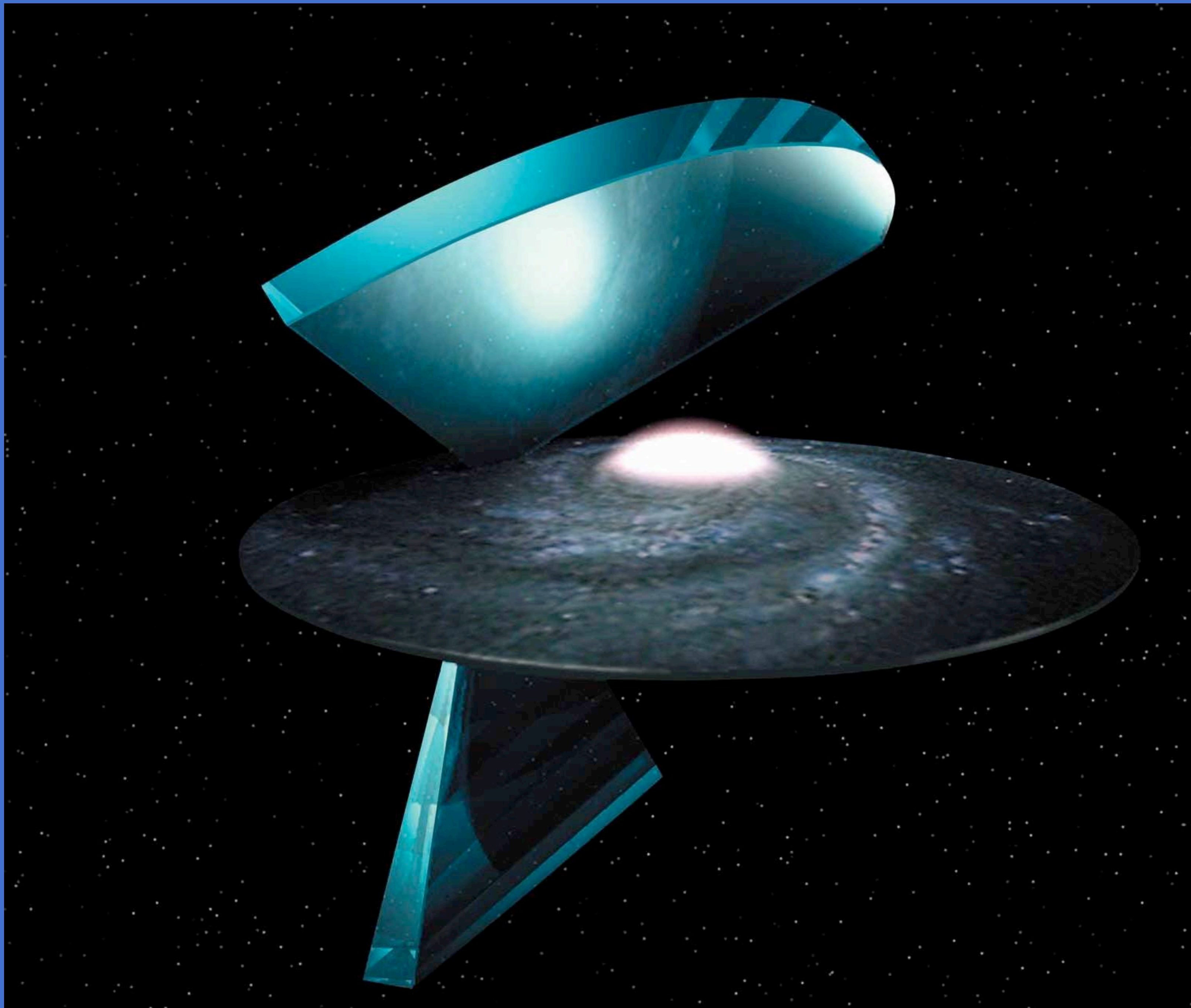

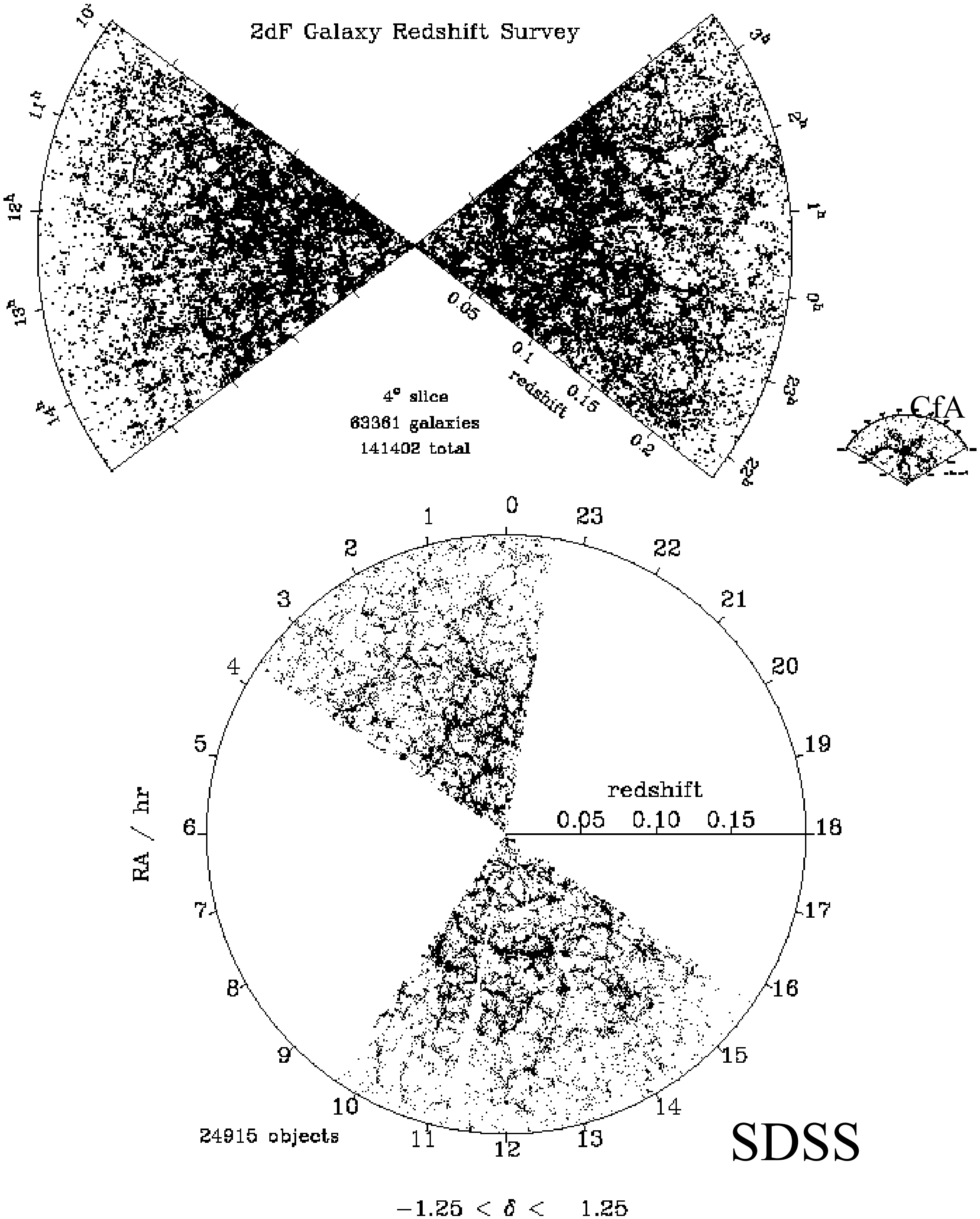

2dF Galaxy Redshift Survey
4° slice
63361 galaxies
141402 total
redshift
CfA
RA / hr
redshift
0.05 0.10 0.15
24915 objects
SDSS
−1.25 < δ < 1.25

A volume-limited sample:

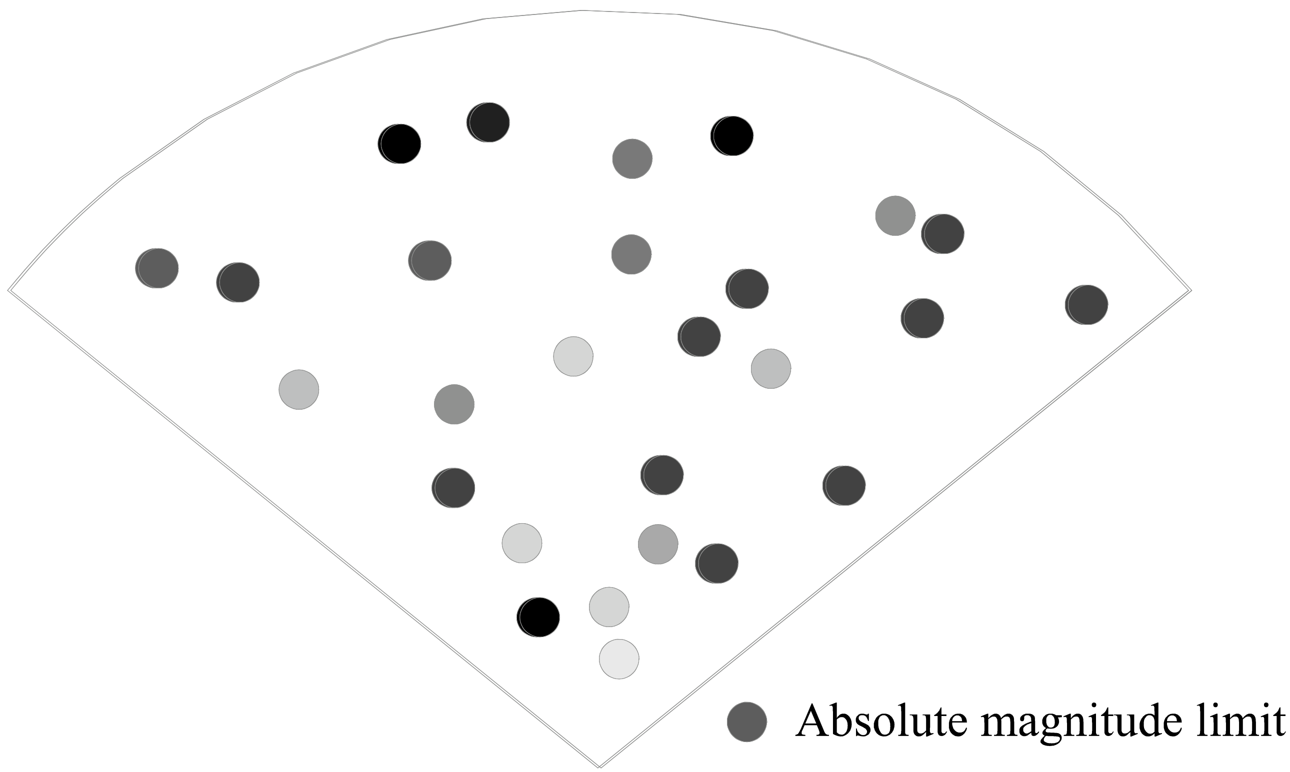

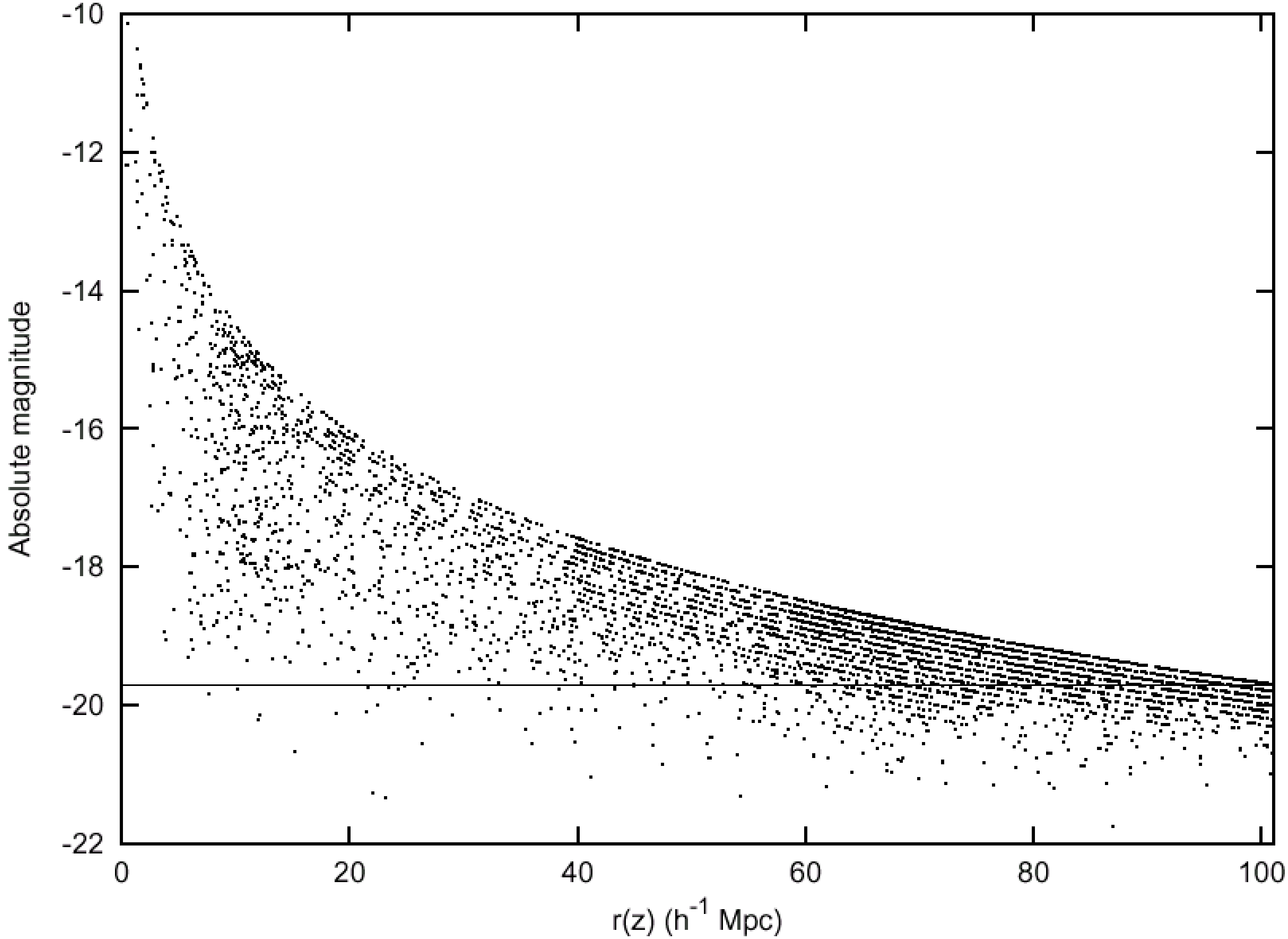

-10
-12
-14
-16
-18
-20
-22
Absolute magnitude
0
20
40
60
80
100
r(z) (h^-1 Mpc)

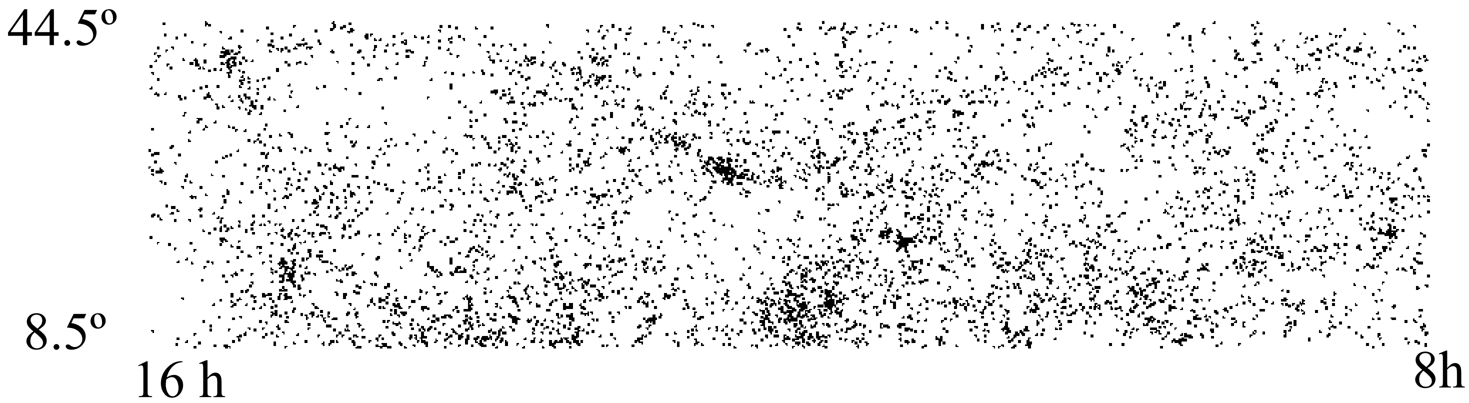

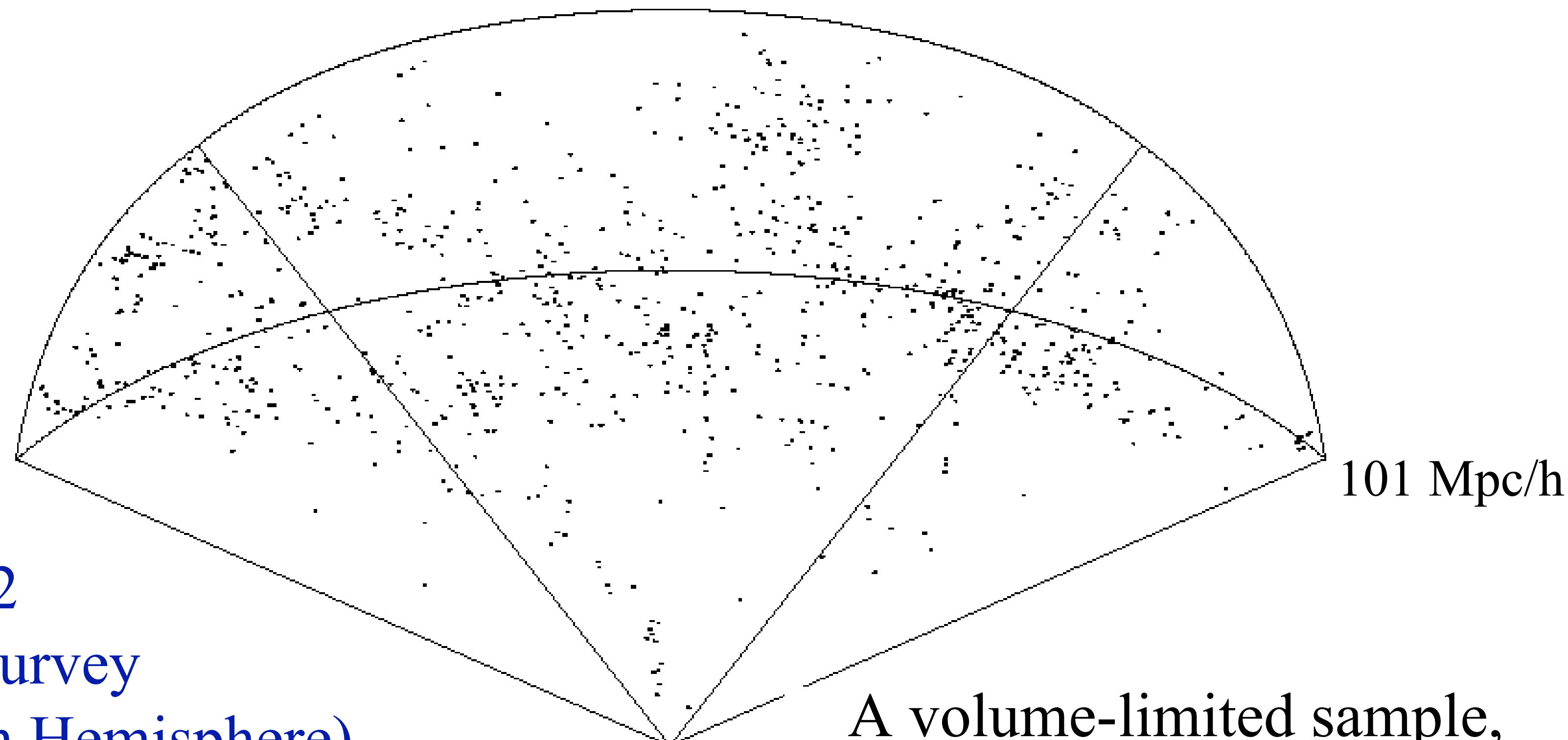

The CfA2 redshift survey (Northern Hemisphere)

A volume-limited sample,
$M < 15.5 - 5\log(D(z)) - 25 - Kz$
N = 905 galaxies

2dFGRS (Southern slice, volume limited sample)

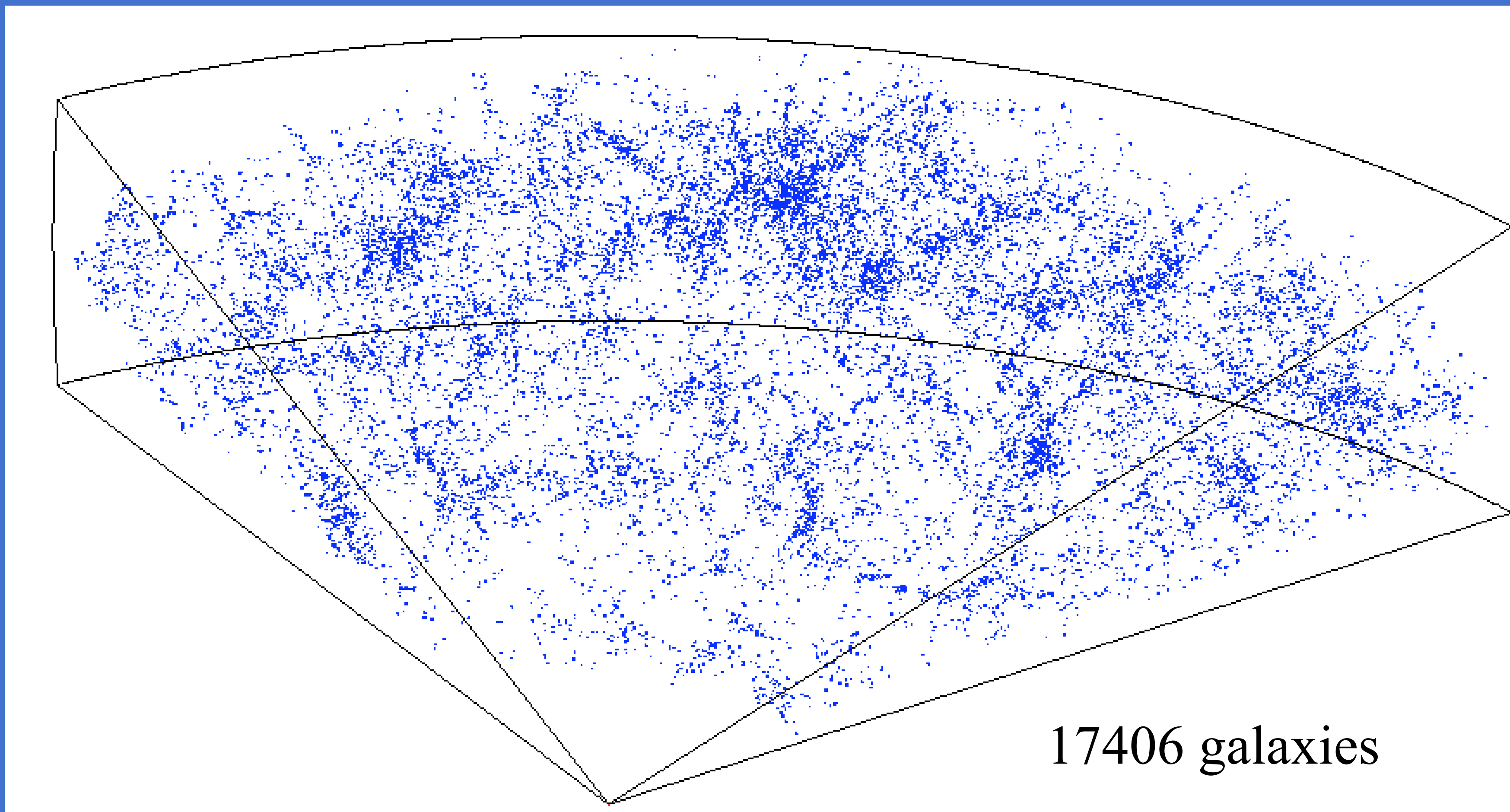

$$v_r = H_0 d + v_p$$

Velocity distortions can be severe:

They can expand a cluster in redshift space in the radial direction five-ten times.

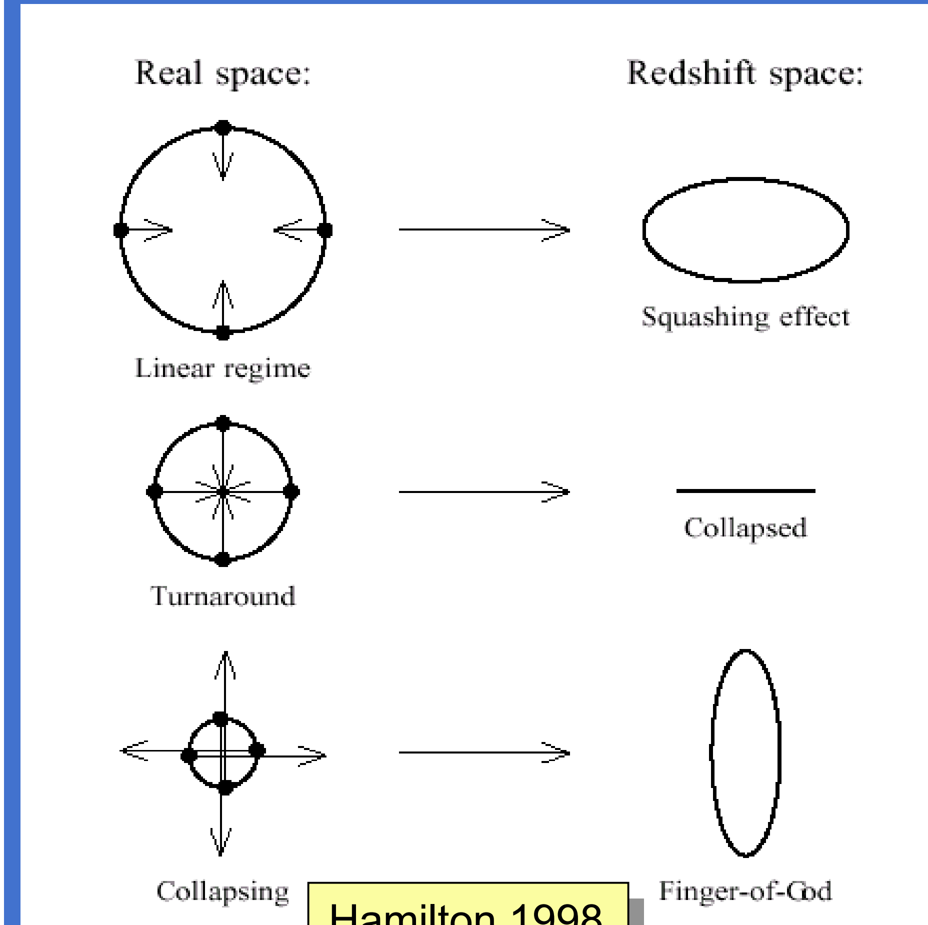

Hamilton 1998

Fingers-of-God are elongated structures caused by a large radial velocity dispersion in rich galaxy clusters.

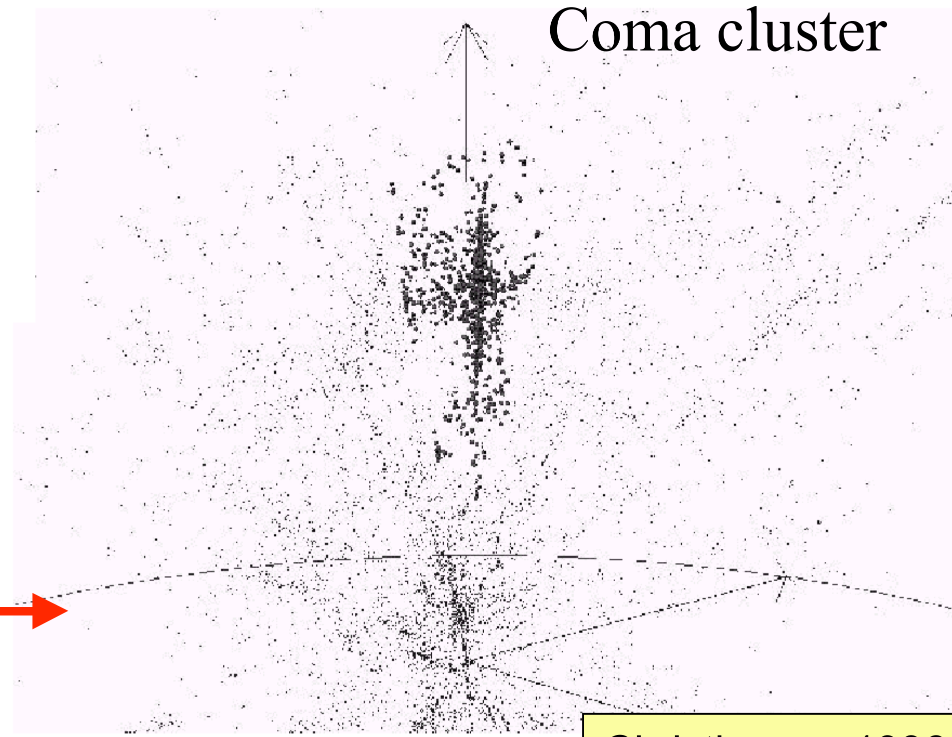

Christiansen 1996

Finger-of-God compression

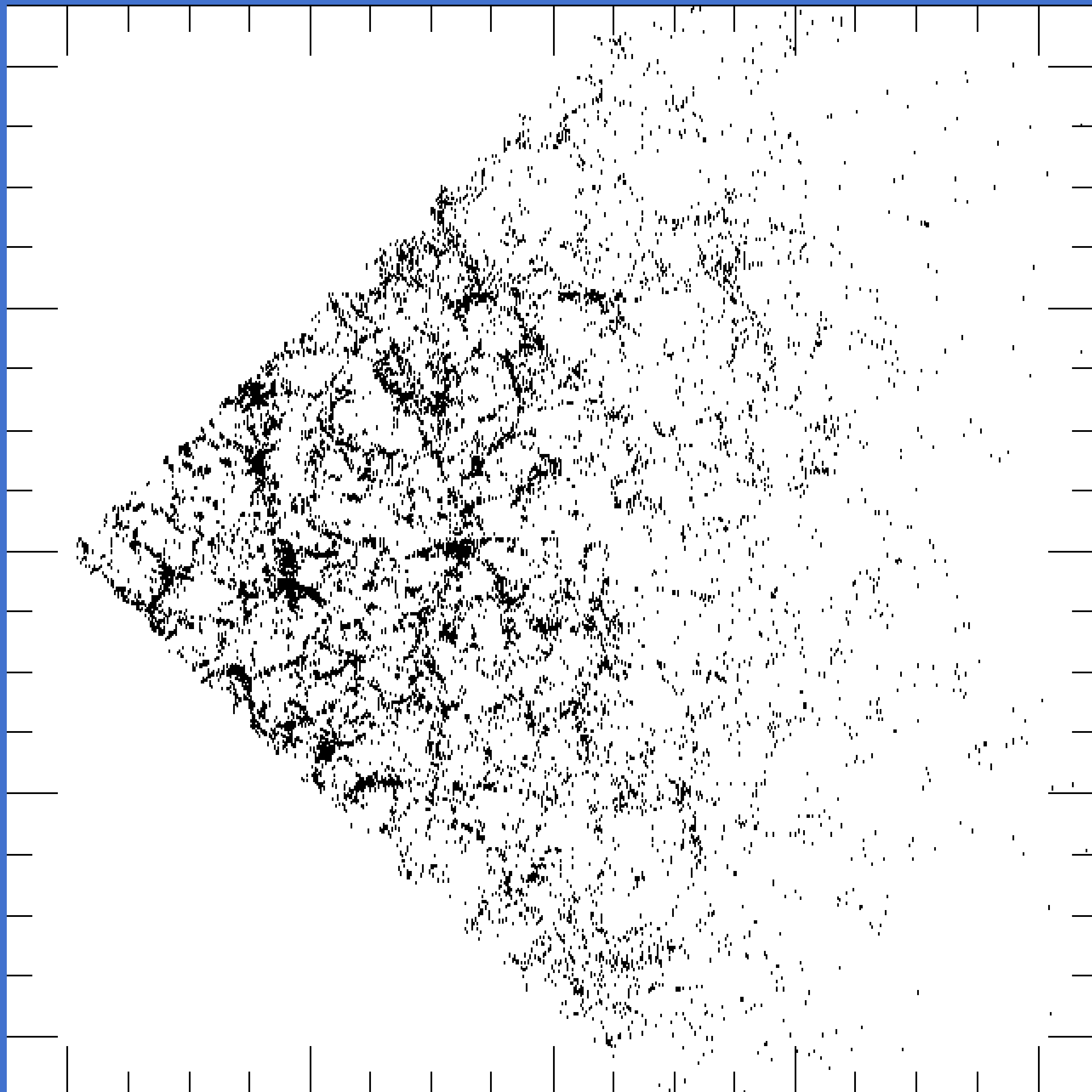

15,055 Galaxies in the 2° southern slice of the 2dF redshift survey (1st public release)

(Tegmark, Hamilton, and Xu astro-ph/0111575)

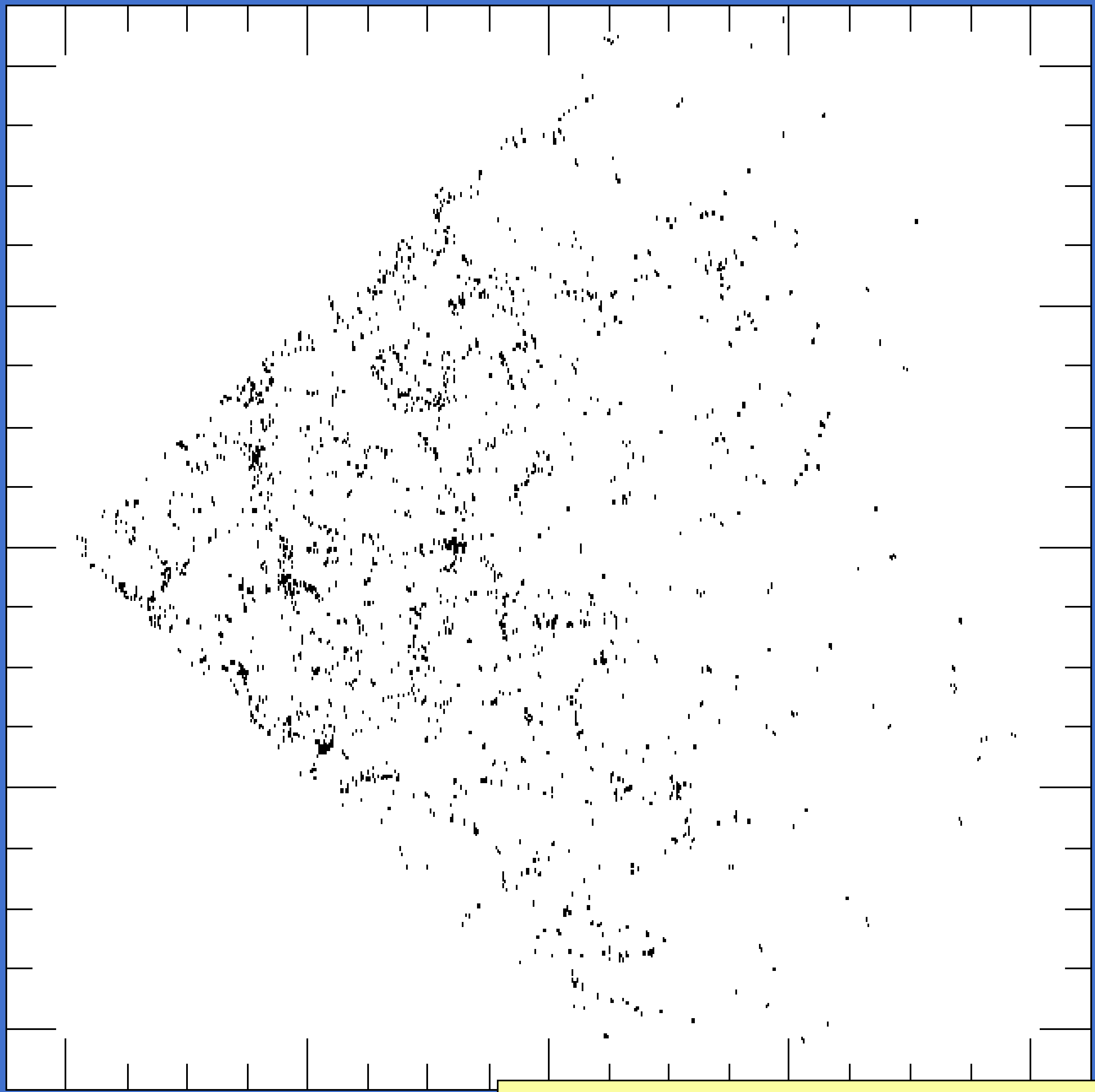

The same galaxies after the FOG effect removal

(Tegmark, Hamilton, and Xu astro-ph/0111575)

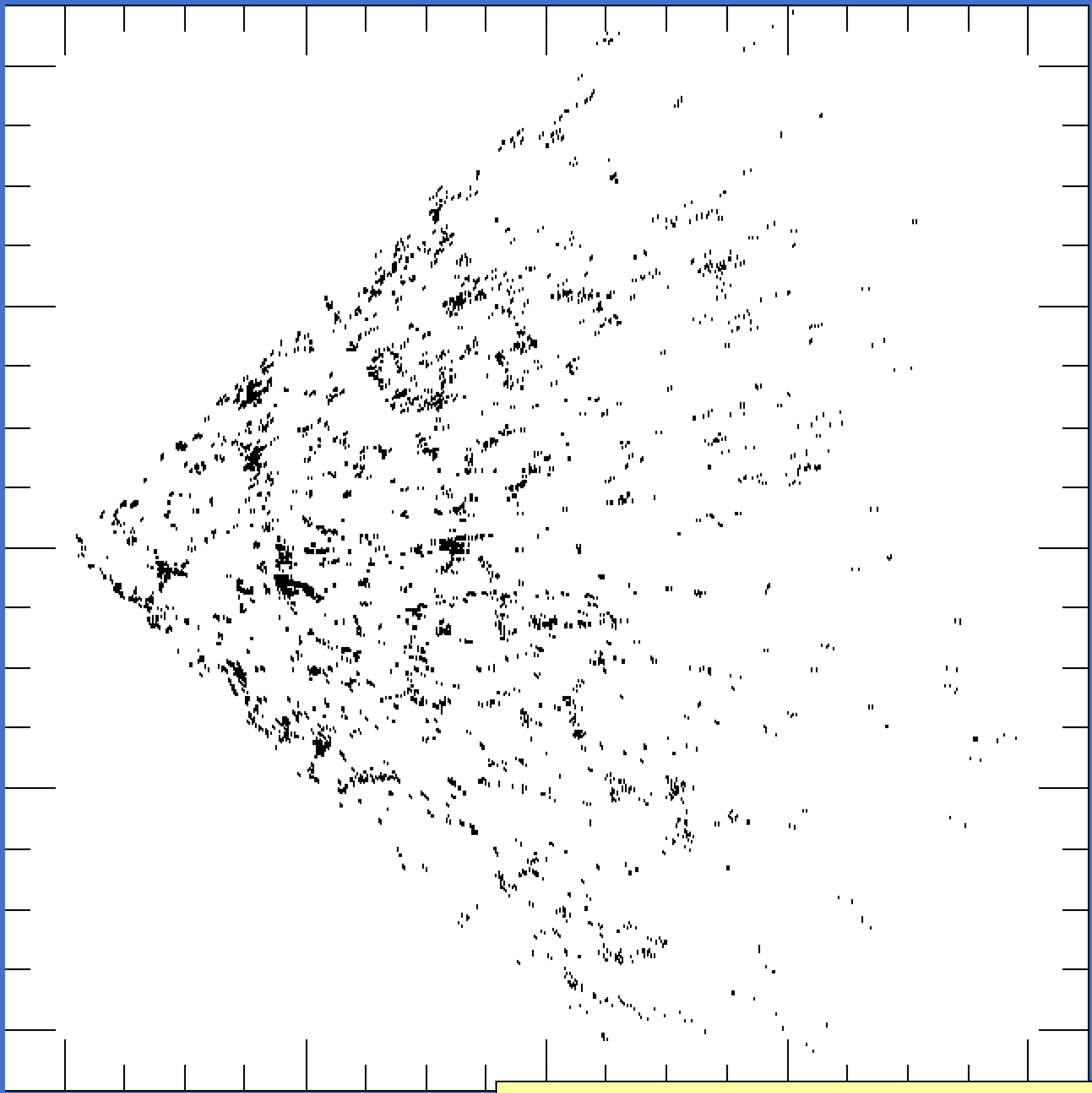

6,211 galaxies belong to a FOG (according to a given density threshold)

(Tegmark, Hamilton, and Xu astro-ph/0111575)

Simulating structure formation: collisionless dark matter

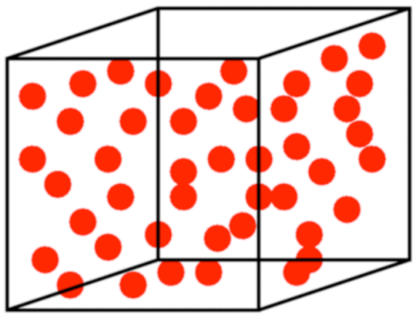

Use a supercomputer to follow the trajectories of 10 million - 1 billion imaginary particles

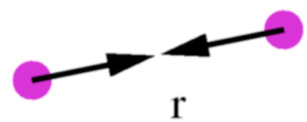

$$F = \frac{G\,m\,m}{r^2}$$

VIRGO

The Virgo consortium uses Cray, SUN & IBM supercomputers (up to 512 processors) in Edinburgh, Durham & Munich to simulate the growth of cosmological structure

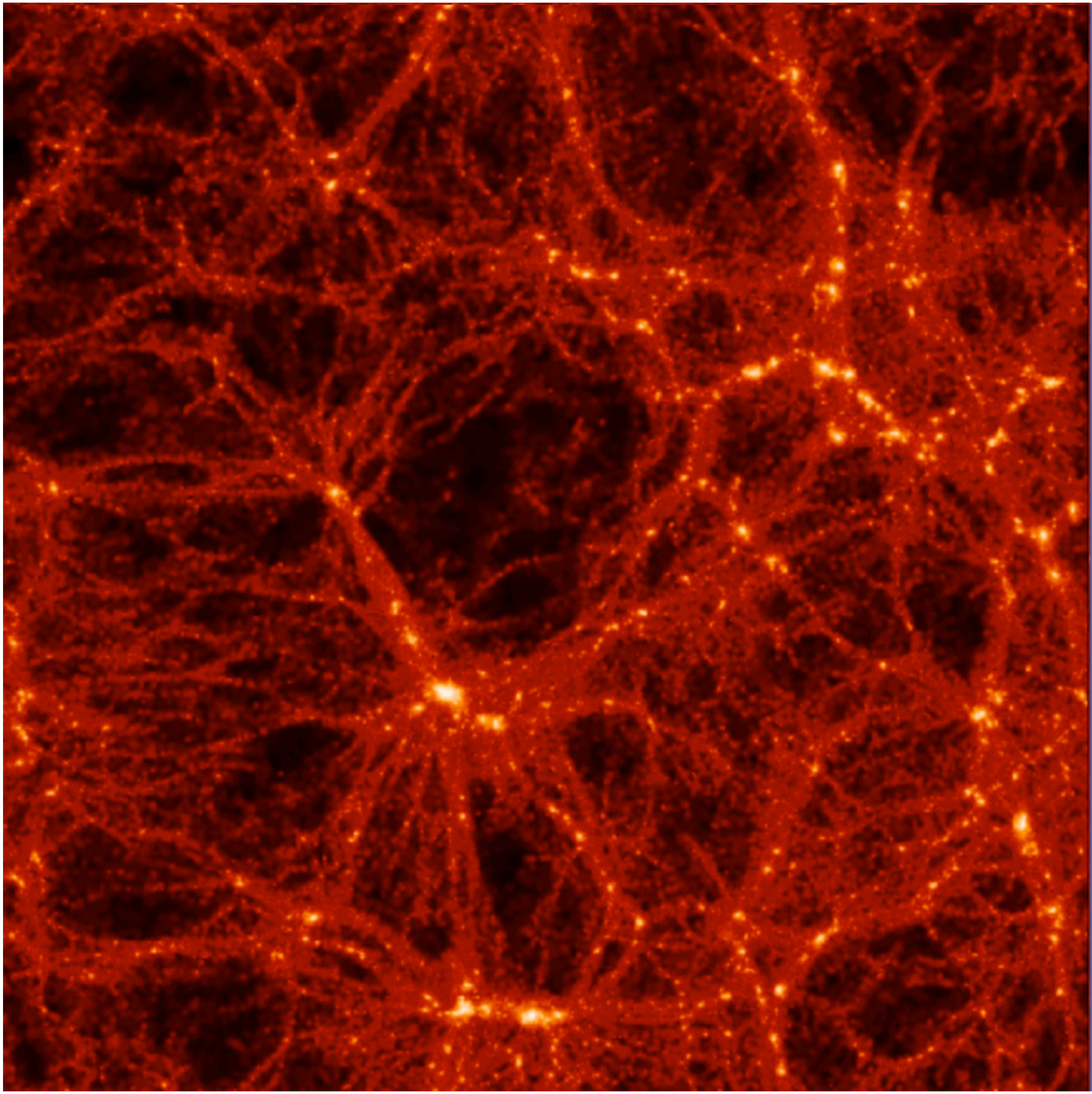

J. Peacock, JENAM ‘04

Forming superclusters (comoving view)

redshift z=3

(1/4 present size)

redshift z=1

(1/2 present size)

Redshift z=0

(today)

The dominant feature of these maps, as of all other galaxy maps of the large-scale structure of the universe, is the network of filaments of different size and contrast, along with relatively empty voids between the filaments. The filamentary network contains different scales, where smaller-scale filaments are also less prominent.

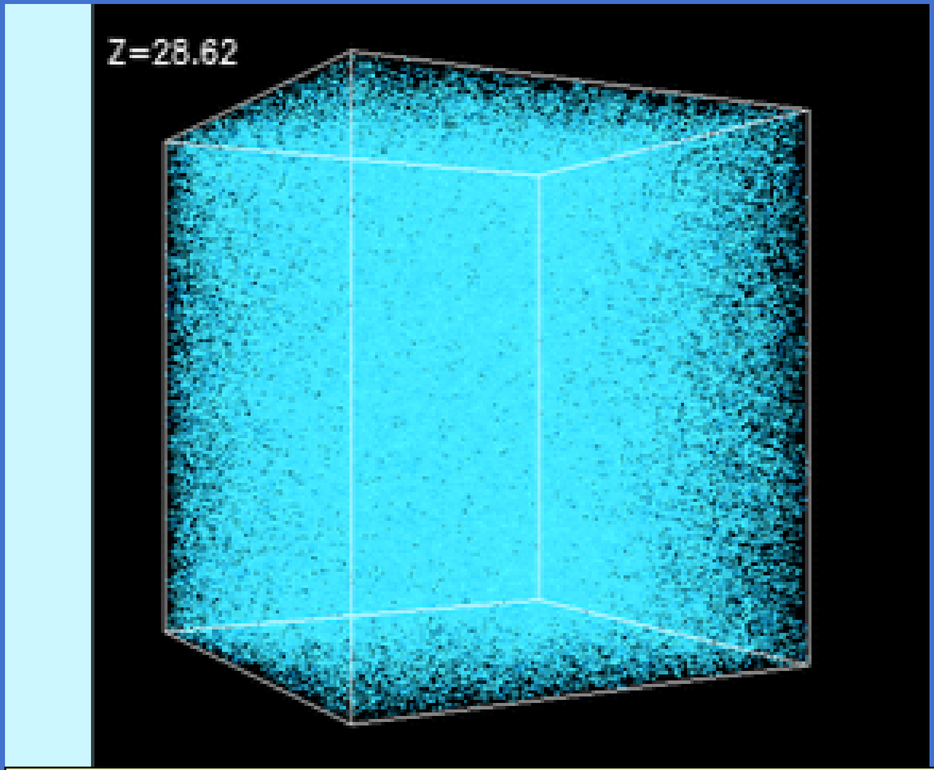

Simulation by Andrew Kravtsov and Anatoly Klypin

43 Mpc

Outline of the talk:

- Galaxies everywhere

(on the sky and in the computer)

- Second-order statistics

(correlation function and power spectrum)

"The central limit theorem asserts that a density distribution is asymptotically Gaussian in the limit where the density results from the average of many independent random processes; and a Gaussian is completely characterized by its mean and variance (the 1st and 2nd irreducible moments)".

A. Hamilton

Correlation Analysis

The two-point correlation function

- Infinitesimal interpretation:

$$dP_{12} = \bar{n}^2[1 + \xi(\mathbf{r})]dV_1 dV_2$$

is the joint probability that in each one of the two infinitesimal volumes dV_1 and dV_2, with separation vector $\mathbf{r}$, lies a galaxy.

is the average number density (intensity)

Diagram from Guzzo (2002) in *Modern Cosmology* (eds. S. Bonometto et al.)

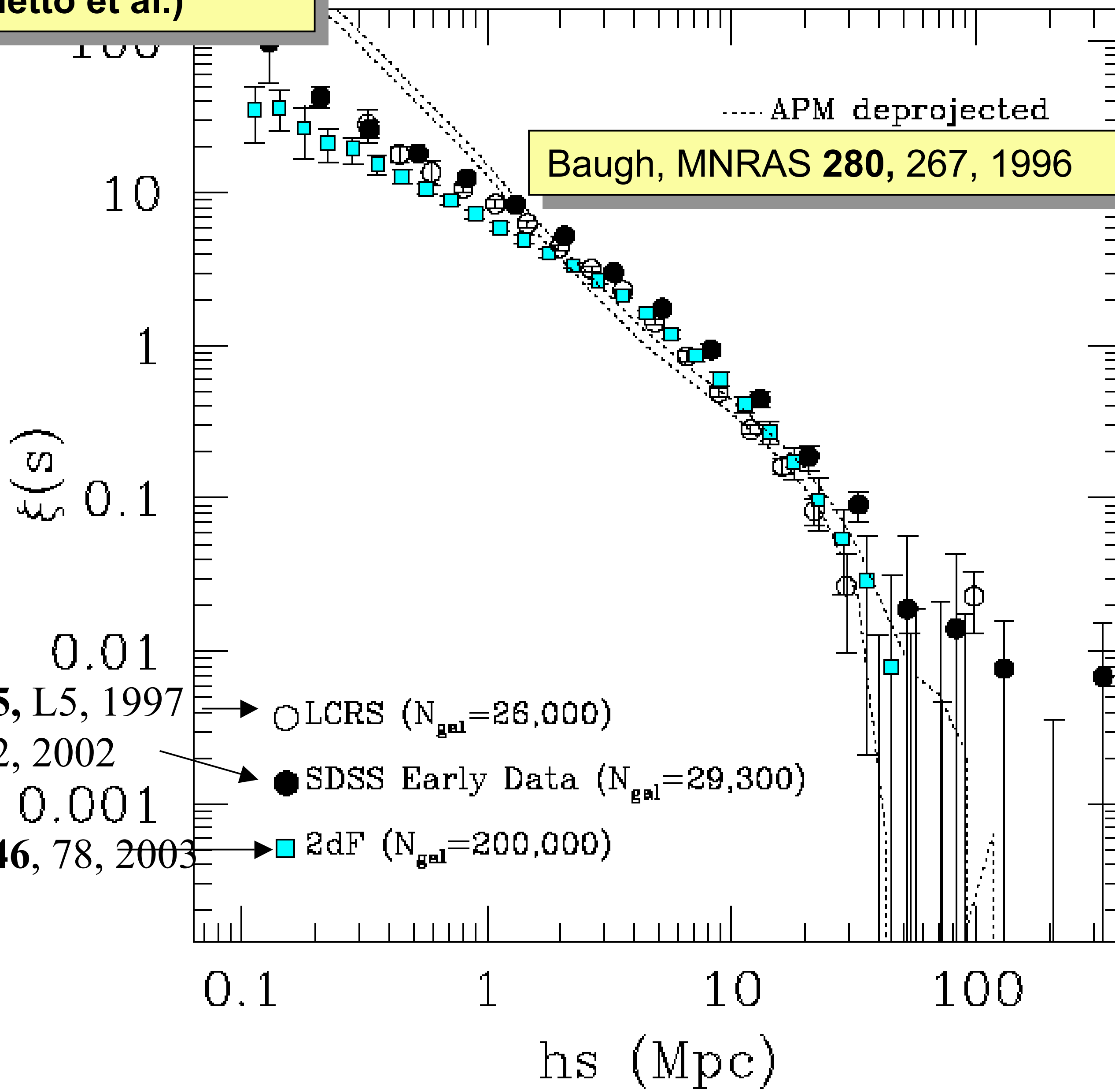

Baugh, MNRAS **280**, 267, 1996

Tucker et al., MNRAS, **285,** L5, 1997

Zehavi et al., ApJ, **571**, 172, 2002

Hawkins et al. MNRAS, **346**, 78, 2003

A segment Cox process is a simple point process with known analytical expression for the correlation function

Stoyan, Kendall, and Mecke (1995)

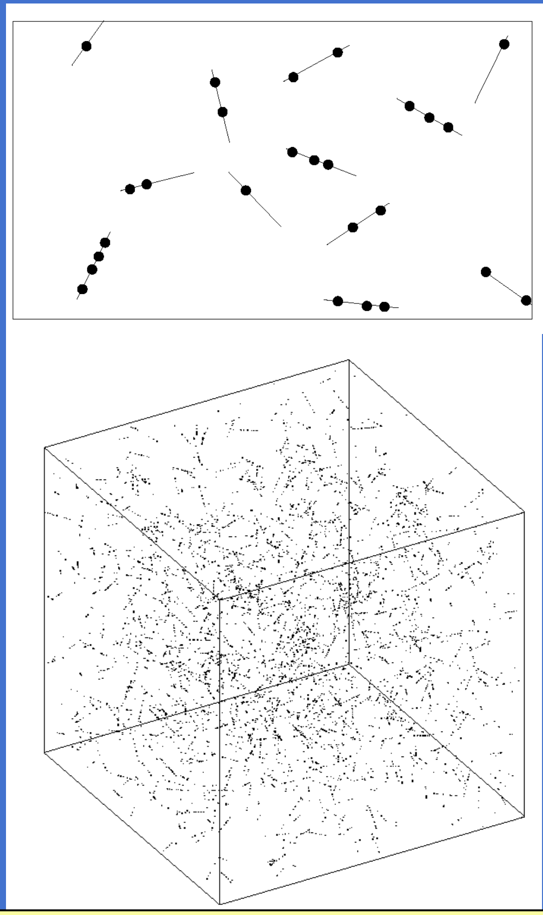

Martínez et al. (1988), MNRAS, 298, 1212

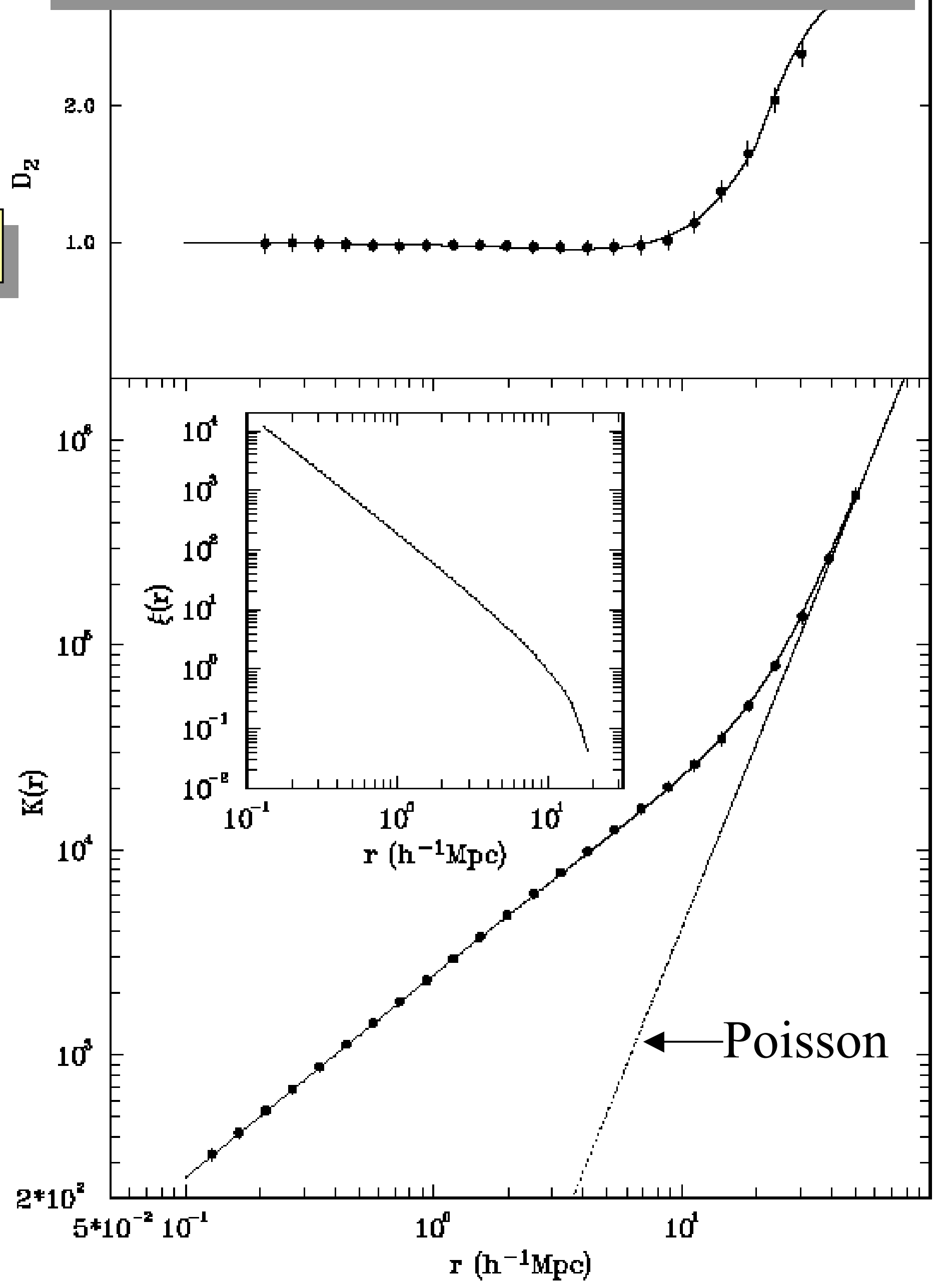

See also Stoyan (1994), Statistics **25,** 267

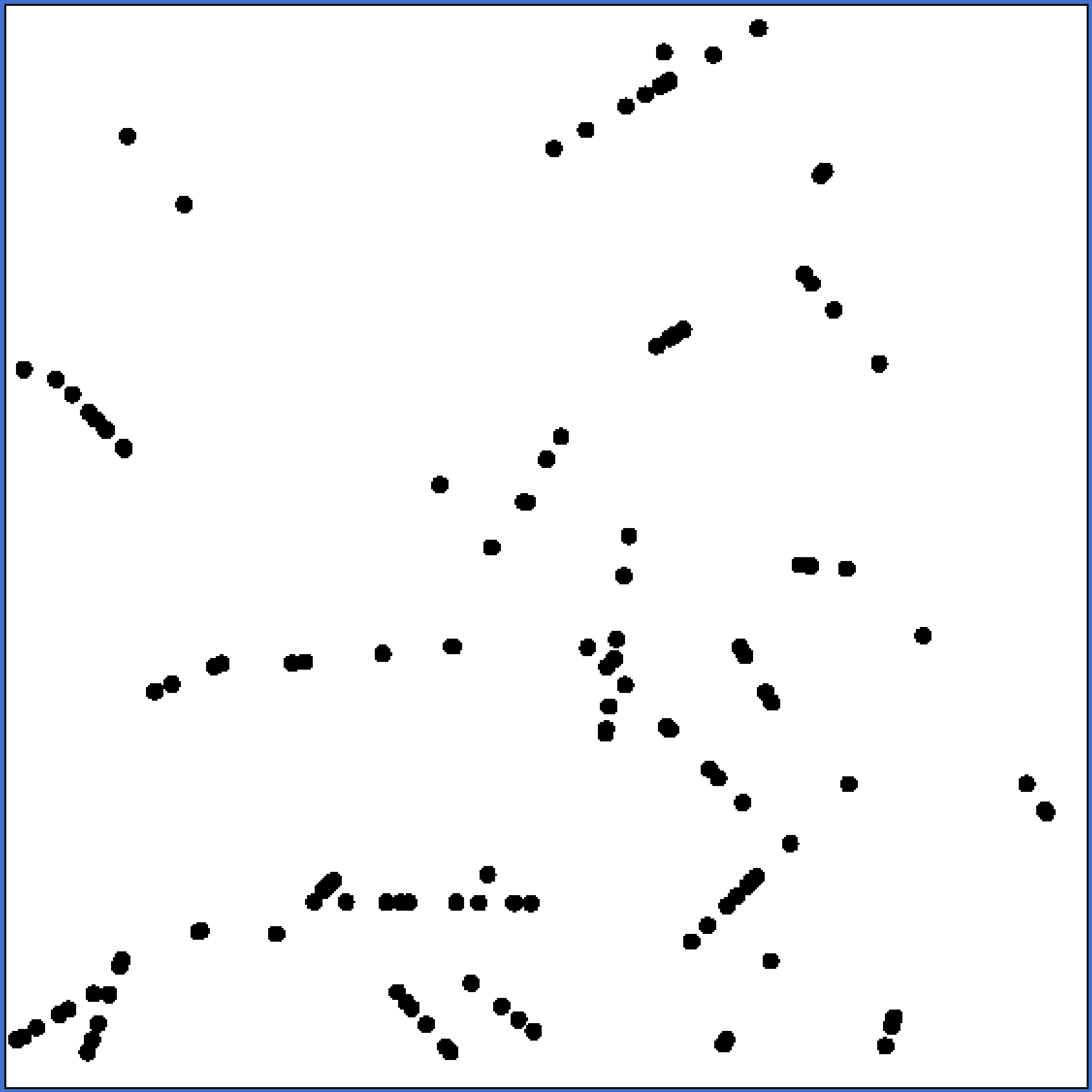

A 2-D slice of the segment Cox process

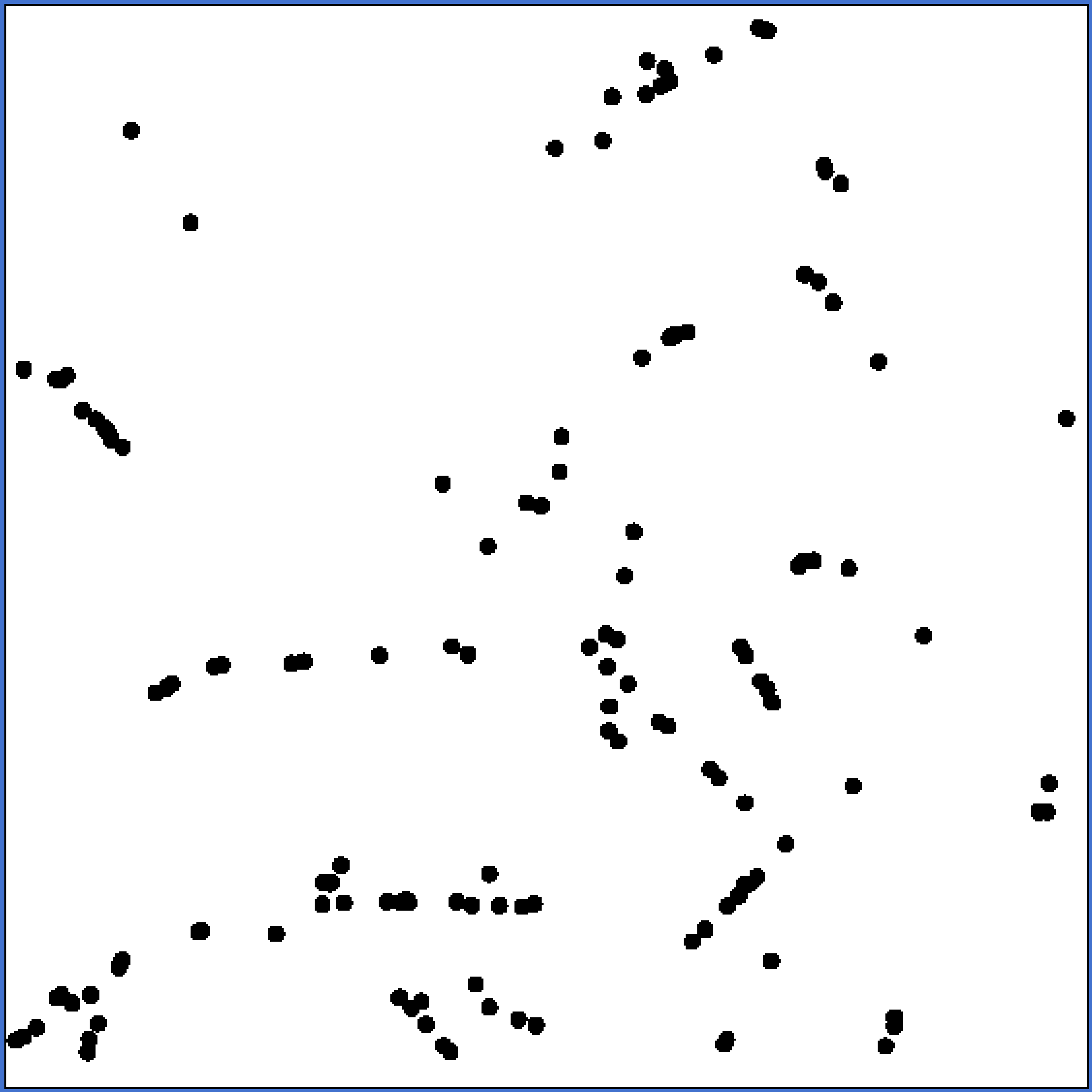

Power-law shifts

Random shifts are distributed according to a power-law density probability function $d^*(r) \propto r^\alpha$.

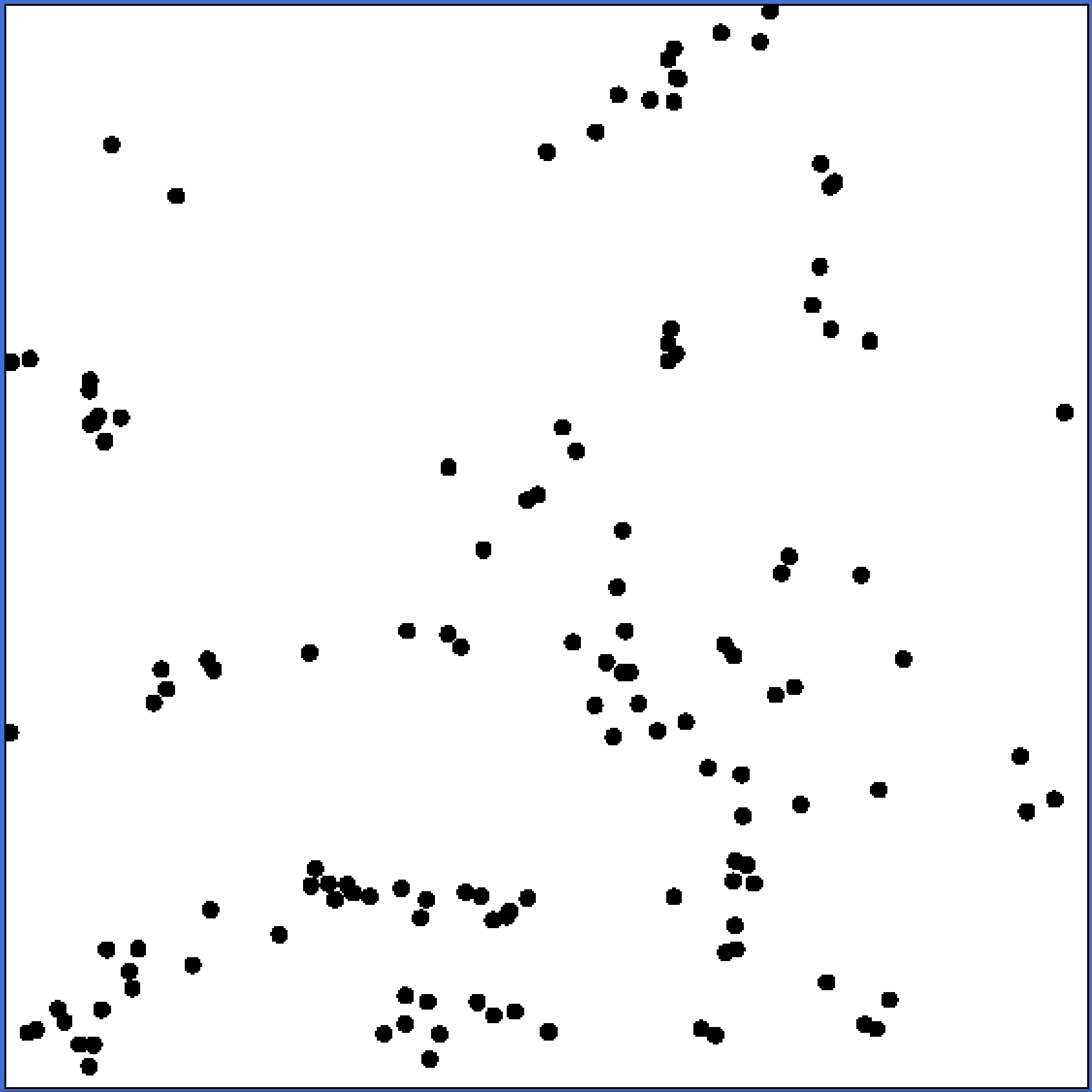

Gaussian shifts

Random shifts are performed by a three-dimensional Gaussian distributed vector with $\sigma = 0.5$.

The two-point correlation function does not describe the filamentary pattern of the galaxy distribution:

Small random displacements do not destroy the filaments but erase the small scale correlations

(Snethlage, Martínez, Stoyan & Saar, A&A 2002)

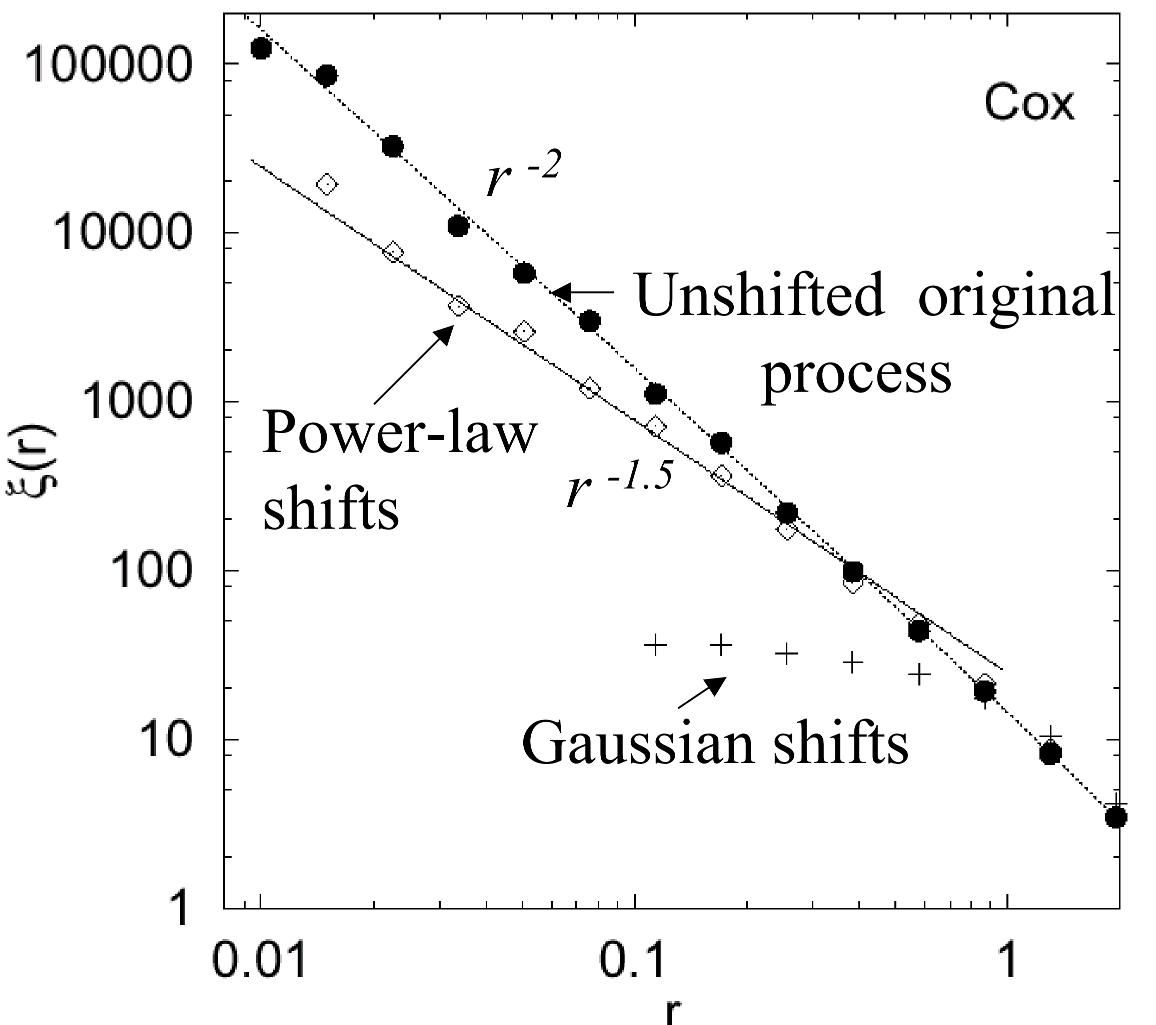

The value γ is reduced by $2(1+\alpha)$. In the example $\alpha = -0.75$ and therefore γ changes from 2 to 1.5.

Power spectrum

Real space

- Correlation function:

$$\boxed{E\left\{\rho(\mathbf{x})\rho(\mathbf{x}+\mathbf{r})\right\} = \bar{\rho}^2\left[1+\xi(\mathbf{r})\right].}$$

- Density contrast:

$$\delta(\mathbf{x}) = \frac{\rho(\mathbf{x})-\bar{\rho}}{\bar{\rho}},$$

$$E\left\{\delta(\mathbf{x})\delta(\mathbf{x}+\mathbf{r})\right\} = \xi(\mathbf{r}).$$

Fourier space (advantages)

- It is more intuitive physically, separating processes on different scales.
- Theoretical model predictions are made in terms of power spectrum.
- The amplitudes for different wavenumbers are statistically orthogonal

$$\boxed{E\left\{\tilde{\delta}(\mathbf{k})\tilde{\delta}^{\star}(\mathbf{k}')\right\} = (2\pi)^3\delta_D(\mathbf{k}-\mathbf{k}')P(\mathbf{k}).}$$

is the Fourier amplitude of the overdensity field δ at a wavenumber $\mathbf{k}$

- Power spectrum — correlation function:

$$P(\mathbf{k}) = \int \xi(\mathbf{r}) e^{i\mathbf{k}\cdot\mathbf{r}}\, d^3r,$$

Fourier transform pair

$$\xi(\mathbf{r}) = \int P(\mathbf{k}) e^{-i\mathbf{k}\cdot\mathbf{r}} \frac{d^3k}{(2\pi)^3},$$

- Isotropy:

$$\xi(r) = 4\pi \int_0^\infty P(k) \frac{\sin(kr)}{kr} \frac{k^2\, dk}{(2\pi)^3}.$$

- Delta-power:

$$\Delta^2(k) = \frac{1}{2\pi^2} P(k) k^3,$$

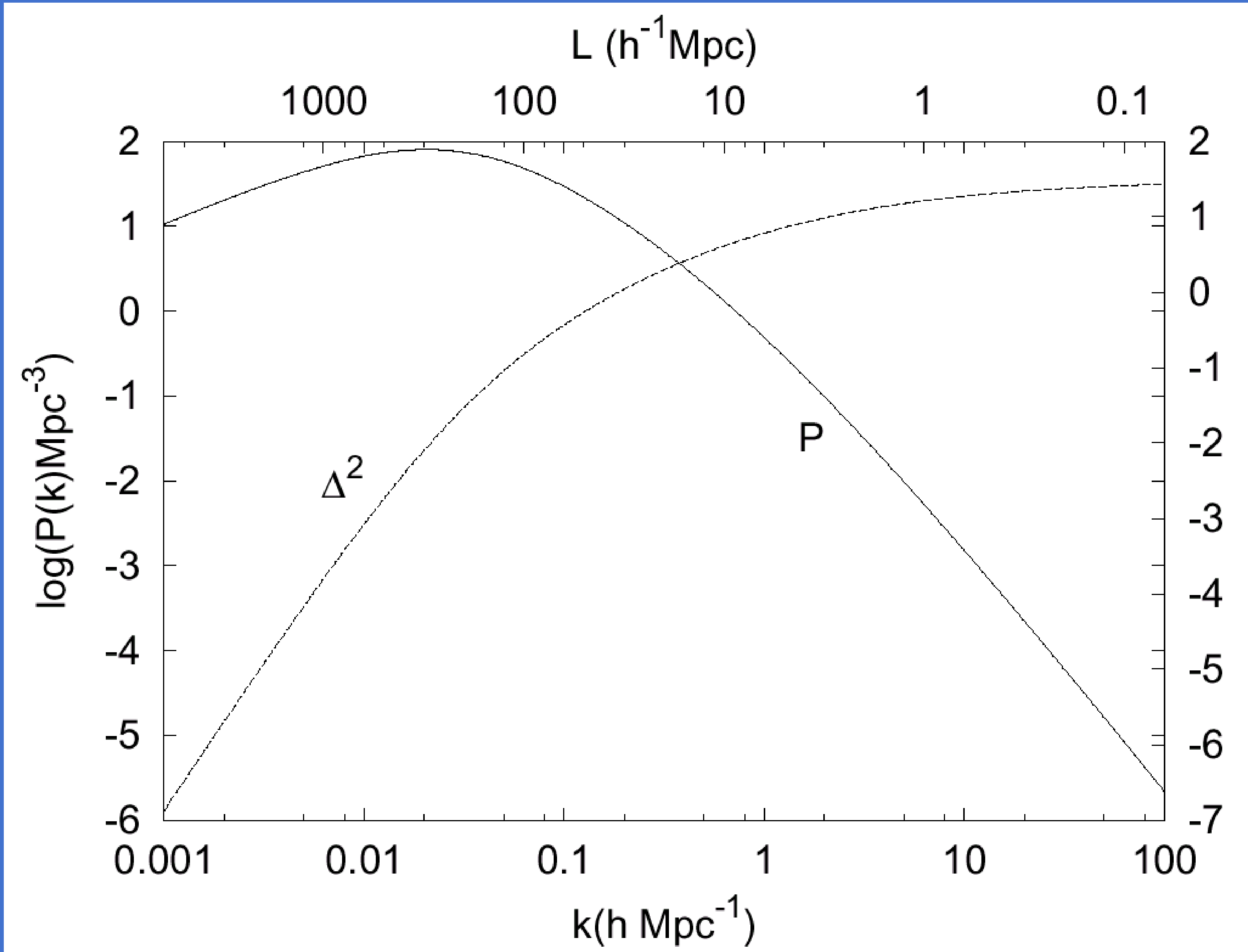

The density contrast power spectrum in a CDM cosmology

2dFGRS power-spectrum results

Dimensionless power:

d (fractional variance in density) / d ln k

Note no large oscillations: pure baryon universe disfavoured

Percival et al. MNRAS 327, 1279 (2001)

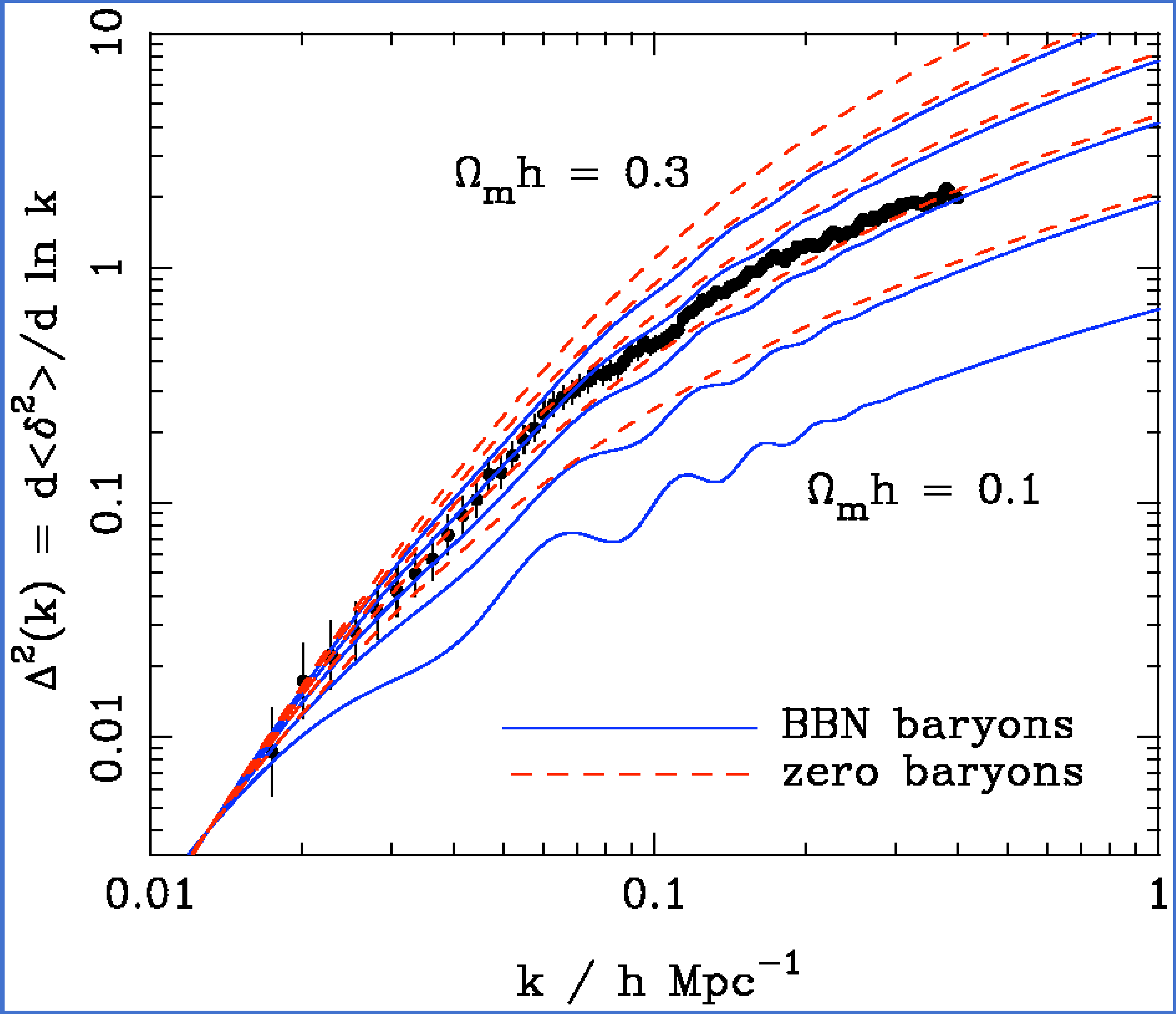

J. Peacock, JENAM '04

Outline of the talk:

- Galaxies everywhere

(on the sky and in the computer)

- Second-order statistics

(correlation function and power spectrum)

- Multiresolution morphology

(consistent estimation of the density field)

Other clustering measures to describre the morphology beyond second order statistics:

- Higher order correlation functions

- Topology and other morphological descriptors provide information about the phase correlation of the density fluctuations in *k*-space

- Shape finders and integral transforms (MGA) are useful to describe the cosmic web

Sergei Shandarin's talk this morning

Minkowski Functionals

Complete morphological description of scalar fields is given by Minkowski functionals ($N+1$ for N-dimensional space).

We start for a:[a]

- point distribution – decorating the points with balls(R),
- continous distribution – slicing by density isolevels.

---

[a] Minkowski functionals: read K.R. Mecke, T. Buchert, H. Wagner, "Robust morphological measures for large-scale structure in the Universe", Astron. Astrophys. 288, 697-704 (1994).

Minkowski functionals

Mecke, Buchert, and Wagner (1994), A&A, 288, 697

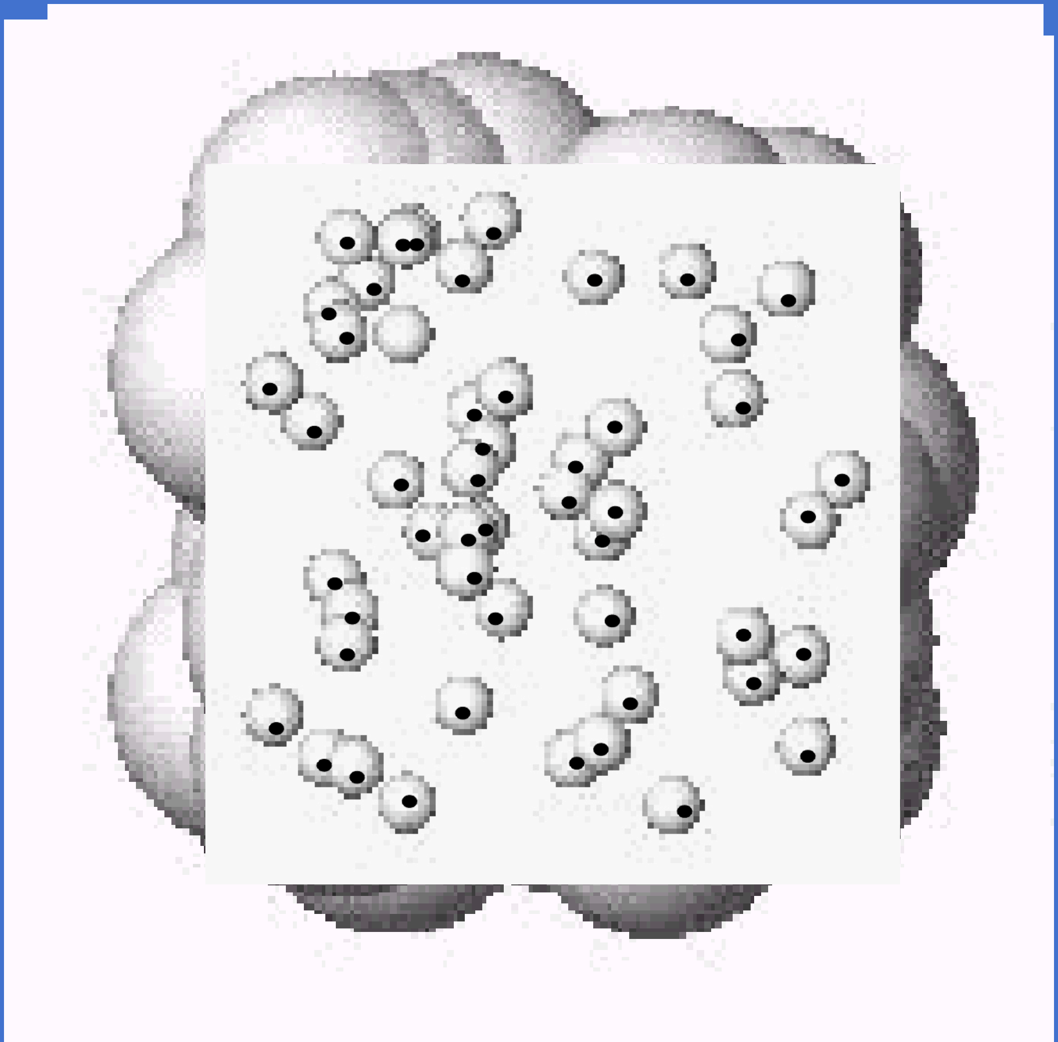

The germ-grain model

$A_r = \cup_{i=1}^{N} B_r(\mathbf{x}_i)$ for the diagnostic parameter r, where $\{\mathbf{x}_i\}_{i=1}^{N}$ represents the galaxy positions and $B_r(\mathbf{x}_i)$ is a ball of radius r centered at point $\mathbf{x}_i$.

In R^3 there are four functionals: the volume V, the surface area A, the integral mean curvature H, and the Euler-Poincaré characteristic χ, related with the genus of the boundary of A_r by $\chi = 1 - g$.

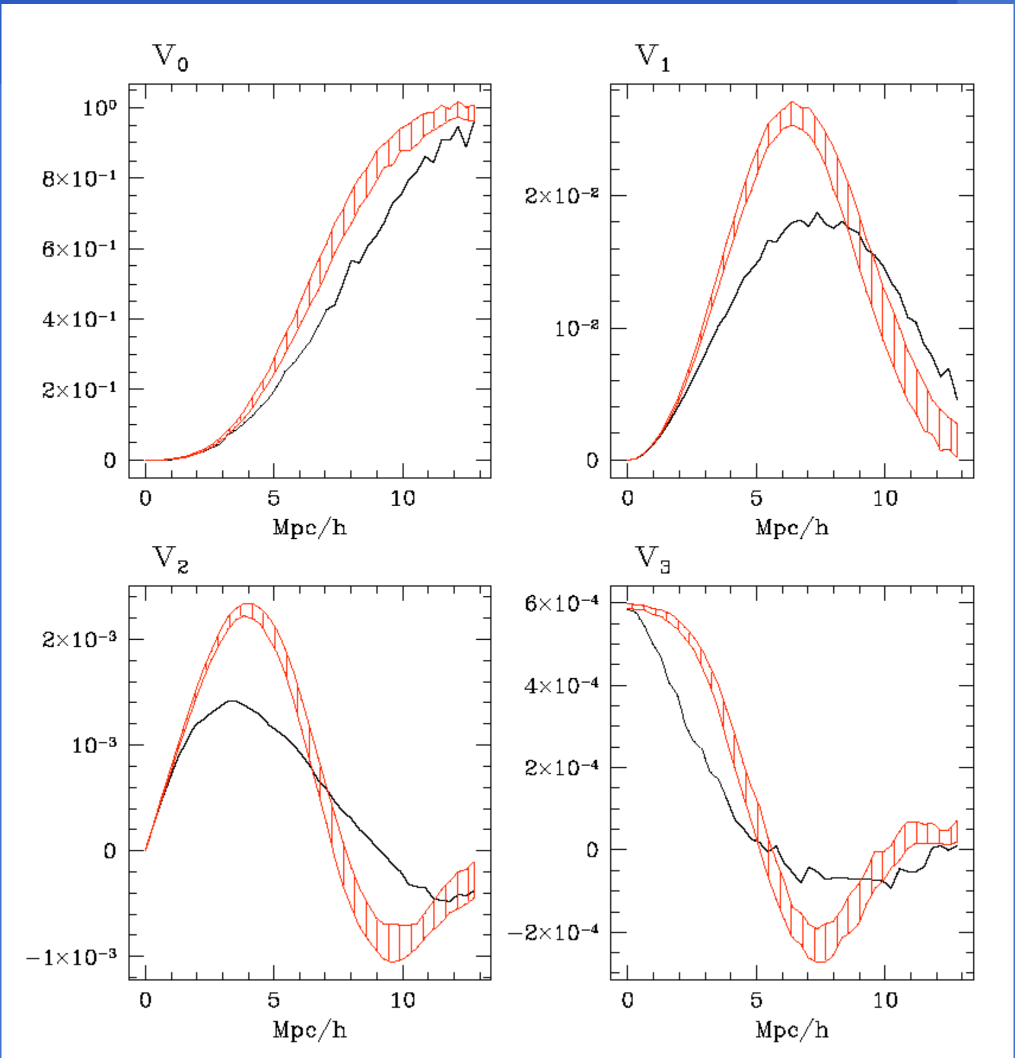

Kerscher & Martínez (1998),

Bull. Int. Statist. Inst. 57-2, 363

GRF

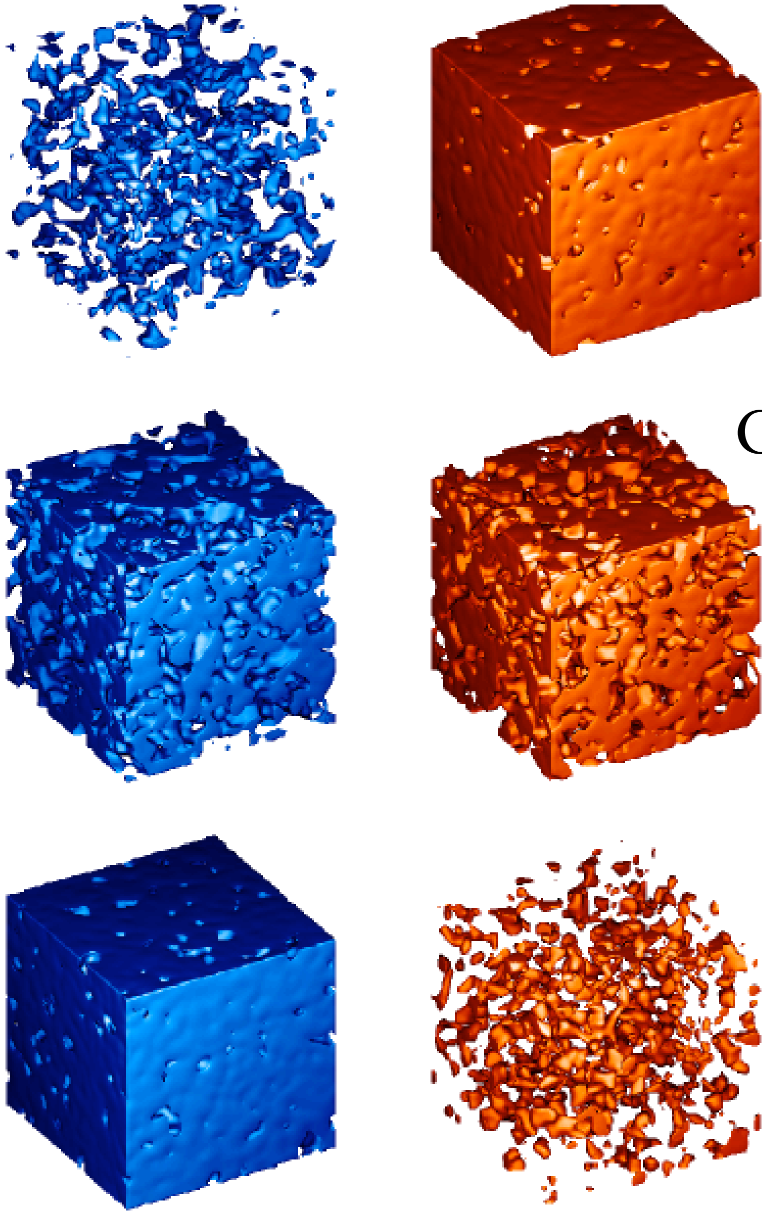

FIG. 1.— Spatial distribution of the low- (left column) and high density (right column) regions for a realization of a Gaussian random field, with comparatively little smoothing. The upper pair shows the 7% low, 93% high density regions, the middle pair stands for 50%–50%, and the lower pair shows the 93% low-density, 7% high-density case.

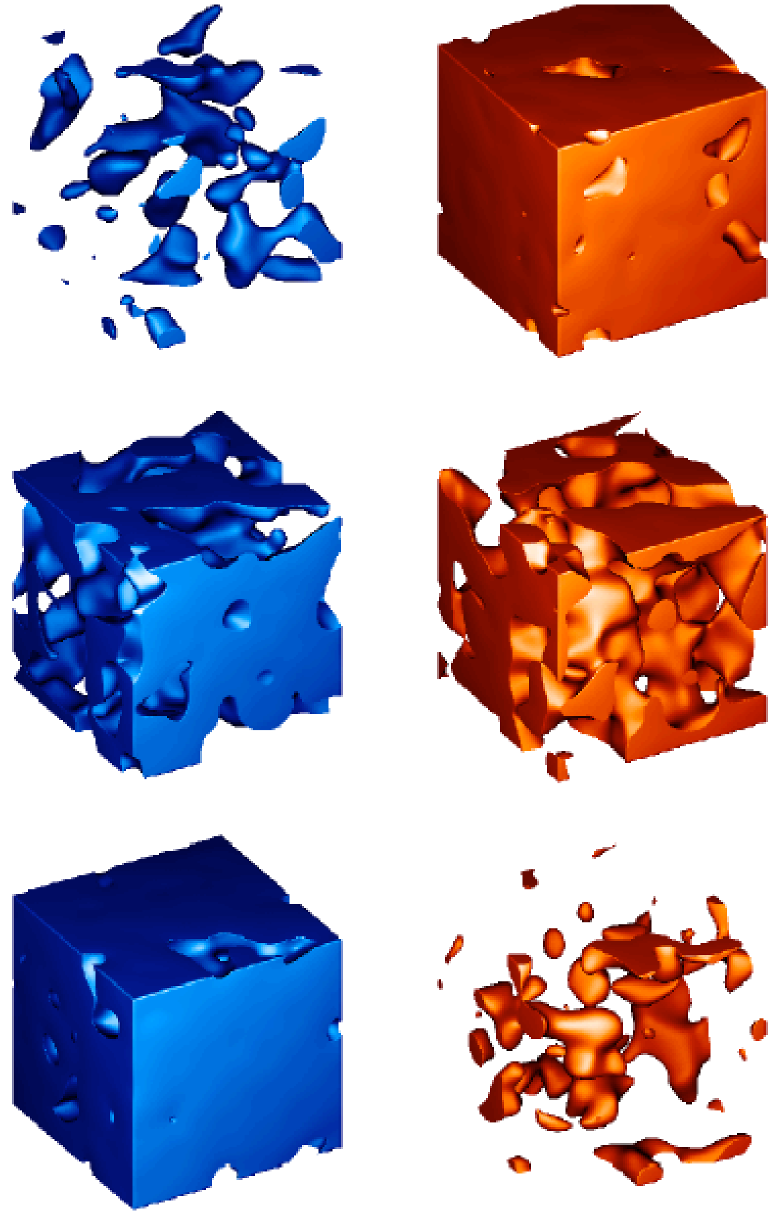

FIG. 2.— Spatial distribution of the low- (left column) and high density (right column) regions for a realization of a Gaussian random field, with heavy smoothing. The upper pair shows the 7% low, 93% high density regions, the middle pair stands for 50%–50%, and the lower pair shows the 93% low-density, 7% high-density case.

Martínez et al. 2004

Gaussian predictions for densities:

- $v_0(\nu) = \frac{1}{2} - \frac{1}{2}\Phi\left(\frac{\nu}{\sqrt{2}}\right)$,
- $v_1(\nu) = \frac{2}{3}\frac{\lambda}{\sqrt{2\pi}} \exp\left(-\frac{\nu^2}{2}\right)$,
- $v_2(\nu) = \frac{2}{3}\frac{\lambda^2}{\sqrt{2\pi}} \exp\left(-\frac{\nu^2}{2}\right)$,
- $v_3(\nu) = \frac{\lambda^3}{\sqrt{2\pi}}(\nu^2 - 1) \exp\left(-\frac{\nu^2}{2}\right)$,
- where $\lambda^2 = \frac{1}{2\pi}\frac{-\xi''(0)}{\xi(0)}$.

Martínez, Starck, Saar, Donoho & Paredes, 2004

Topological genus (Euler-Poincaré characteristic)

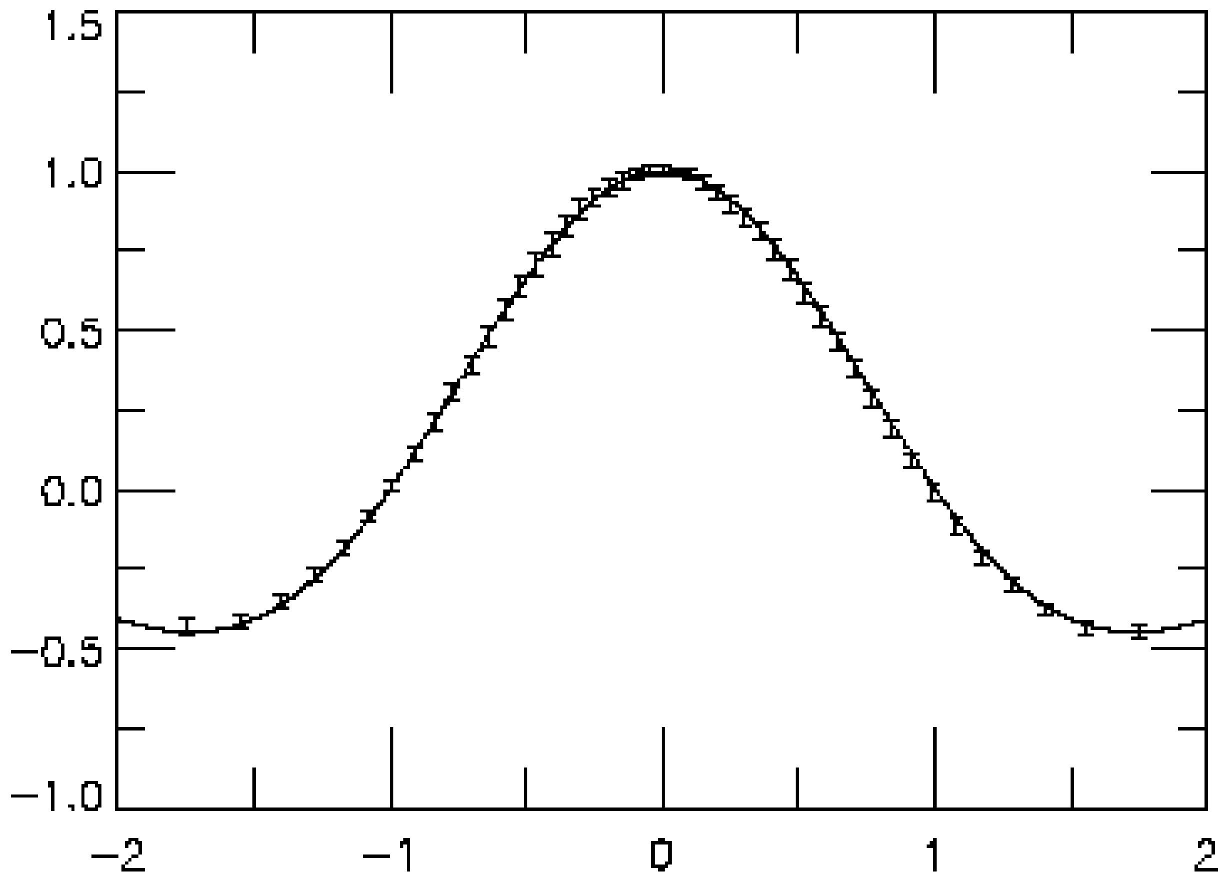

FIG. 3.— The average genus curve for 50 realizations of a Gaussian random field with $P(k) =\sim k^{-1}$ together with the expected analytical result (solid line). Error bars are 1 σ deviations.

Minkowski functionals

Already explained in Sergei Shandarin's talk

Let F_ϕ be the excursion set of a field $\phi(\mathbf{x})$ (all points where $\phi(\mathbf{x}) \geq \phi$). For a 3-D field the Minkowski functionals are:

- $V_0(\phi) = \int_{F_\phi} d^3x$ (volume),
- $V_1(\phi) = \frac{1}{6}\int_{\delta F_\phi} dS(\mathbf{x})$ (surface area),
- $V_2(\phi) = \frac{1}{6\pi}\int_{\delta F_\phi} \left(\frac{1}{R_1(\mathbf{x})} + \frac{1}{R_2(\mathbf{x})}\right) dS(\mathbf{x})$

  (integrated mean curvature of the boundary),

- $V_3(\phi) = \frac{1}{4\pi} \int_{\delta F_\phi} \frac{1}{R_1(\mathbf{x}) R_2(\mathbf{x})} dS(\mathbf{x})$ (integrated Gaussian curvature of the boundary).
- $V_3 = \chi = \frac{(1 - g)}{2} =$
  \# of isolated regions − \# of holes (g is the topological genus).

Arguments:

- density deviation $\nu_\sigma = \dfrac{\phi_c - \bar{\phi}}{\sigma_\phi}$,
- Gaussianized volume fraction ν_G:
  $v_f = 1 - \frac{1}{\sqrt{2\pi}} \int_{\nu_G}^{\infty} \exp(-x^2/2) dx.$

Lattice algorithm (Kendrick invariants):
a lattice of a step a, with N vertices.
In the excursion set: N_0 vertices, N_1 segments, N_2 faces, N_3 cells.

A better algorithm: SURFGEN

Talk by Sergei Shandarin

$$
\begin{aligned}
v_0 &= \frac{1}{N} N_3, \\
v_1 &= \frac{1}{aN}\left(-\frac{2}{3}N_3 + \frac{2}{9}N_2\right), \\
v_2 &= \frac{1}{a^2 N}\left(\frac{2}{3}N_3 - \frac{4}{9}N_2 + \frac{2}{9}N_1\right), \\
v_3 &= \frac{1}{a^3 N}\left(-N_3 + N_2 - N_1 + N_0\right).
\end{aligned}
$$

Smoothing

$$\rho(\mathbf{x}) = \frac{1}{N} \sum_{i}^{N} K_h \left(\frac{\mathbf{x} - \mathbf{x}_i}{h} \right) ,$$

where $K(\mathbf{x})$ is a distribution function:

$$\int K(\mathbf{x})\, d\mathbf{x} = 1, \qquad \int \mathbf{x} K(\mathbf{x})\, d\mathbf{x} = 0.$$

To choose of the band with h is an art!

- Techniques:
  - sample point, sandbox, gather estimators:
    $h = h(\mathbf{x}_i)$
  - balloon, scatter estimators:
    $h = h(\mathbf{x})$.
  - choose h to minimize
    $\text{MSE} = E[\tilde{f}(\mathbf{x}) - f(\mathbf{x})]^2 = \text{Var}(\tilde{f}(\mathbf{x})) + [\text{Bias}(\tilde{f}(\mathbf{x}))]^2$

The à trous wavelet transform

One-dimensional signals $s(l)$:

Already explained in Jean-Luc's talk

- Decomposition (and reconstruction)

$$s(l) = c_{0,l} = c_{J,l} + \sum_{j=1}^{J} w_{j,l}.$$

- The scaling function

$$\frac{1}{2}\phi(\frac{x}{2}) = \sum_{k} h(k)\phi(x-k).$$

- Define the wavelet:

$$\frac{1}{2}\psi(\frac{x}{2}) = \phi(x) - \frac{1}{2}\phi(\frac{x}{2}).$$

$$c_{j+1,l} = \sum_k h(k) c_{j,l+2^j k}.$$

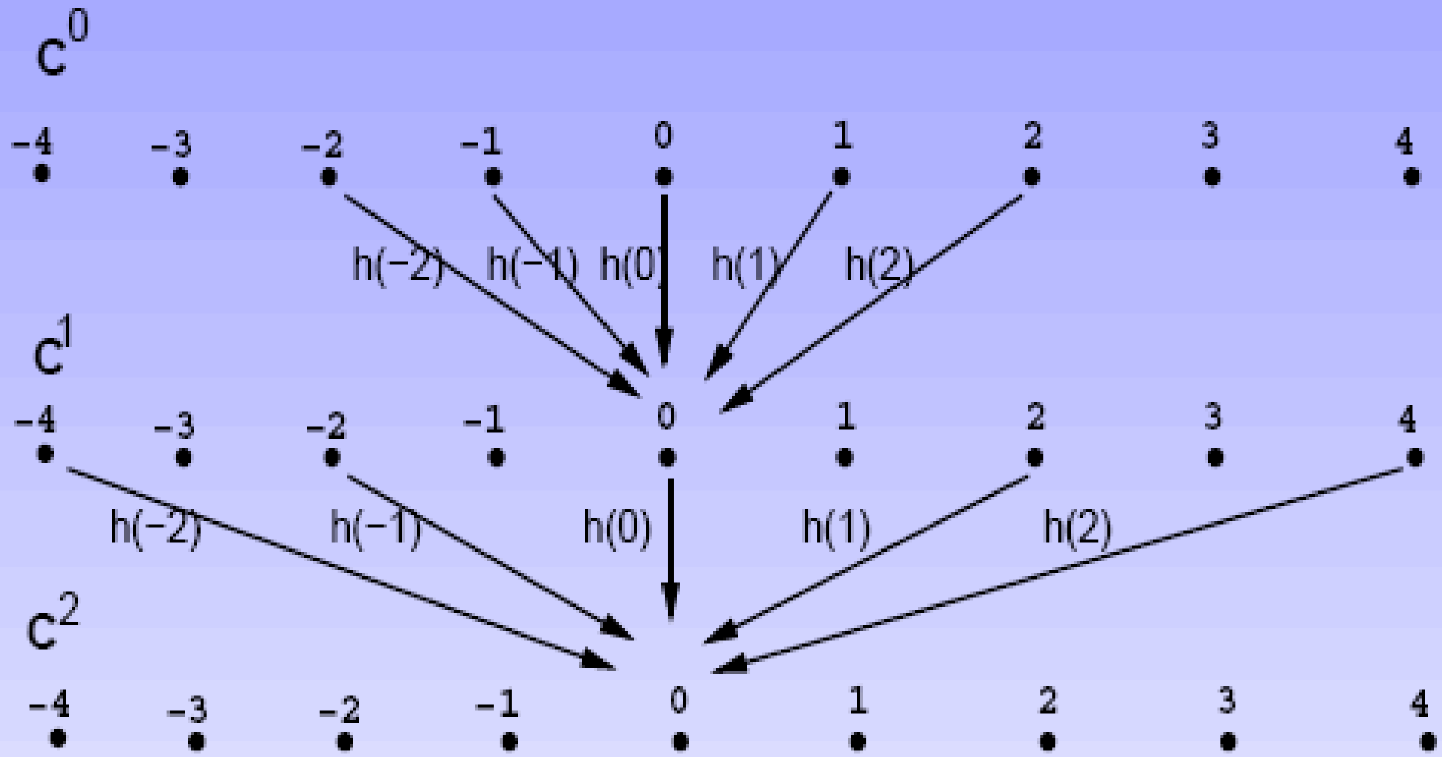

- The wavelet coefficients are:

$$w_{j+1,l} = c_{j,l} - c_{j+1,l}.$$

- The scaling function

$$\phi(x, y, z) = \phi(x)\phi(y)\phi(z),$$

- decomposition (and reconstruction)

$$s(l, m, n) = c_{0;l,m,n} = c_{J;l,m,n} + \sum_{j=1}^{J} w_{j;l,m,n}.$$

- Smooth:

$$c_{j+1;l,m,n} = \sum_{i} \sum_{k} h(i)h(k)h(o)c_{j;l+2^j i,m+2^j k,n+2^j o}.$$

J data sets for all dimensions.

The B_3 spline

$$\phi(x) = \frac{1}{12}\left(|x-2|^3 - 4|x-1|^3 + 6|x|^3 - 4|x+1|^3 + |x+2|^3\right), \qquad -2 \le x \le 2.$$

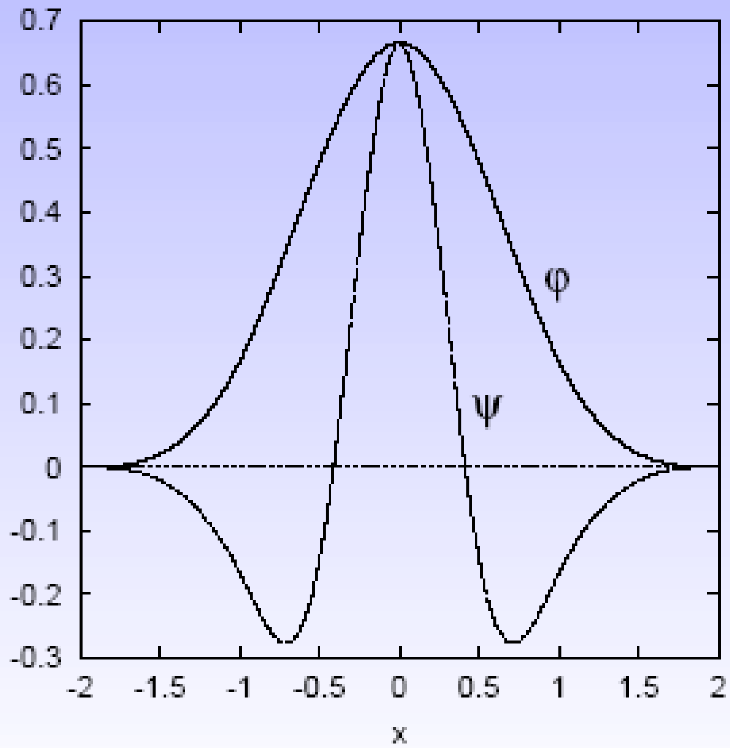

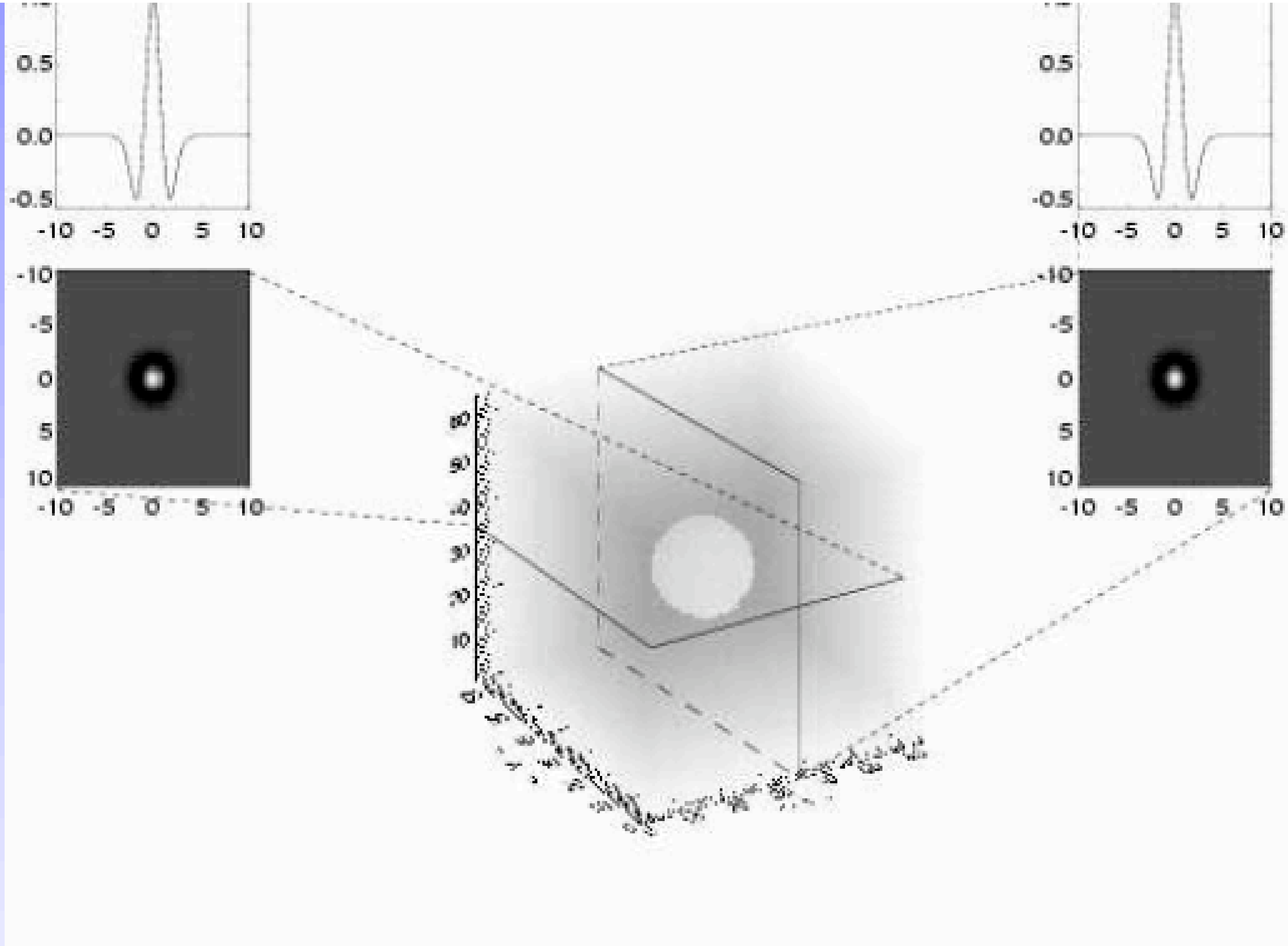

The 3-D B_3 spline generated wavelet

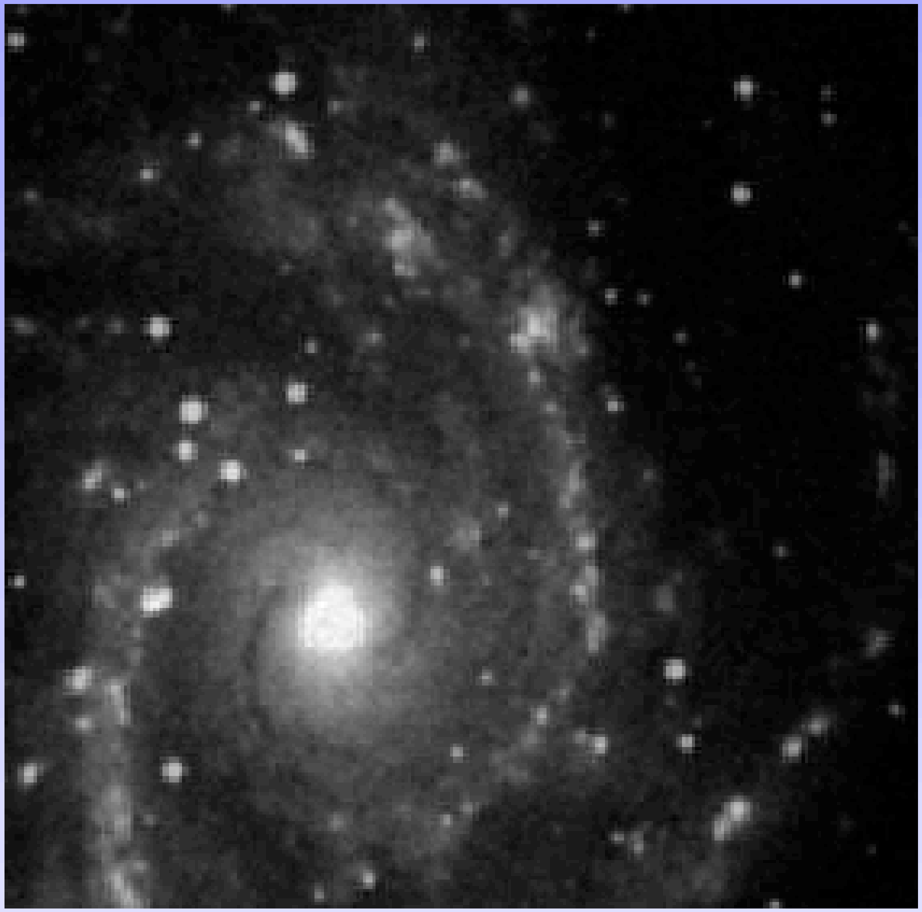

Data – NGC 2997

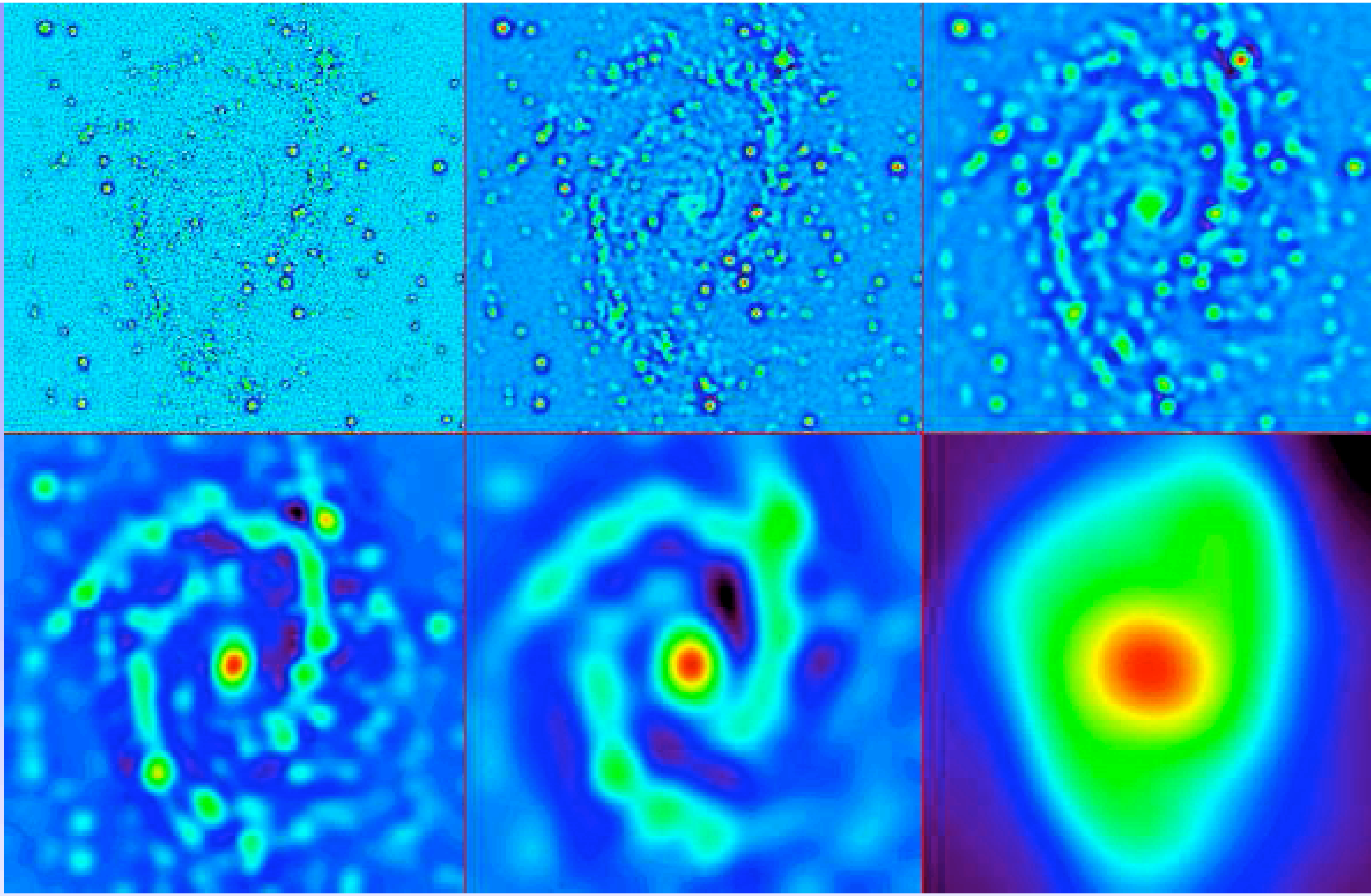

À trous transform of the NGC 2997 data

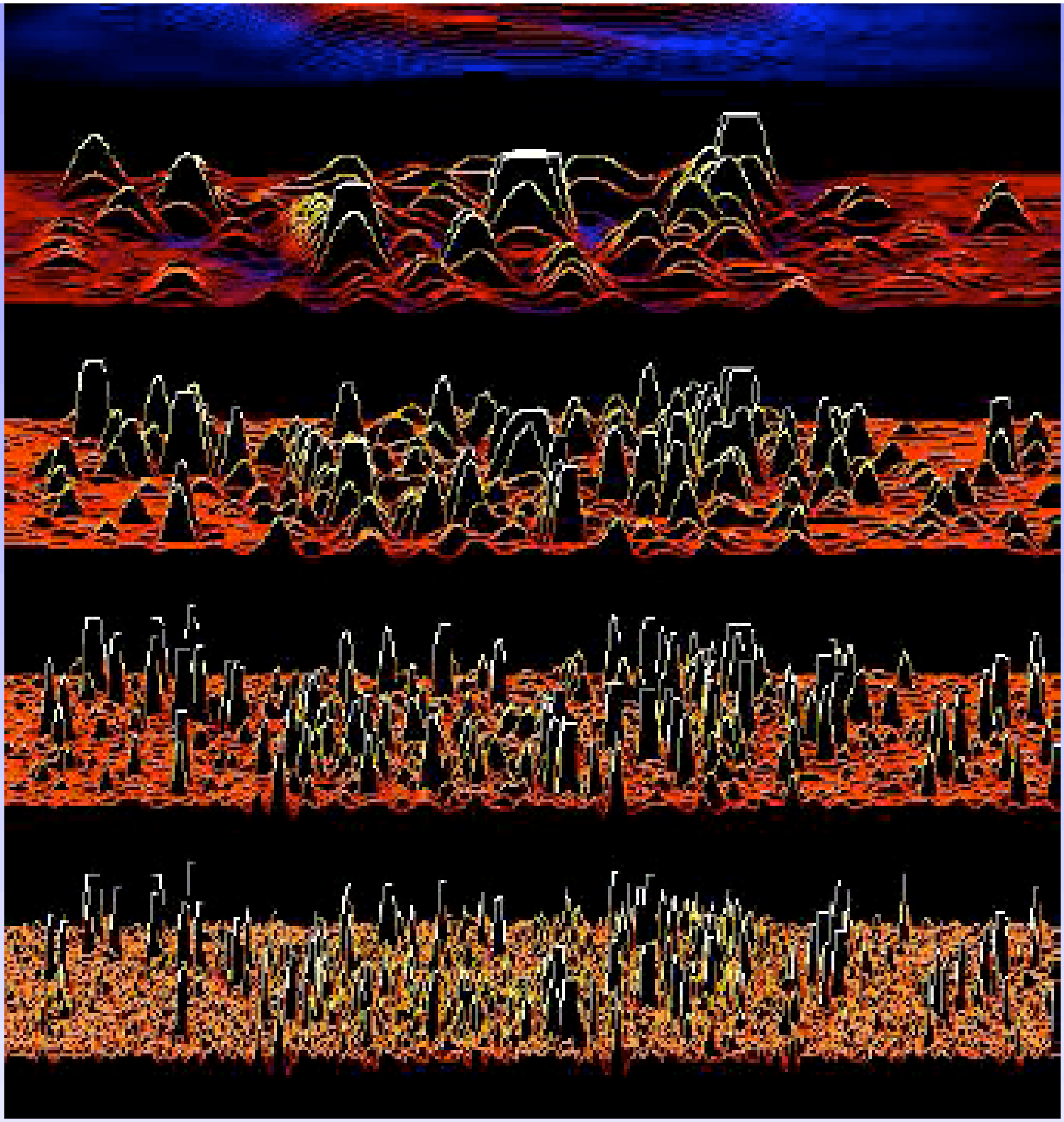

À trous transform, wavelet amplitudes

PixInsight

- A comercial software made and tested by amateur astronomers

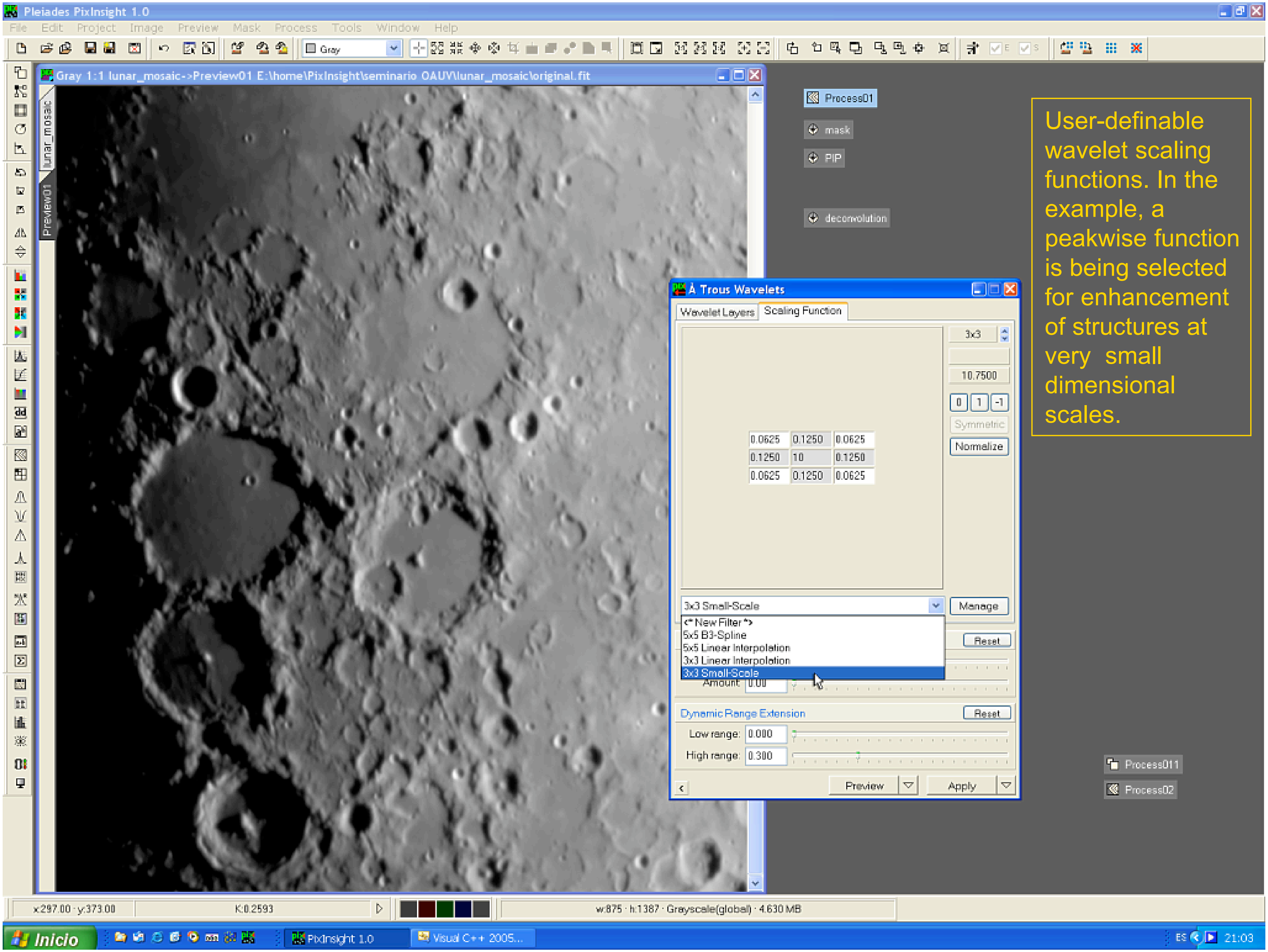

User-definable wavelet scaling functions. In the example, a peakwise function is being selected for enhancement of structures at very small dimensional scales.

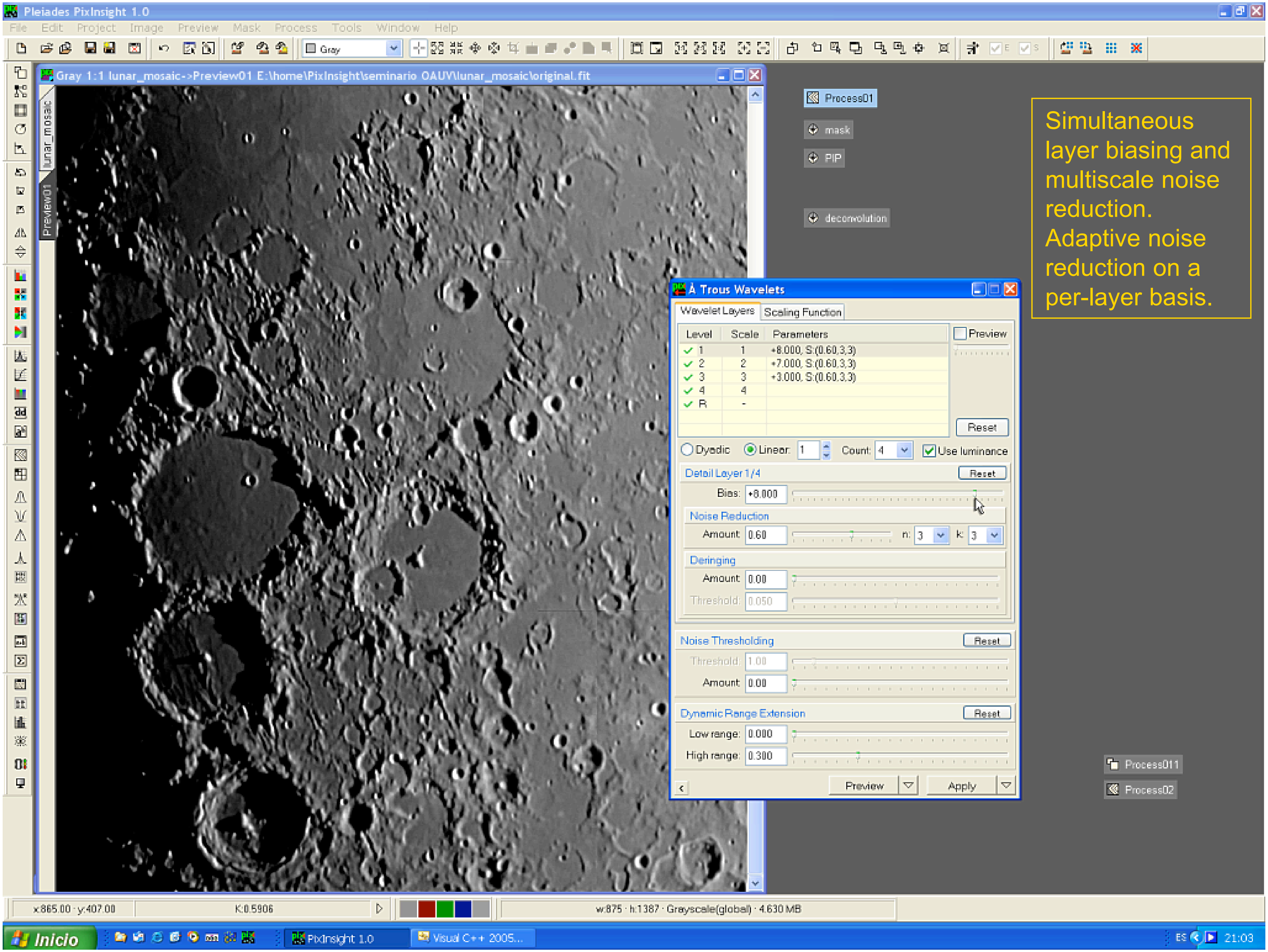

Simultaneous layer biasing and multiscale noise reduction. Adaptive noise reduction on a per-layer basis.

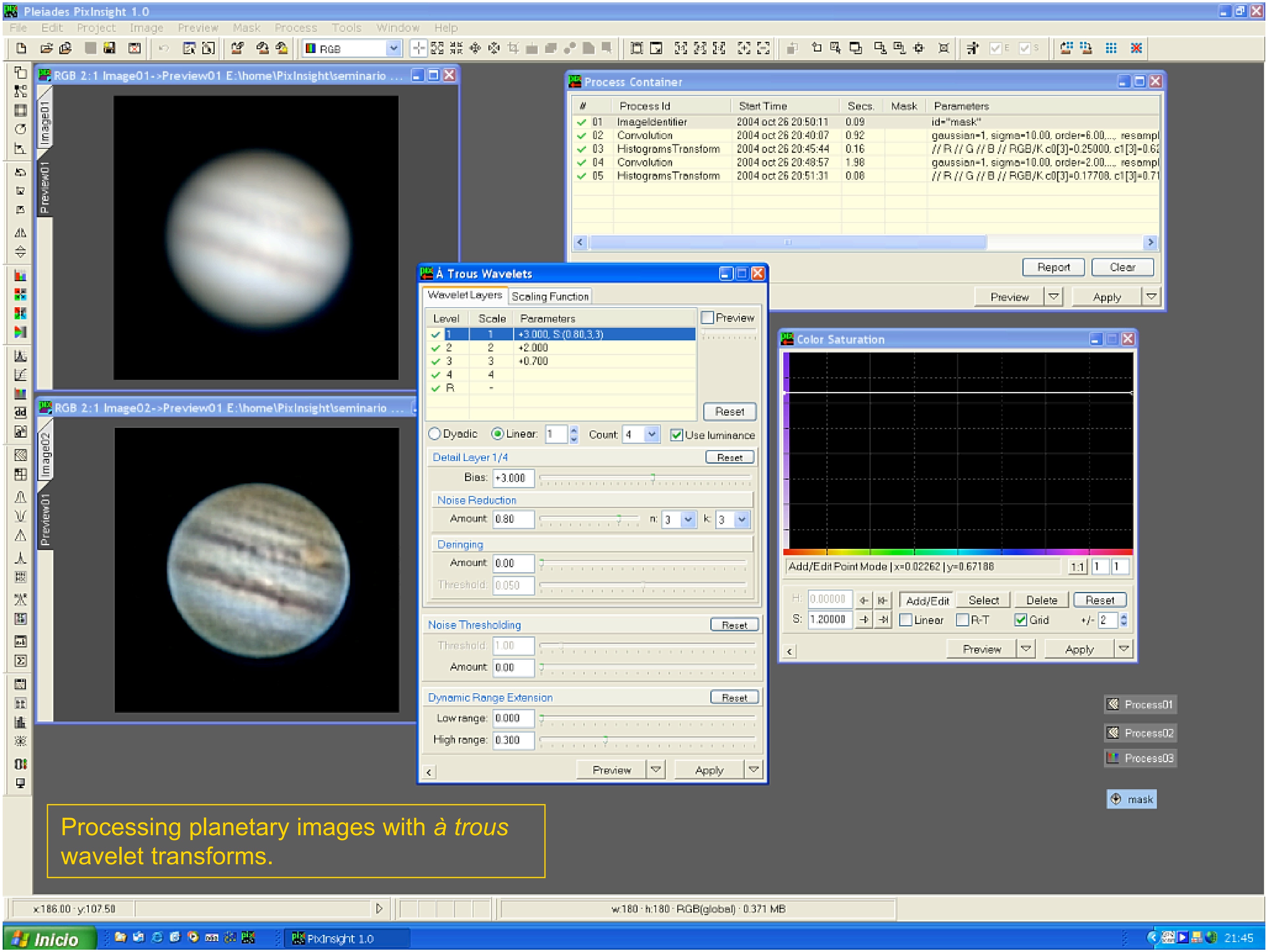
Pleiades PixInsight 1.0
File Edit Project Image Preview Mask Process Tools Window Help
RGB 2:1 Image01->Preview01 E:\home\PixInsight\seminario ...
RGB 2:1 Image02->Preview01 E:\home\PixInsight\seminario ...
Image01
Preview01
Image02
Process Container
Process Id Start Time Secs. Mask Parameters
01 ImageIdentifier 2004 oct 26 20:50:11 0.09 id="mask"
02 Convolution 2004 oct 26 20:40:07 0.92 gaussian=1, sigma=10.00, order=6.00,... resampl
03 HistogramsTransform 2004 oct 26 20:45:44 0.16 // R // G // B // RGB/K c0[3]=0.25000, c1[3]=0.62
04 Convolution 2004 oct 26 20:48:57 1.98 gaussian=1, sigma=10.00, order=2.00,... resampl
05 HistogramsTransform 2004 oct 26 20:51:31 0.06 // R // G // B // RGB/K c0[3]=0.17708, c1[3]=0.71
Report Clear
Preview Apply
À Trous Wavelets
Wavelet Layers Scaling Function
Level Scale Parameters
1 1 +3.000, S:(0.80,3,3)
2 2 +2.000
3 3 +0.700
4 4
R -
Preview
Reset
Dyadic Linear: 1 Count: 4 Use luminance
Detail Layer 1/4 Reset
Bias: +3.000
Noise Reduction
Amount: 0.80 n: 3 k: 3
Deringing
Amount: 0.00
Threshold: 0.050
Noise Thresholding Reset
Threshold: 1.00
Amount: 0.00
Dynamic Range Extension Reset
Low range: 0.000
High range: 0.300
Preview Apply
Color Saturation
Add/Edit Point Mode | x=0.02262 | y=0.67188
1:1 1 1
H: 0.00000 Add/Edit Select Delete Reset
S: 1.20000 Linear R-T Grid +/- 2
Preview Apply
Process01
Process02
Process03
mask
Processing planetary images with *à trous* wavelet transforms.
x:186.00 · y:107.50
w:180 · h:180 · RGB(global) · 0.371 MB
Inicio
PixInsight 1.0
21:45

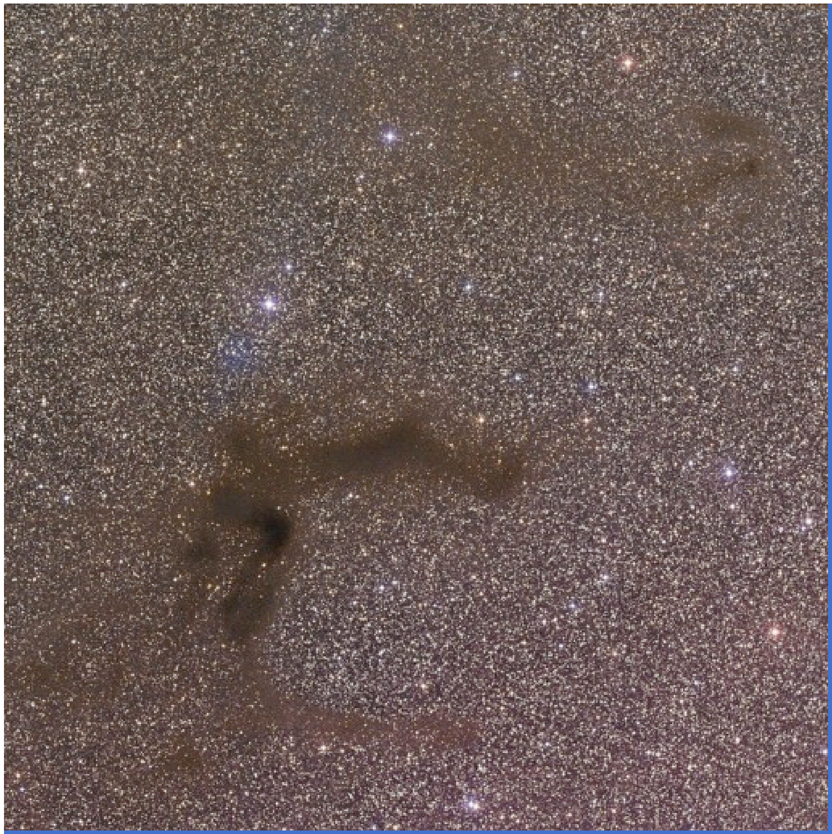

1. Original Composite RGB image

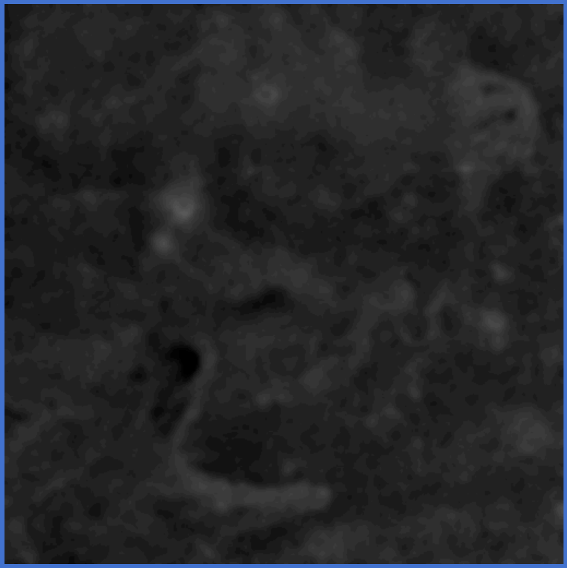

2. Stars removed by multiscale processing (small scale layers removed in *à trous* wavelet transform).

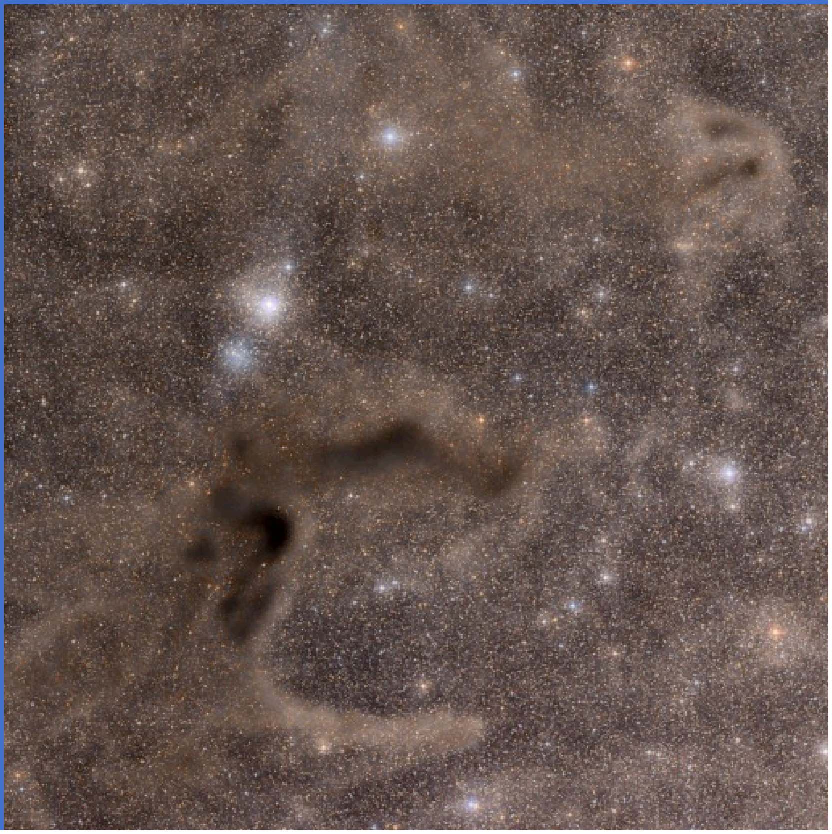

3. Large dimensional scales enhanced with *à trous* wavelet transform. Stars and small-scale structures re-inserted after wavelets processing.

Barnard 142/143 Region DSS Image

Processing in PixInsight by Vicent Peris (PTeam)

NGC 7662 image by Vicent Peris (PTeam) / Processing in PixInsight

TROBAR 0.6 m Ritchey-Chretien Telescope @ f/25 / Canon 300D digital SLR camera

1. Original RGB image

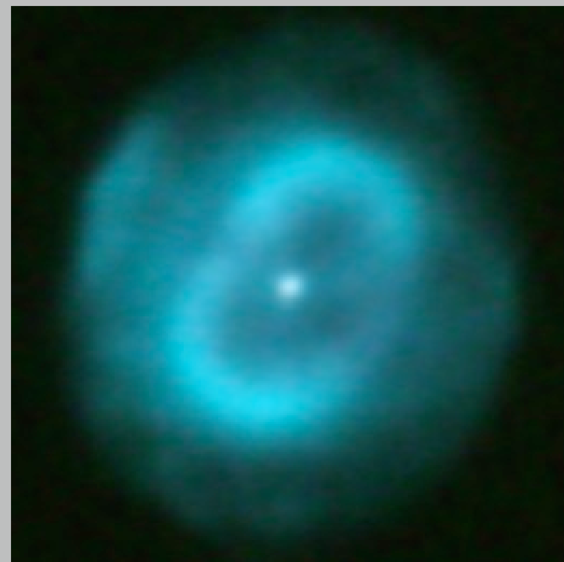

2. Small-scale noise reduction with *à trous* wavelet transform

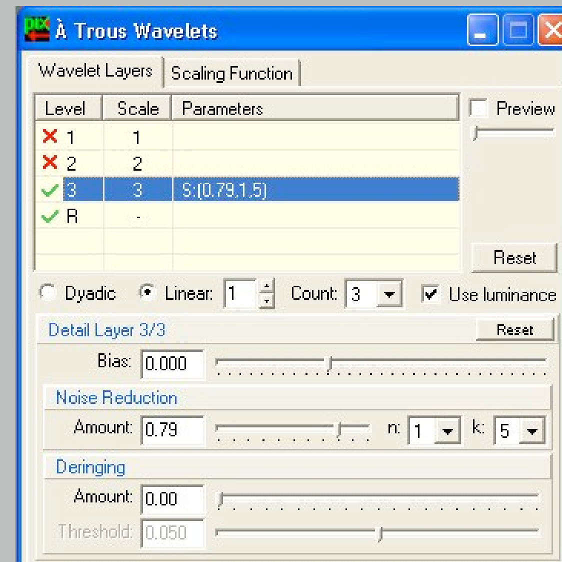

Suppression of small-scale wavelet layers. Adaptive noise reduction on the third wavelet layer.

3. Regularized Richardson-Lucy deconvolution / Color enhancement processing.

Comparison with HST image.

•PixInsight is a high-performance, flexible and modular image processing software specialized in astrophotography.

•It consist of a low-level processing engine, a sophisticated graphical user interface, and a programming environment to build high-level processing tools and their associated user interfaces.

•A limited edition of PixInsight (LE) has been released as a freeware application.

•PixInsight Home Page: http://pleiades-astrophoto.com/pixinsight/

Wavelet smoothing

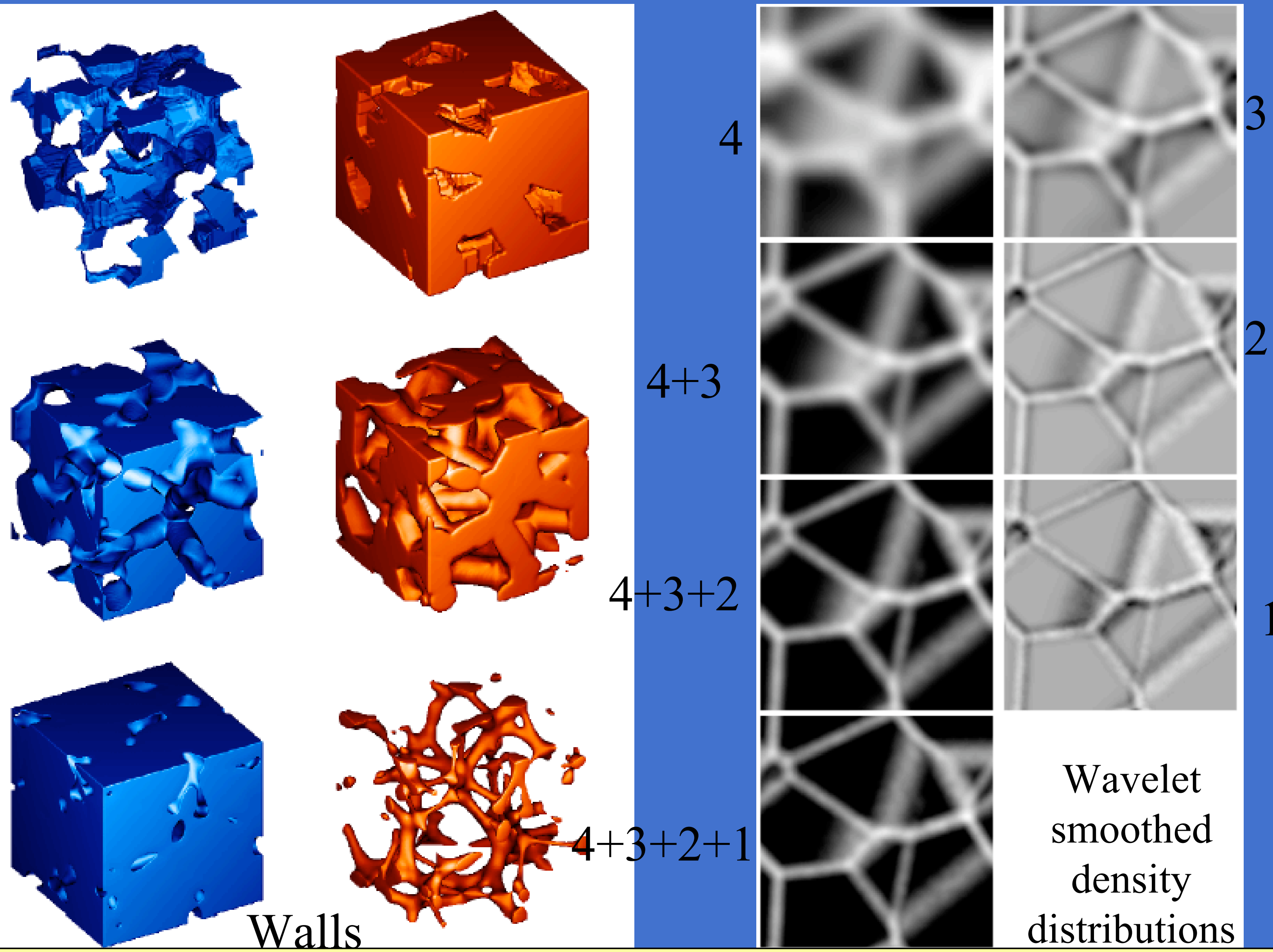

van de Weygaert talk also dealed with an adaptive method to find the density field using Delaunay tessellations

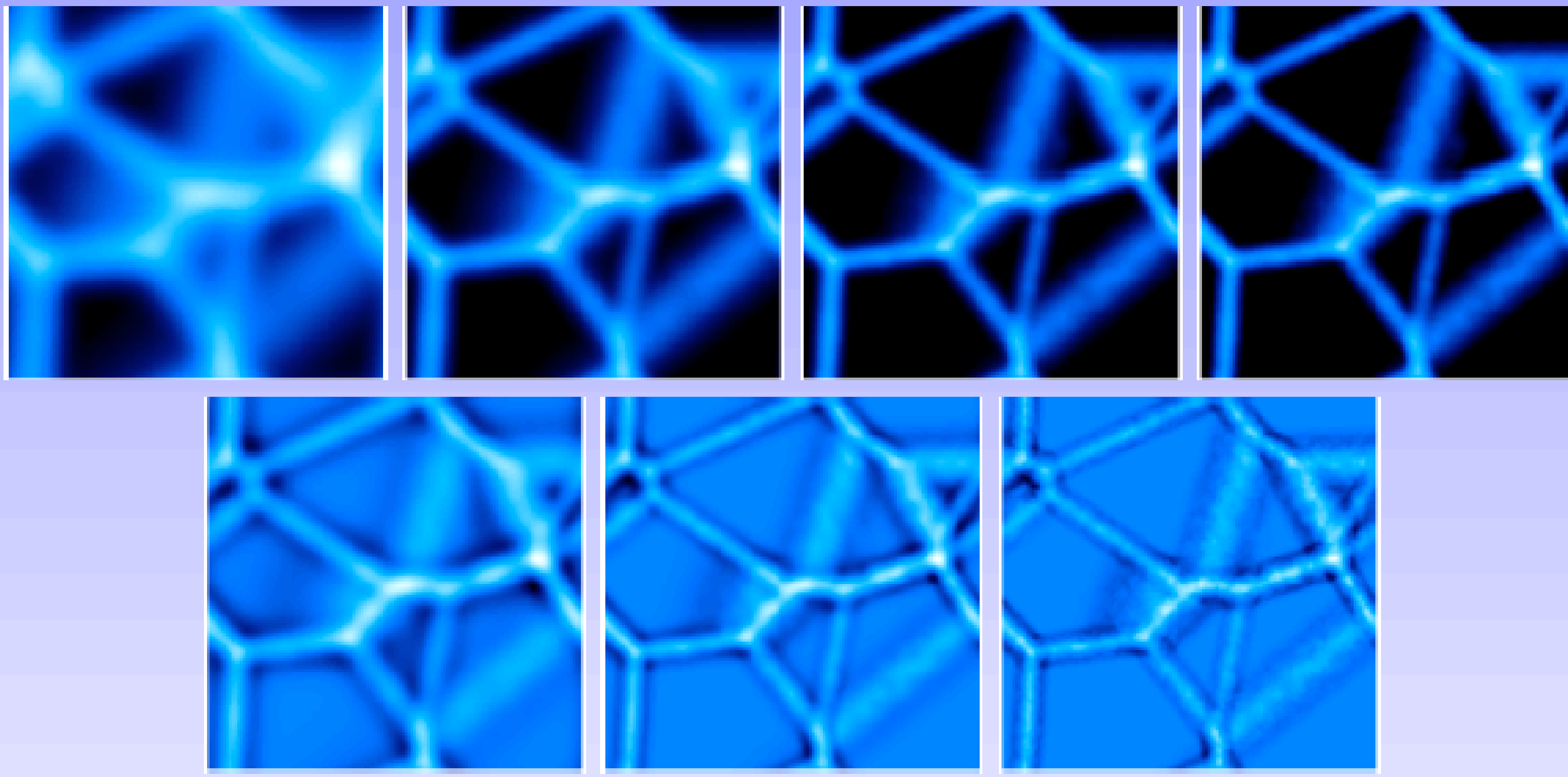

Á trous density (slices) for a Voronoi walls sample (square root scale).

The multiresolution world

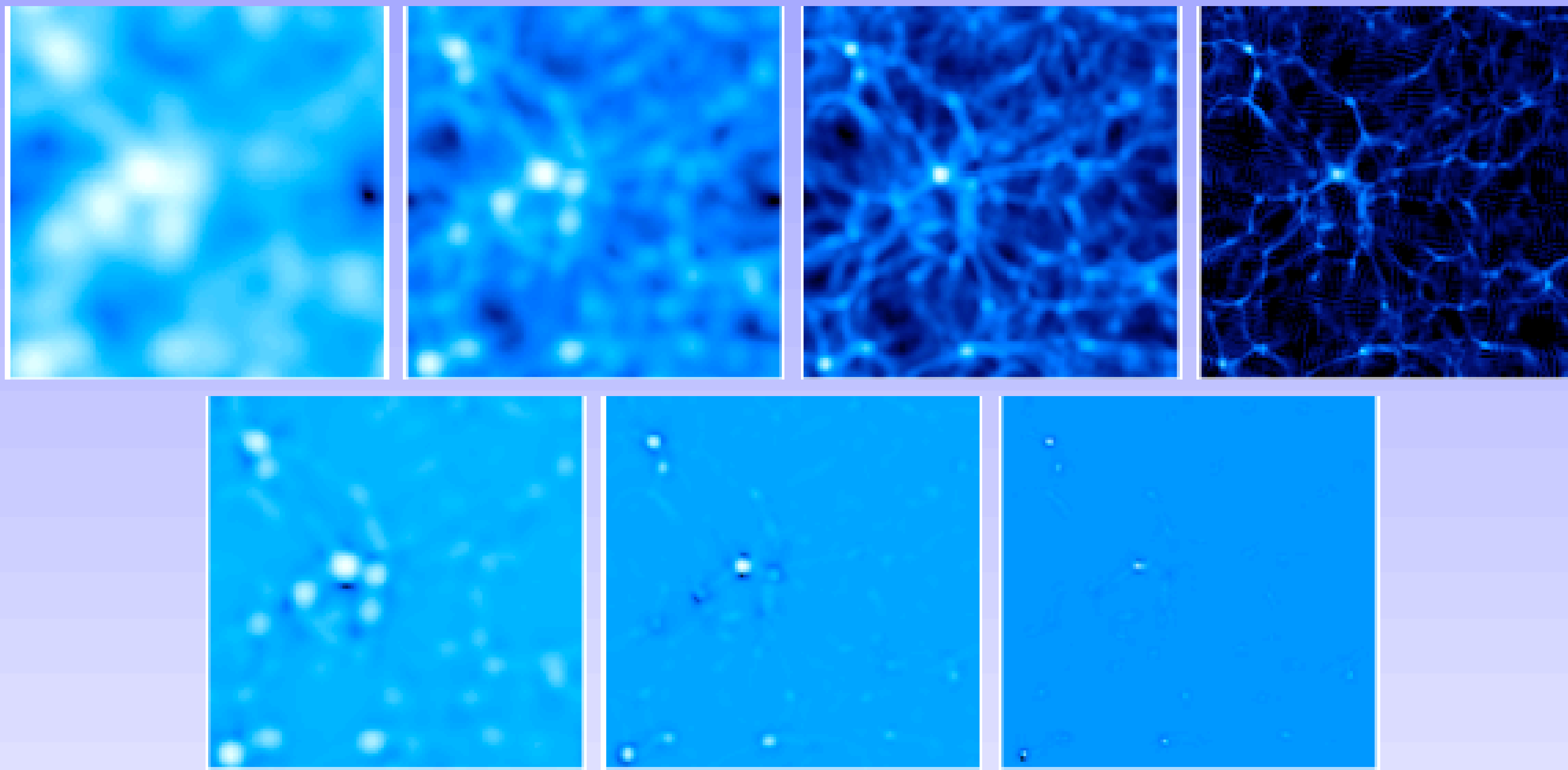

Á trous density slices for an N-body model structure (logarithmic scale).

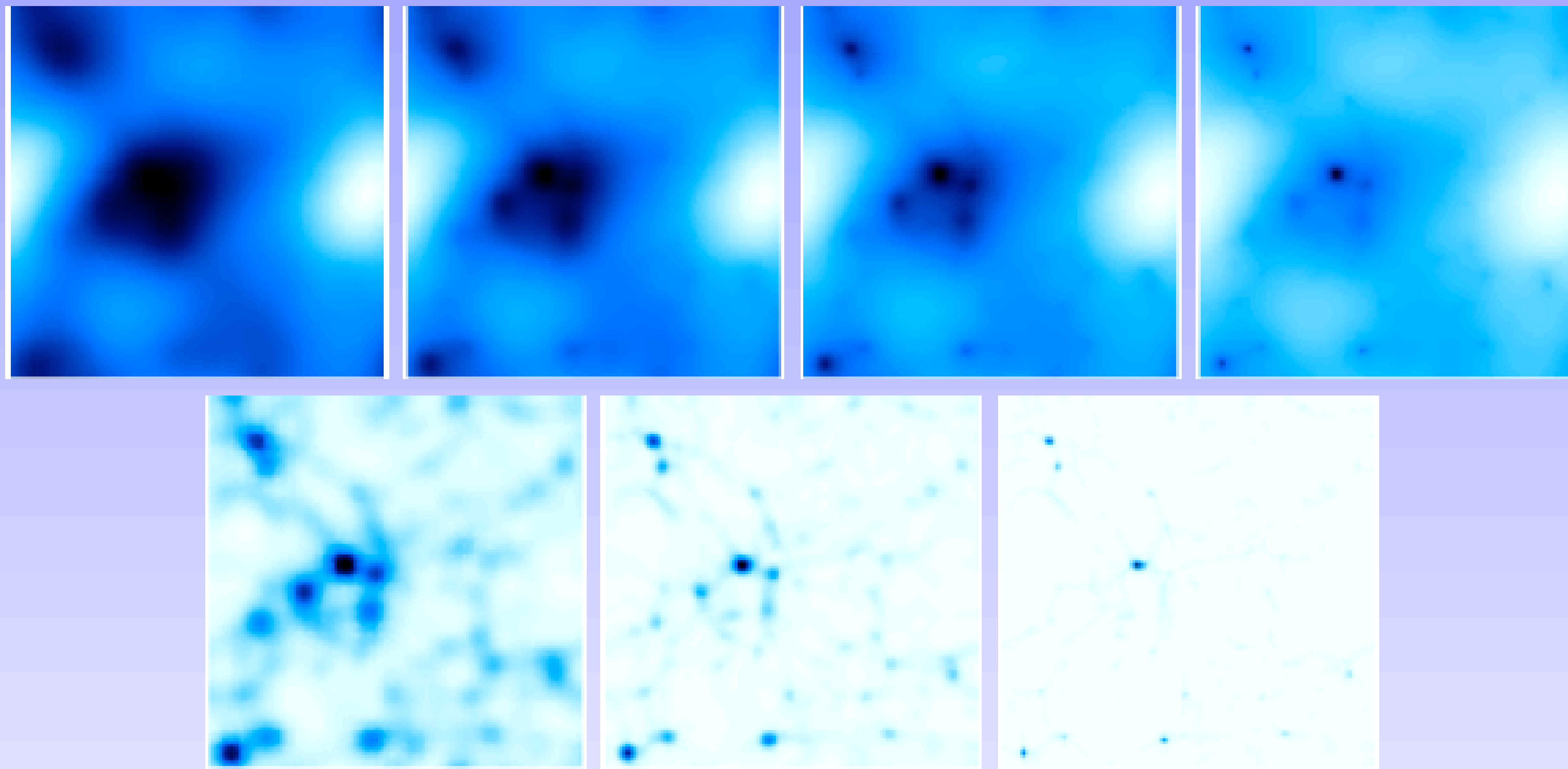

Á trous potential (slices) for the N-body model above (linear scale).

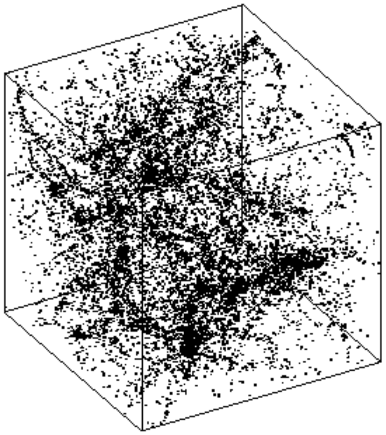

N- body simulation

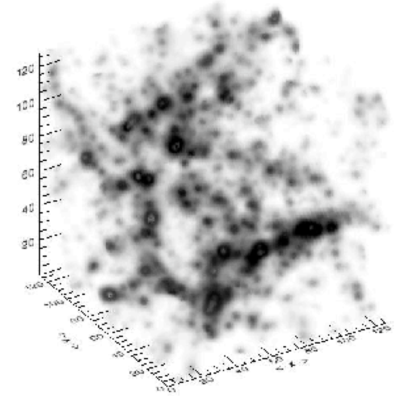

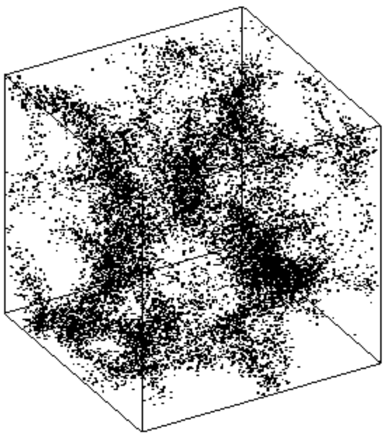

Voronoi model –
populating
filaments

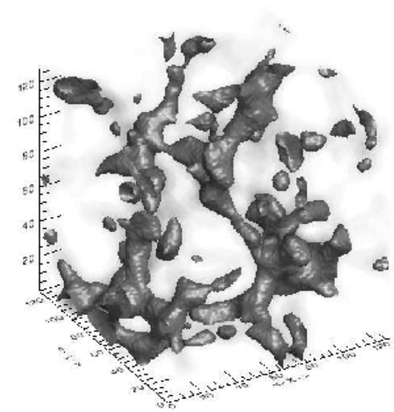

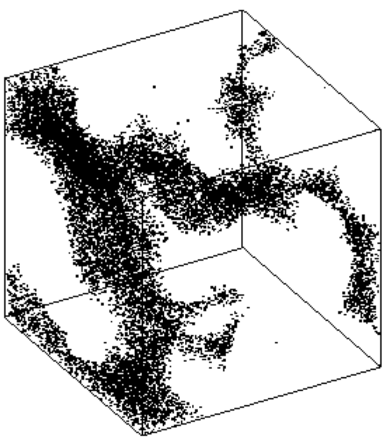

Swiss-Cheese model
dominated by huge voids

About 15000 points

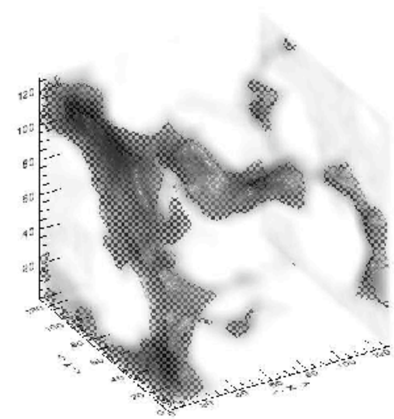

Gaussian smoothing

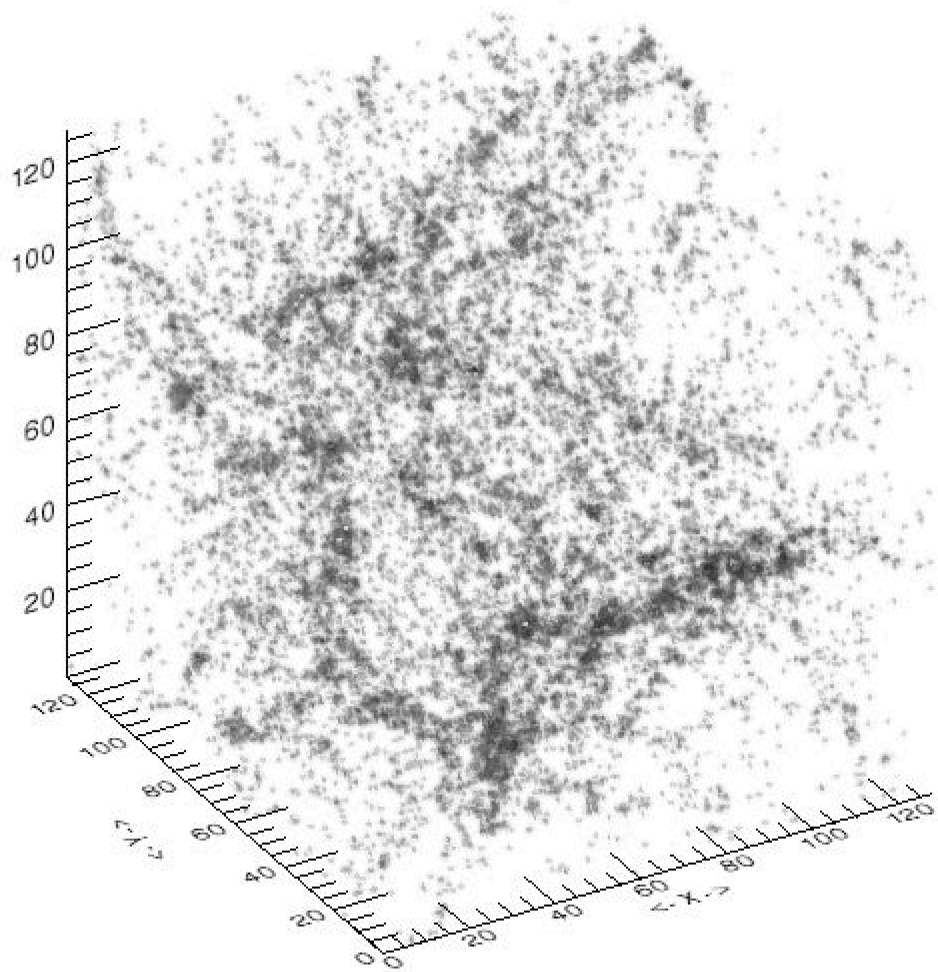

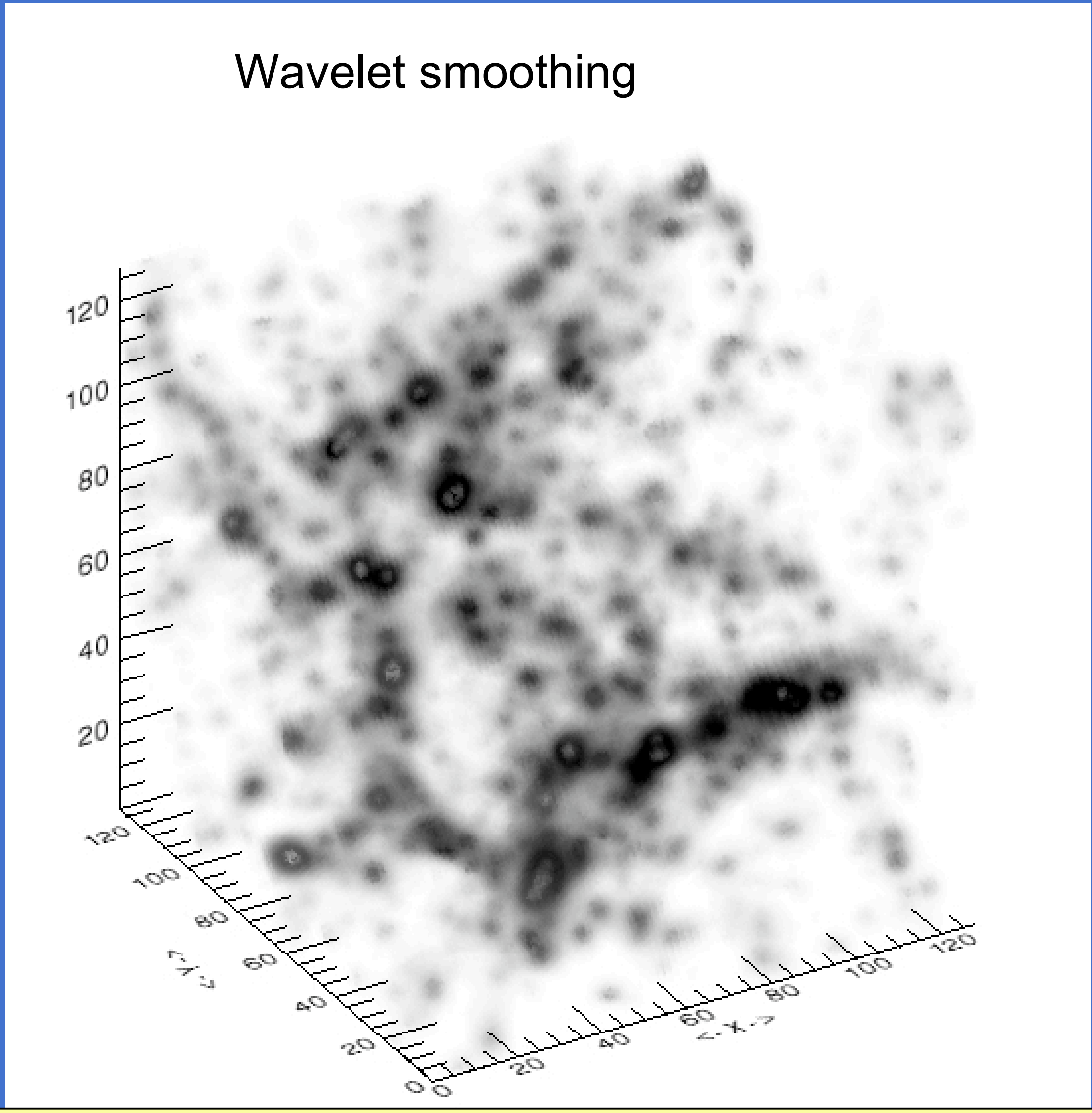

The wavelet density field keeps information at all scales due to its multiscale nature, and represents an unique reconstruction, which does not depend on a given band width.

Wavelet cleaning

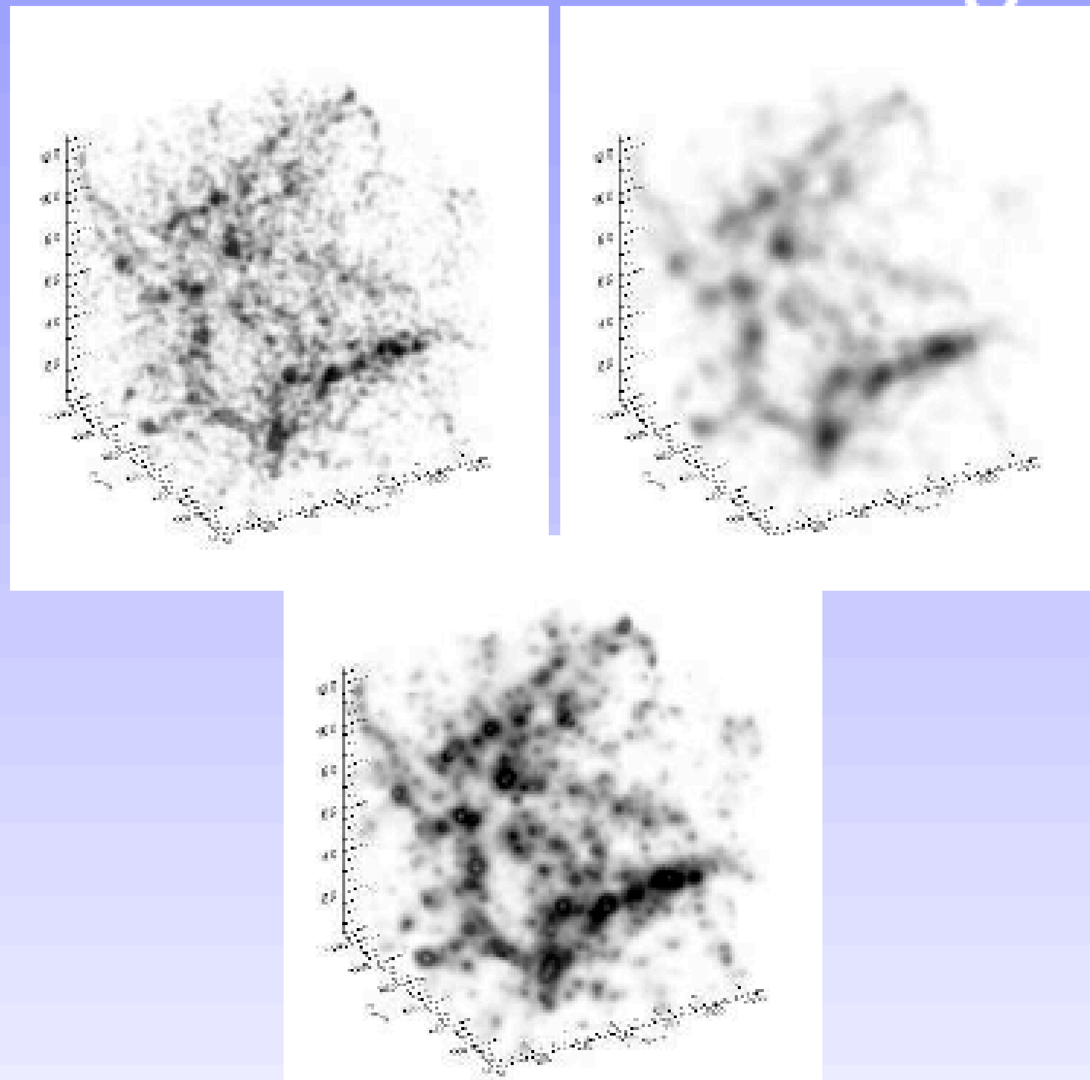

Left – Gaussian $\sigma = 1$ Mpc smoothing, middle – wavelet cleaning, right – Gaussian $\sigma = 3$ Mpc smoothing.

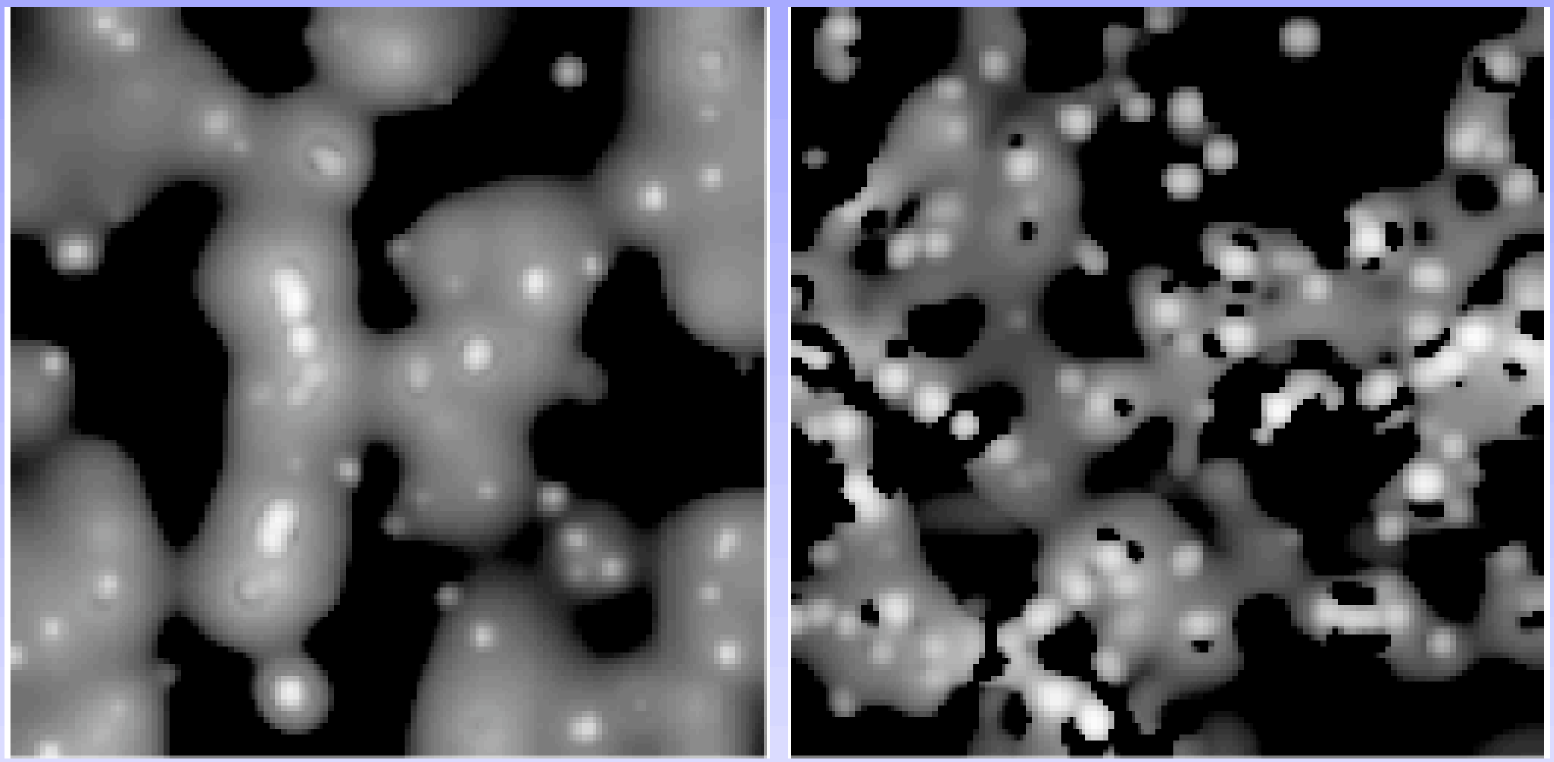

Wavelet cleaning of a model galaxy distribution (left – a successful attempt, right – overcleaning).

Denosing technique explained in Jean-Luc's talk

Ringing artifacts

Gaussian smoothing (n body)

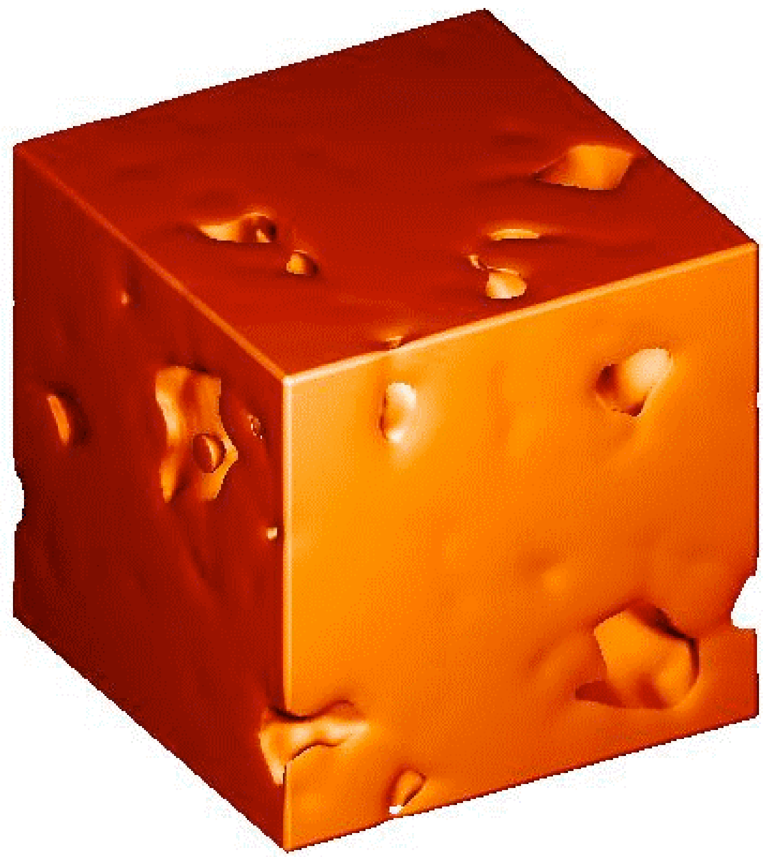

Wavelet smoothing (n-body)

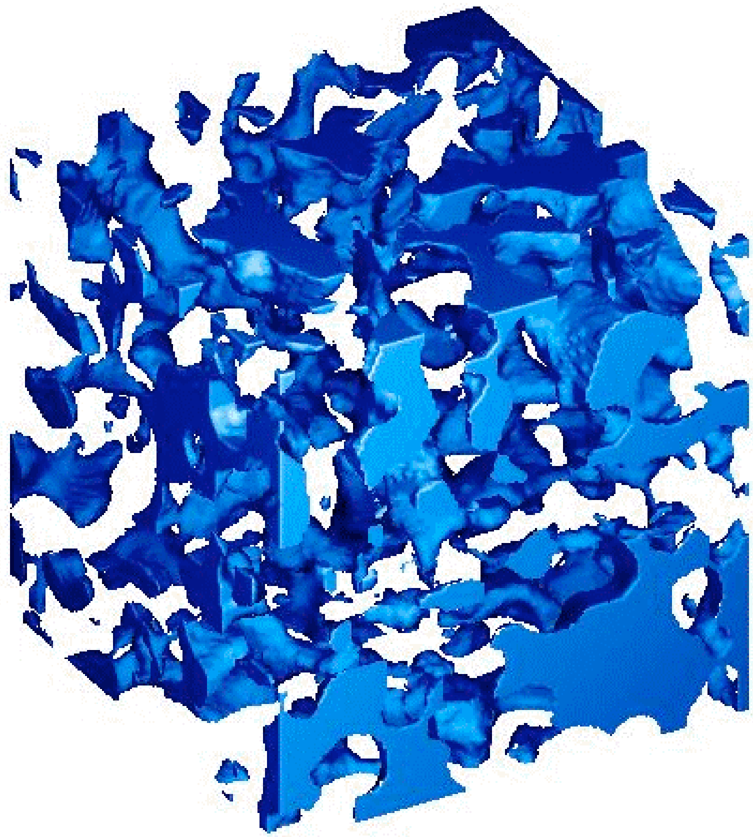

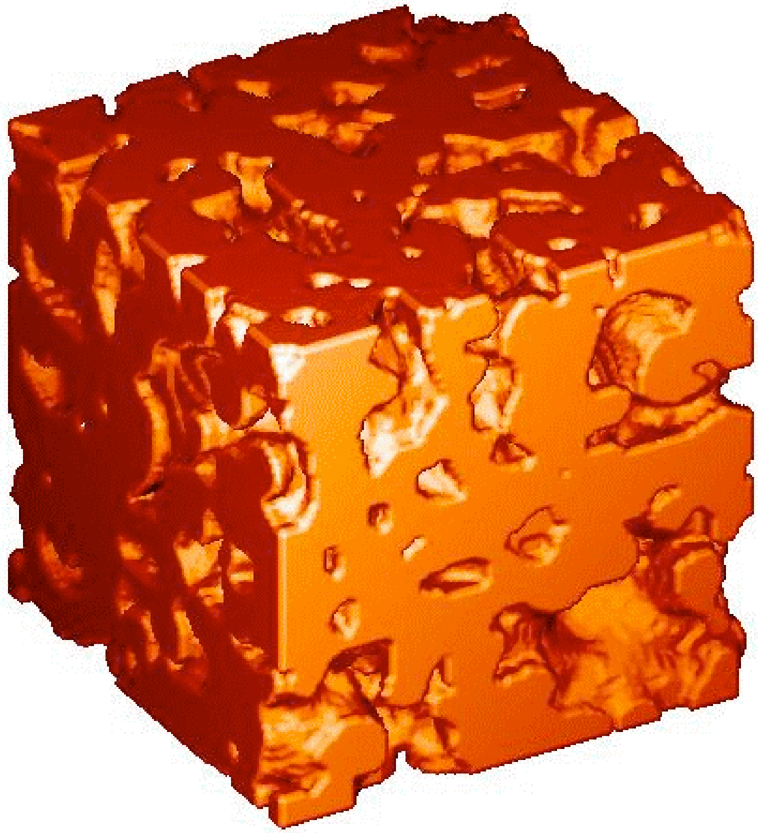

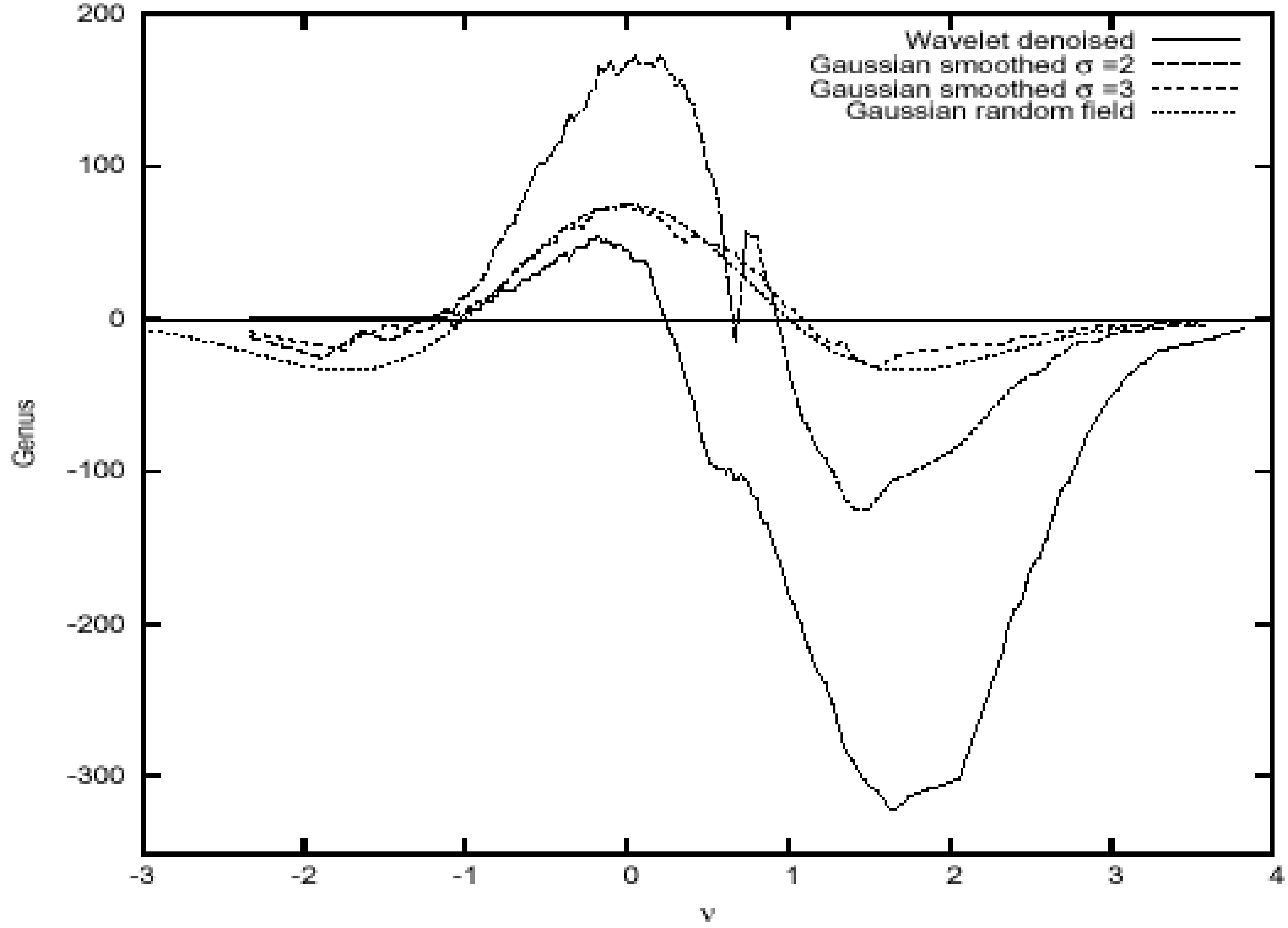

The genus curve of this adaptive reconstructed density field is much more informative because it is unique and does not depend of the particular choice of the filter radius. Additionally, the genus curves of Gaussian-smoothed density fields mimic those of Gaussian random fields, describing thus more the properties of the filter than the real morphology of the density distribution.

Voronoi filaments

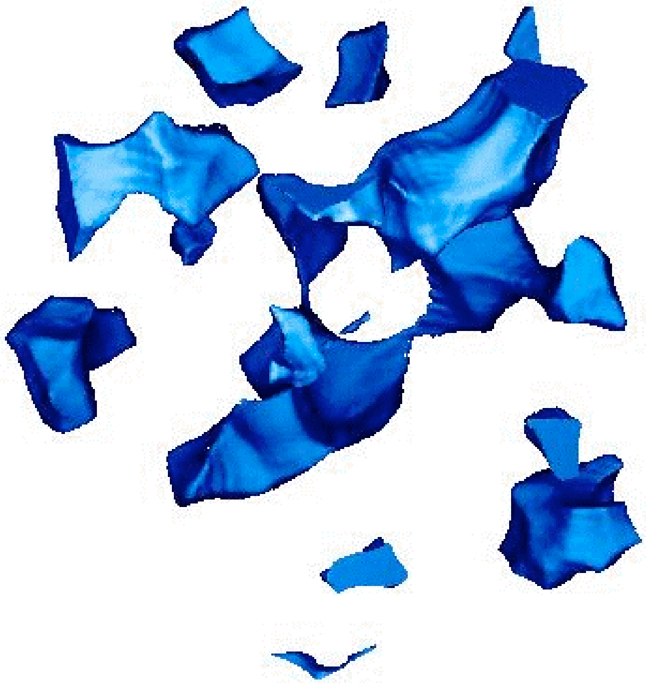

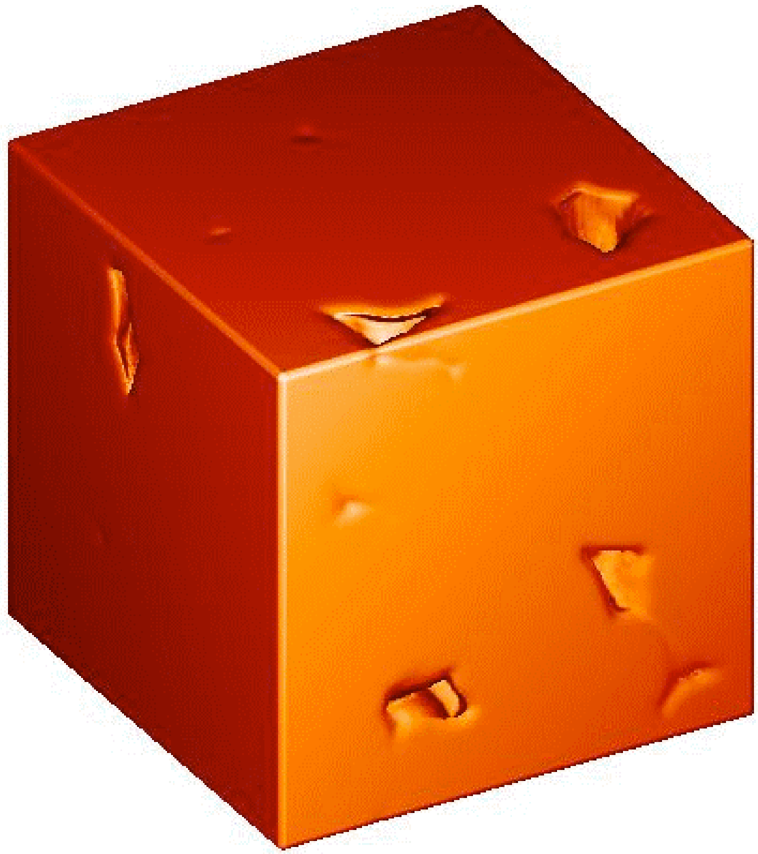

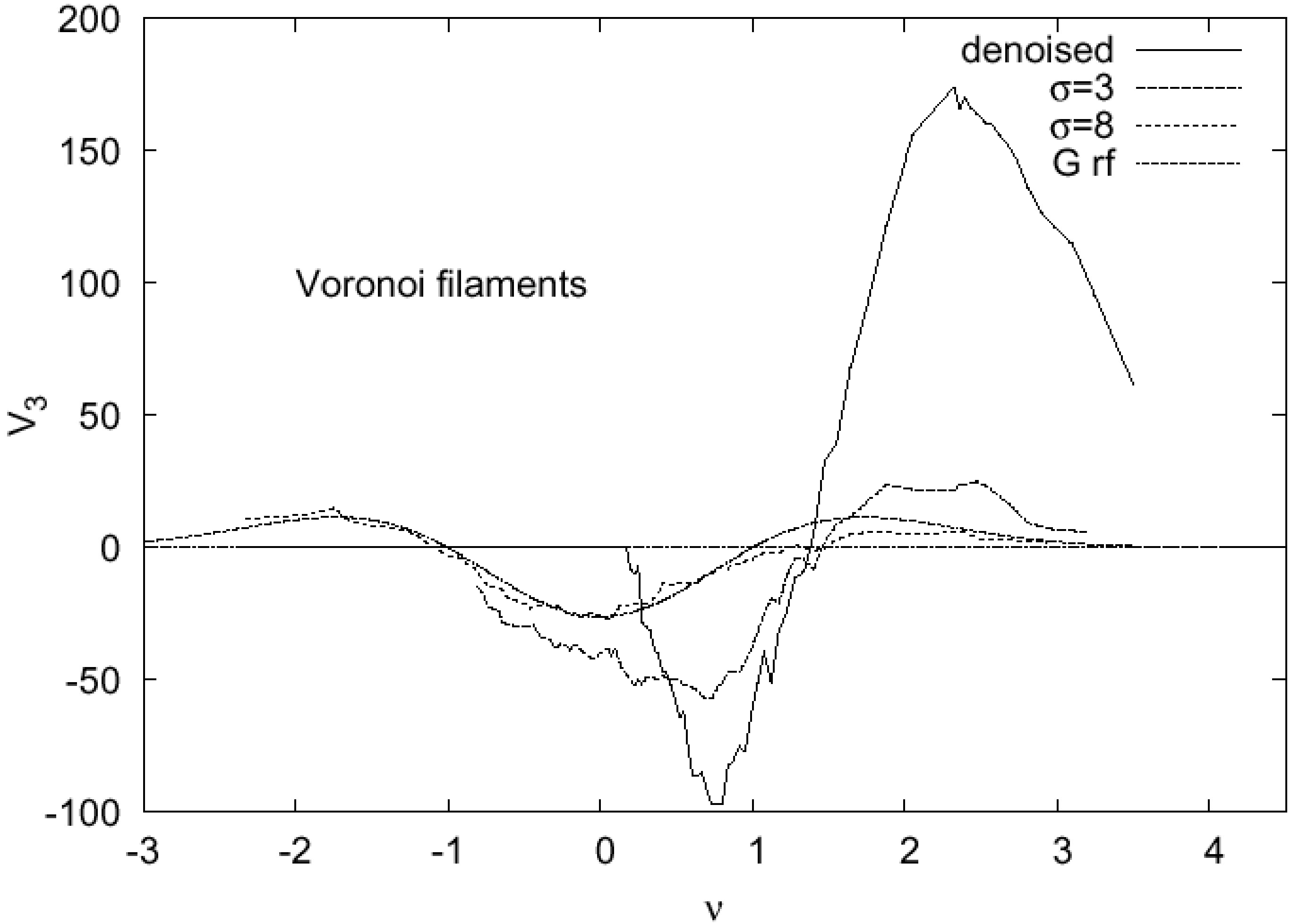

denoised
σ=3
σ=8
G rf
Voronoi filaments
V_3
200
150
100
50
0
-50
-100
-3
-2
-1
0
1
2
3
4
ν

Swiss Cheese

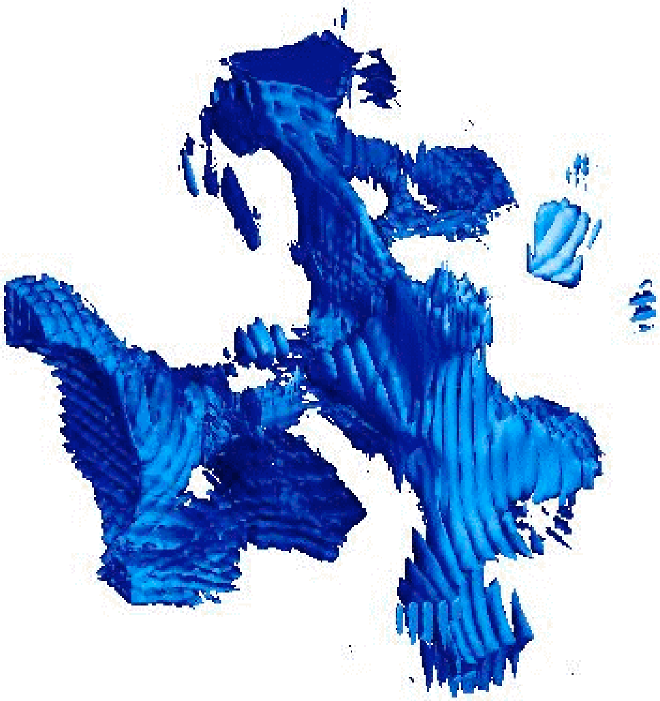

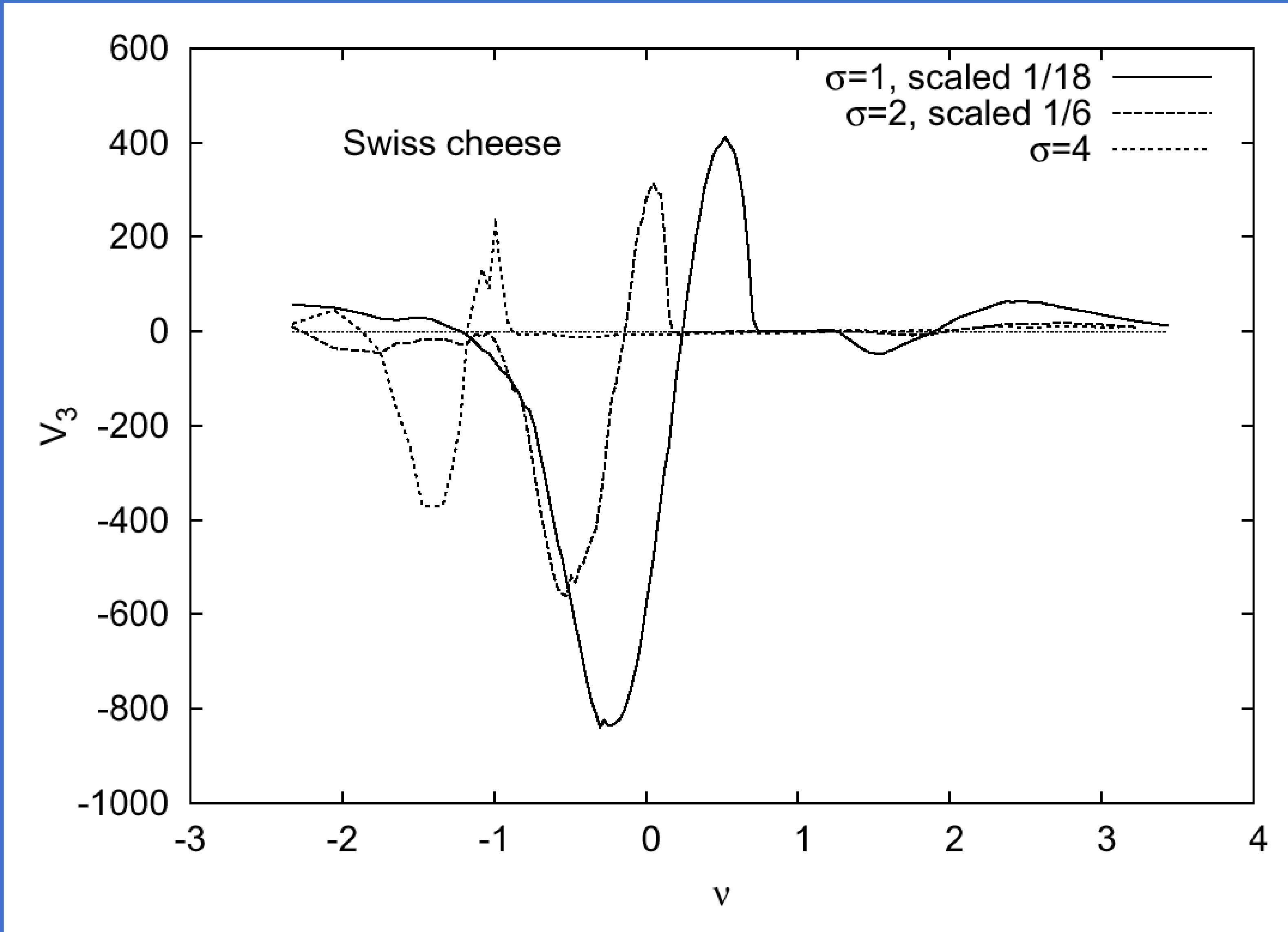

Swiss cheese
σ=1, scaled 1/18
σ=2, scaled 1/6
σ=4
600
400
200
0
-200
-400
-600
-800
-1000
V_3
-3
-2
-1
0
1
2
3
4
ν

2dfGRS northern slice

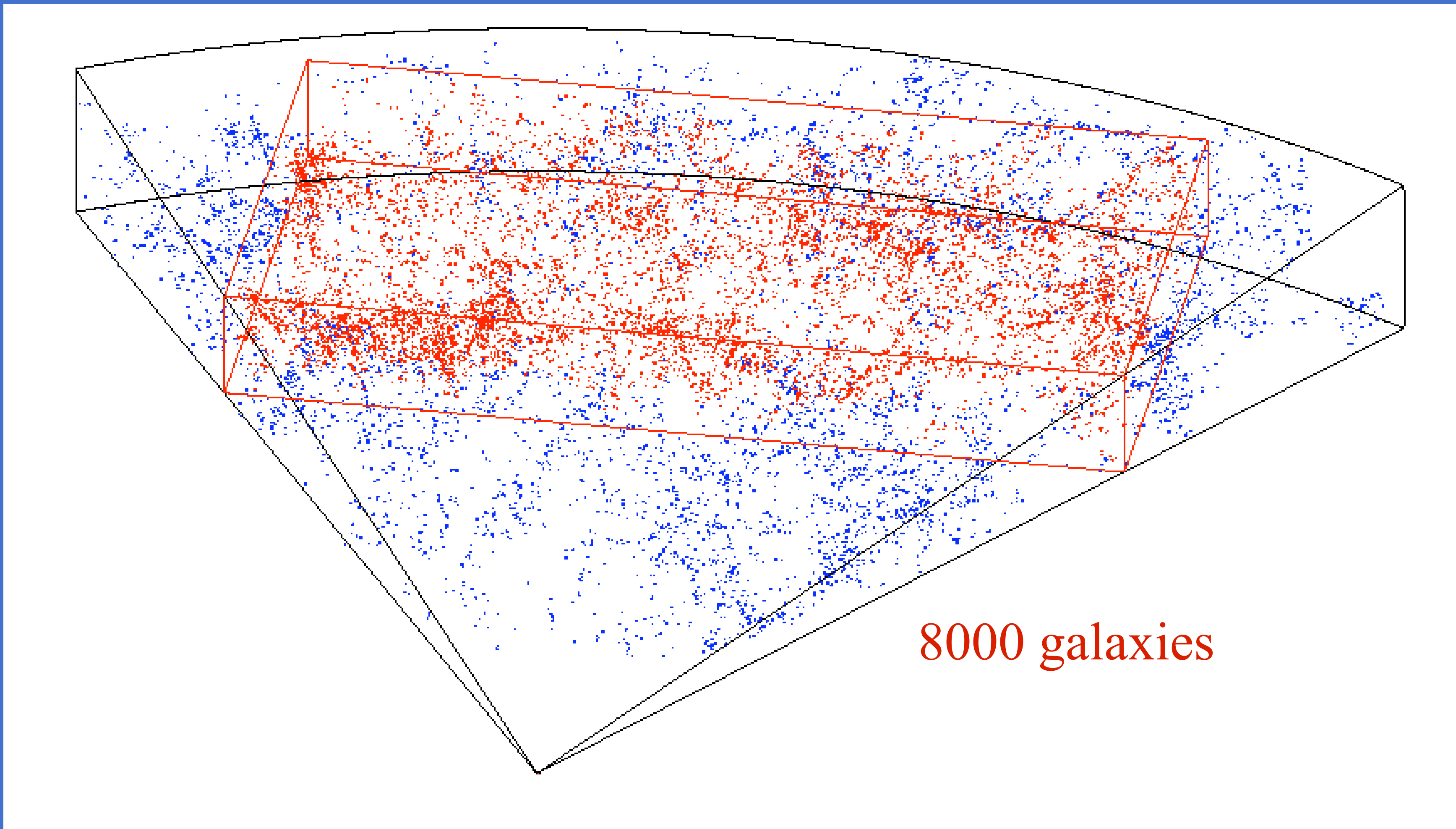

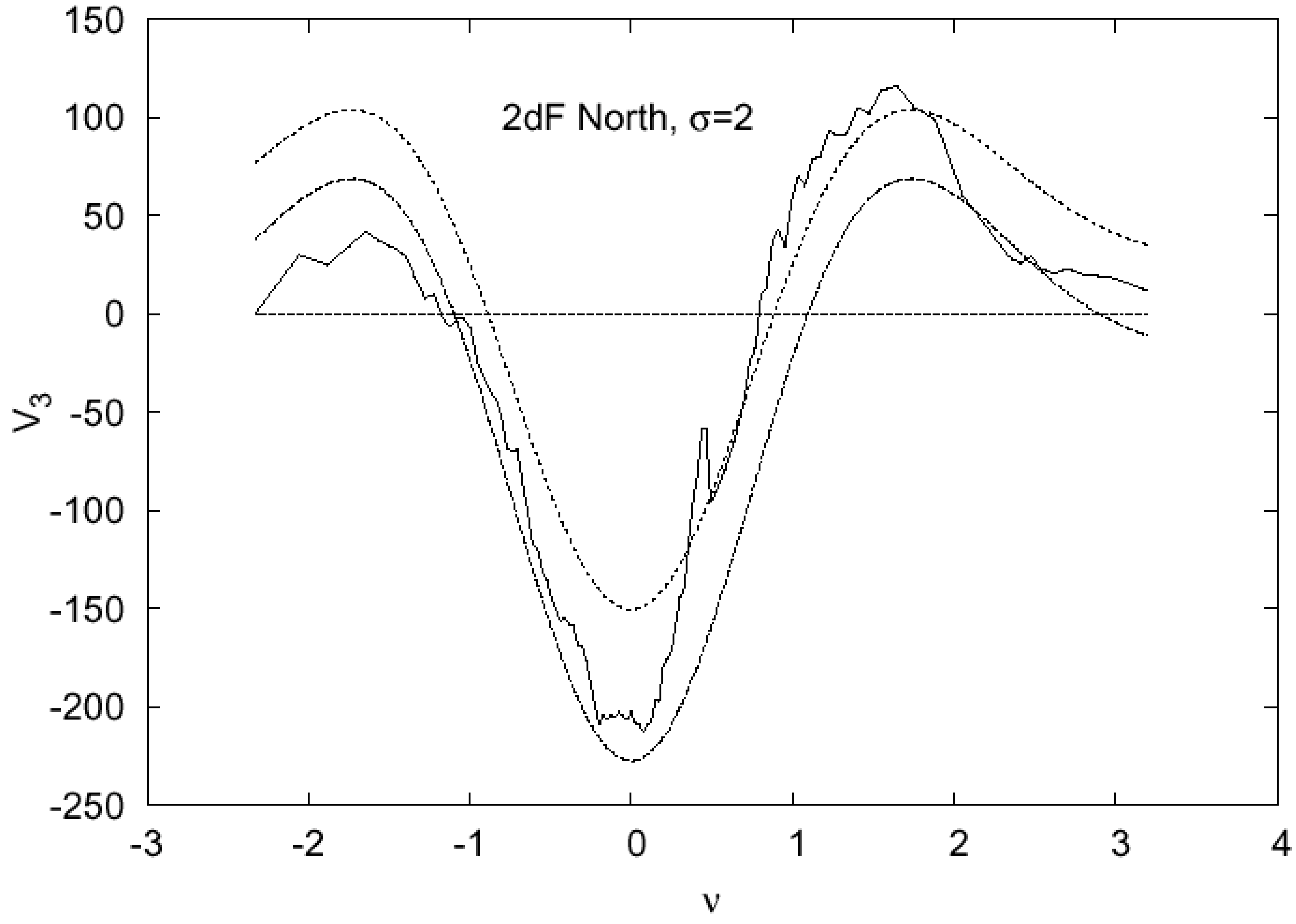

2dF North, σ=2
150
100
50
0
-50
-100
-150
-200
-250
V_3
-3
-2
-1
0
1
2
3
4
ν

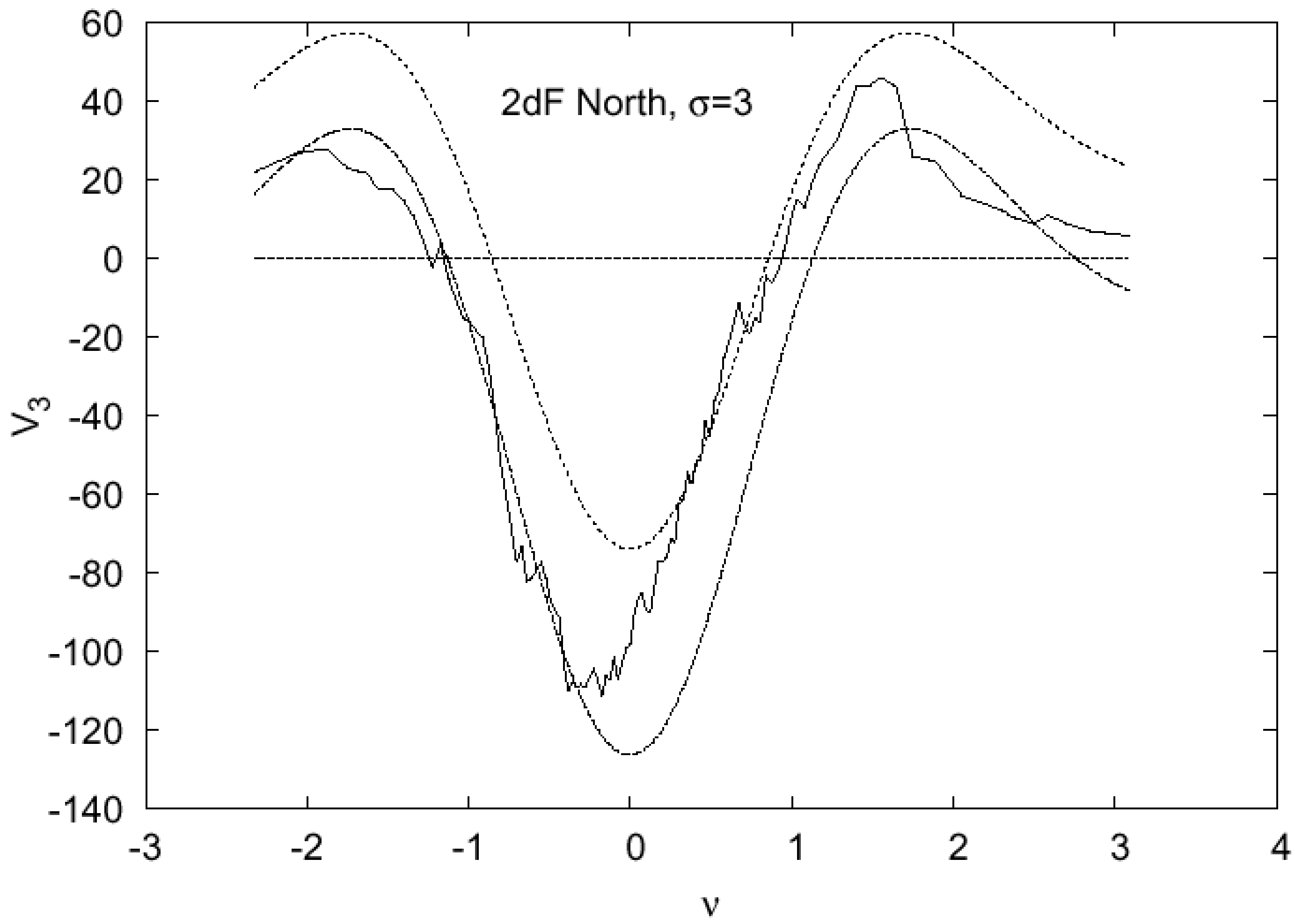
2dF North, σ=3
60
40
20
0
-20
-40
-60
-80
-100
-120
-140
V3
-3
-2
-1
0
1
2
3
4
ν

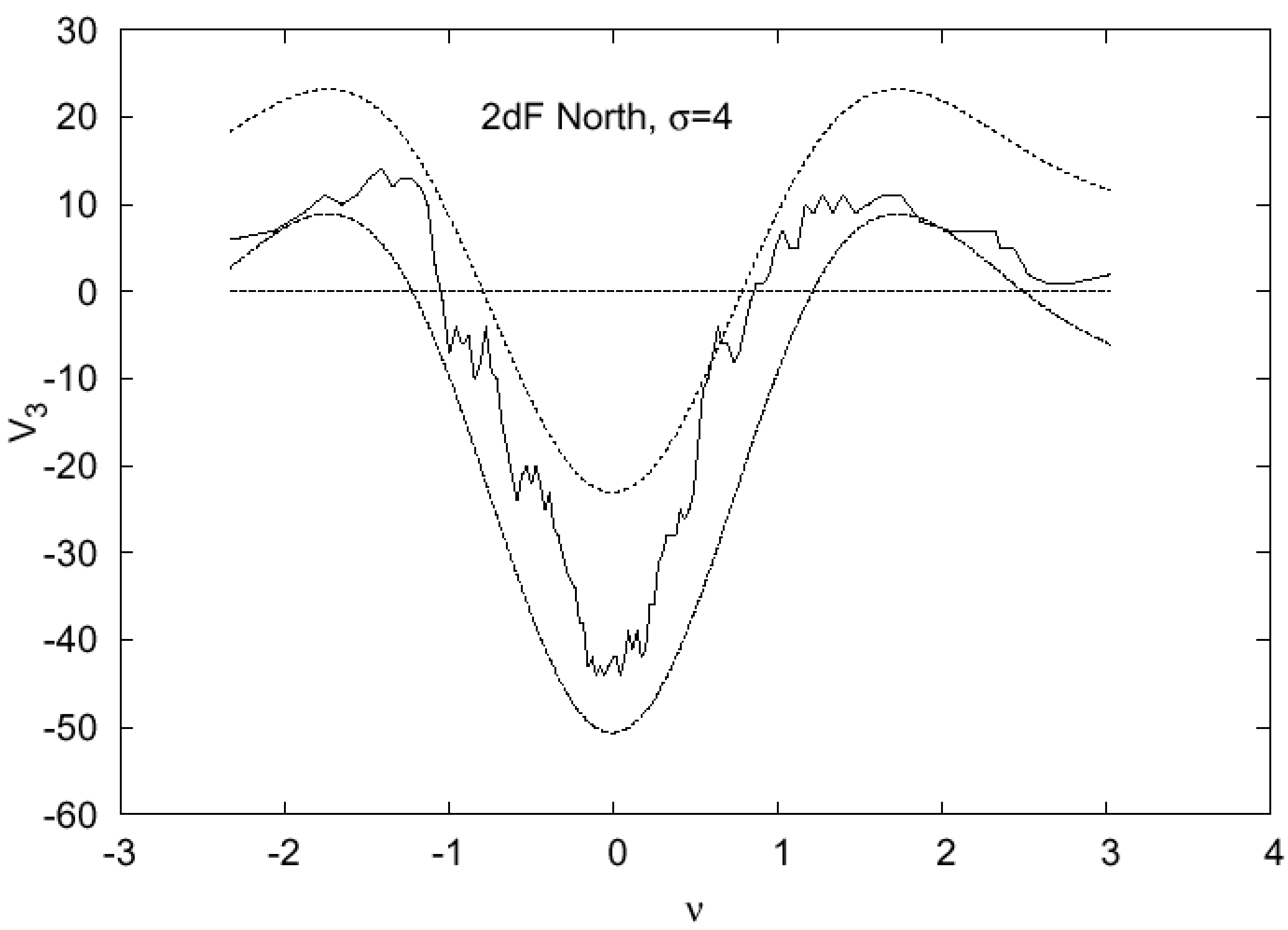

2dF North, σ=4
30
20
10
0
-10
-20
-30
-40
-50
-60
V3
-3
-2
-1
0
1
2
3
4
ν

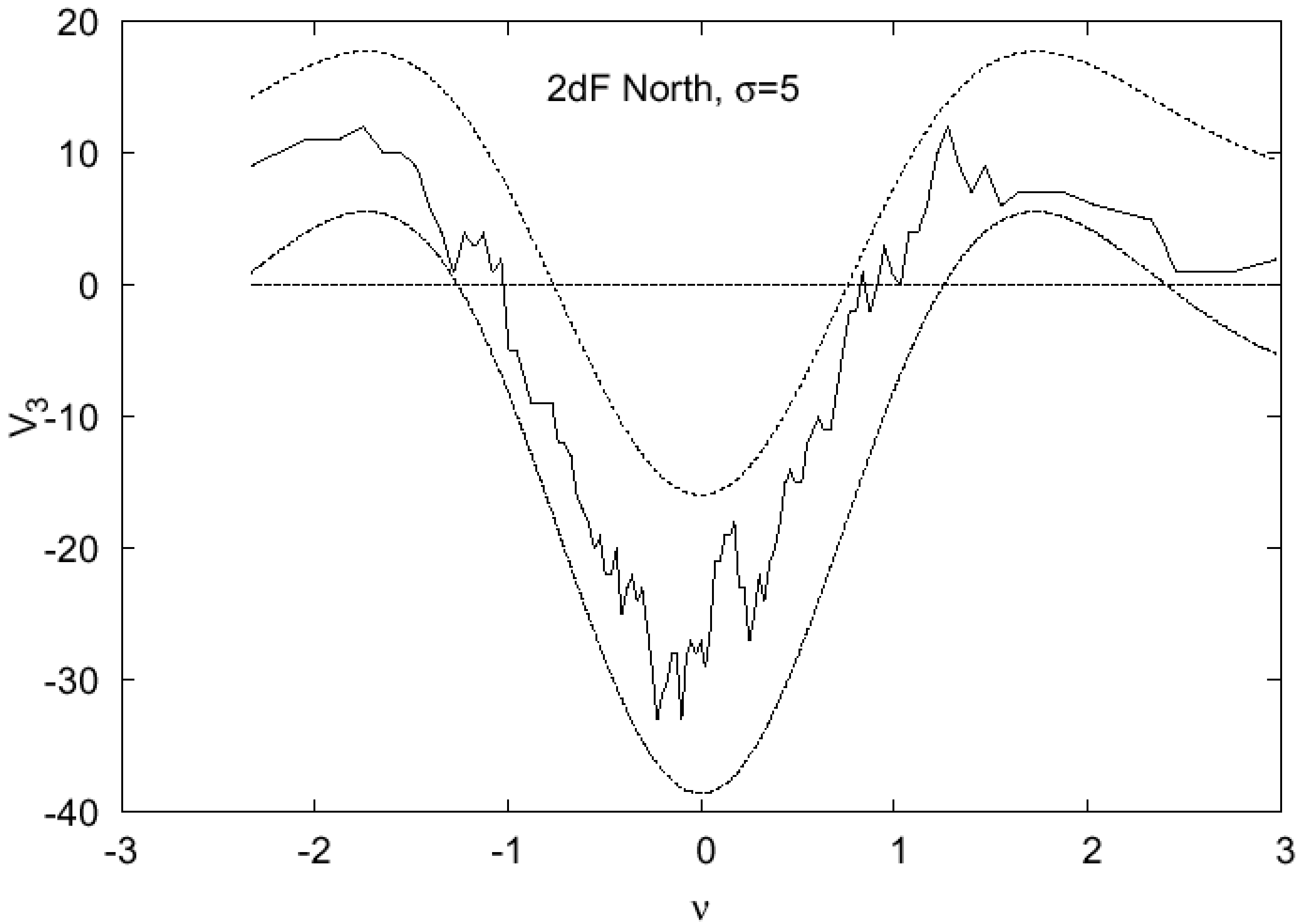

2dF North, σ=5
20
10
0
-10
-20
-30
-40
V_3
-3
-2
-1
0
1
2
3
ν

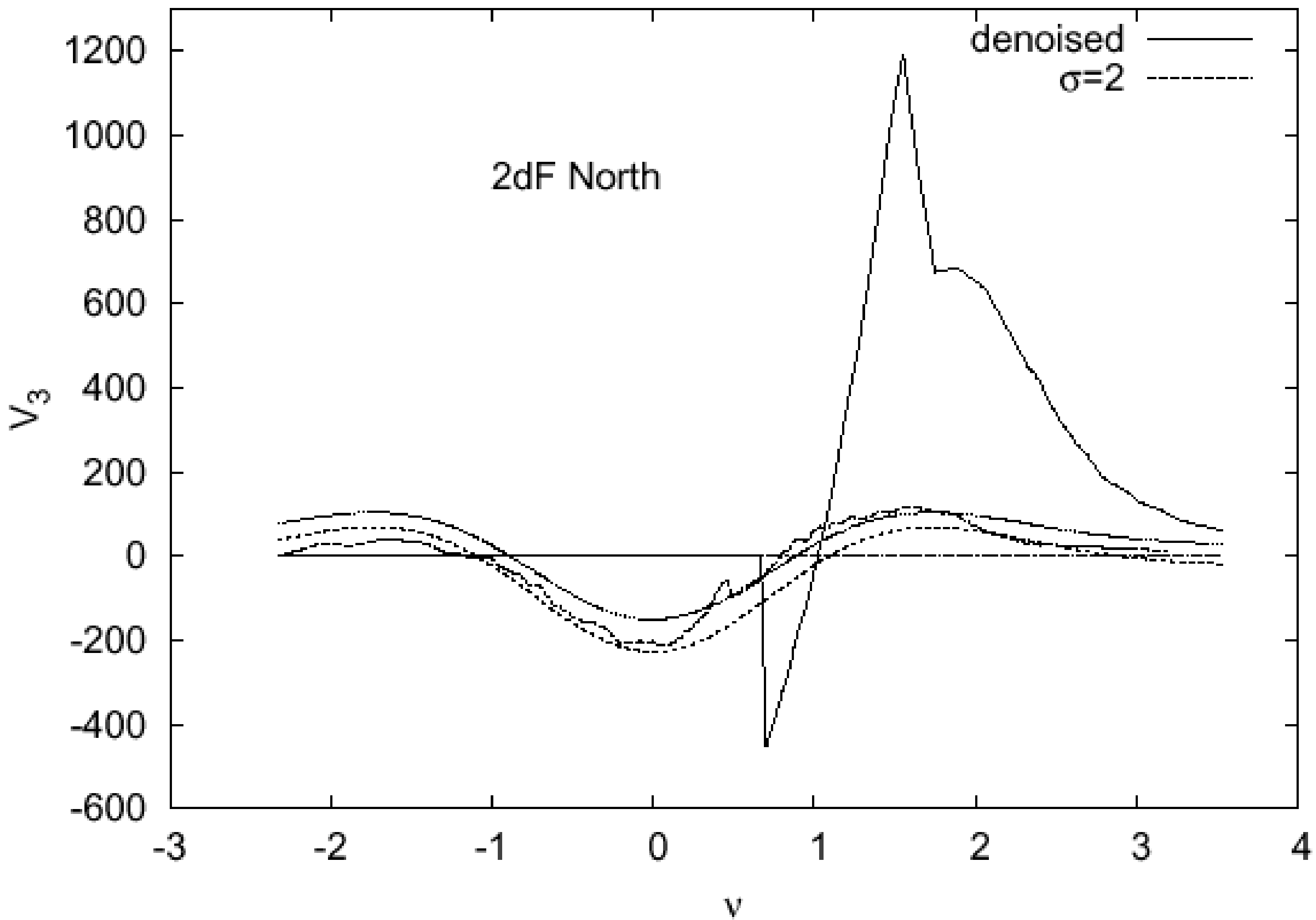

denoised
σ=2
2dF North
1200
1000
800
600
400
200
0
-200
-400
-600
V_3
-3
-2
-1
0
1
2
3
4
ν

We have seen that Gaussian smoothing, as usually applied, introduces a strong Gaussian signal for any kind of distribution, erasing small scale non-Gaussian features

Coles & Lucchin pointed out this idea already in 1995

We see that the multiscale representation retains the non-Gaussian nature of the initial samples; the Minkowski functionals are far from Gaussian

In contrast, Gaussian smoothing smears matter into low-density regions and generates density distributions, which resemble Gaussian random fields, as shown by the Minkowski functionals shown in the previous sections.

Conclusions

- Quantitative descriptors -being reliable, robust, unbiased, and physically interpretable- are needed to extract cosmological information from the data.
- We have shown a consistent method to estimate the density field in an optimal way that ensure that the topology of the reconstructed field reflects the true underlying topology of the point process.
- The method is suitable for the galaxy distribution which has a genuinely multiscale structure, with non-linear structures like filaments, sheets and prominent clusters.

If you want to know more...